

Ion Beam Characterization and Engineering of Strain in Semiconductor Multilayers

Thesis submitted for the degree of

Doctor of Philosophy

by

S.V.S. Nageswara Rao



**School of Physics
University of Hyderabad
Hyderabad - 500 046 India
December 2002**



Dedicated to

Lord Sri Venkateswara Swamy

DECLARATION

I hereby declare that the work embodied **in this thesis entitled "Ion Beam Characterization and Engineering of Strain in Semiconductor Multilayers"** carried out by me, under the supervision of **Prof. Anand P. Pathak**, School of Physics, University of Hyderabad, Hyderabad, India, has not been submitted for any other degree or diploma either in part or in full to this or to any other University or Institution.

Place: Hyderabad

Date: 27-12-02

(S.V.S. Nageswara Rao)

CERTIFICATE

This is to certify that the work described in this dissertation entitled "**Ion Beam Characterization and Engineering of Strain in Semiconductor Multilayers**" has been carried out by **Mr. S.V.S. Nageswara Rao** under my direct supervision for the full period prescribed under PhD. ordinances of the University and the same has not been submitted for any other degree or diploma to this or any other University or Institution.

Place: *Hyderabad*

Date: *27.12.02*

S. S. Nageswara Rao
27.12.02
(Dean, School of Physics)

DEAN I/C
School of Physics
University of Hyderabad
Hyderabad 500 046 INDIA

Anand P. Pathak
(Prof. Anand P. Pathak)

Prof. ANAND P. PATHAK
SCHOOL OF PHYSICS

ACKNOWLEDGMENTS

I would like to thank all those who have, directly or indirectly, helped or encouraged or motivated me in successful completion of this thesis. It is really difficult to do complete justice to this section of the thesis because unfortunately we don't keep logbooks for this purpose! However all the names are permanently written in my heart and I thank all of them. It is really my pleasure to get a chance to work with many great researchers and I sincerely thank all of them.

I am completely indebted to Prof. Anand P. Pathak, a constant source of encouragement, inspiration, help, knowledge and advices which are very much useful for both the academic and personal life. I sincerely thank him for his invaluable guidance, keen observation, patience, support and teaching. I feel I am very lucky for getting him as my PhD supervisor who has taught me several crucial concepts and trained me in getting expertise. I enjoyed the kind of team work we did in collaboration with several scientific institutions. Once again I thank him for establishing collaboration with several institutes and organisations in India and abroad and for providing all facilities and help in making out this work. Most of the times he treated me like his son but at the same time he is not confined only to fatherliness. He is like my father only while taking responsibility of my future but in addition he played many roles: for example like an elder brother while giving advices and like a friend many times. I have tried to learn all of his good qualities but I should admit that I could reach his (light) velocity. I request him to forgive me for any mistakes if I did in the course of work. Finally I thank all his family members for providing homely atmosphere during our meetings on several occasions.

I express my deep sense of gratitude to Dr. D.K. Avasthi for his invaluable teaching, training and advices during my course of experimental and developmental work at NSC, New Delhi. He has helped me in planning and performing several experiments and provided all necessary facilities to execute this work. I sincerely thank him for teaching several concepts involved in accelerator based experimental research. I am very lucky to get a chance to learn several experimental techniques and skills directly from such an expert. I also thank his family for providing homely and friendly atmosphere during festivals, celebrations and other meetings.

I express my sincere thanks to our school's present dean, Prof. S.N. Kaul and all former deans for providing all facilities that are needed to complete this thesis work. I thank Prof. V.S.S. Sastry for his kind help on many occasions. I would like to thank Dr. Ashok Chatterjee, Dr. Prashanta K. Panigrahi and Dr. Vipin Srivastava for their kind concern and teaching, in the initial days of my research while I was attending their M. Phil classes. Once again I thank Dr. Panigrahi for his continuous encouragement and motivation. I express my cordial thanks to Mr. Abraham for his patience and helping nature. Also I thank all teaching and non teaching staff of the school.

I would like to express my sincere thanks to NSC, New Delhi for providing financial support through an UFUP project and **CSIR, India** for SRF. Also I cordially thank CSIR for foreign travel grants to present our results in an international conference (CAAR1 17) at University of North Texas, Denton, USA.

It is my great pleasure to have nice seniors like Dr. V. Harikumar, Dr. Azher M. Siddiqui, Dr. L.N.S. Prakash Goteti and Dr. Santanu Ghosh in our group. I am grateful to them for providing fundamental knowledge which is still driving my research activities. I thank Dr. Siddiqui and Dr. Ghosh for laying the foundations in experimental physics and Dr. Prakash for laying the foundations in theoretical physics specially quantum mechanics and solid state physics. I specially thank Dr. Prakash for digging out my analytical skills and Dr. Siddiqui for introducing me to the scientific community in India. Also I thank all these people for their nice company and encouragement.

I thank my colleague Ms. G.B.V.S. Lakshmi for extending her support in planning and performing experiments. She has helped a lot while developing the experimental facilities that are need to pursue this work. I must admit the fact that I may not have finished this work within this time span without her cordial help. I sincerely thank all my colleagues Ms. Anita Tiwari, Mr. Arun and Mr. Suryanarayana for their kind support and motivation, especially while visiting other institutes. I used to visualize and learn some crucial concepts while clarifying Mr. Arun's doubts. I thank him for this and also for his company and specially for providing humorous atmosphere.

I am grateful to Mr. B.V.N. Phani Kumar for his all kinds of support. He is the first person ever I know from our school and many times his advices helped me a lot. I cordially thank Mr. Phani Murali Krishna, Mr. Naga Srinivas, Mr. Prem, Mr. Manoj Kumar, Ms. Raishma Mr. Pammy, Mr. Bharadwaj for their help, useful suggestions during the course of work. I also I thank them for making lively personal life in the campus. I express my sincere thanks to Dr. Sri Ramana, Dr. Anita Semwal, Dr. Sateesh and Dr. Srinath for their kind motivation and encouragement. I would like to thank Mr. M^{TV} Rao and Mr. Mukunda for their kind help in critical situations, for their encouragement and for providing lively personal. I would like to thank Mr. Sarkar, Mr. Senthil, Mr. Sudhir, Mr. Bashid, Mr. Sanjeev, Mr. Mani, Mr. Ajit, Mr. Sunil, Mr. Prasanna, Mr. Ajay, Mr. Chaitanya and all other research scholars.

I express my cordial thanks to my VAX lab mates Mr. Satya, Mr. Kalyan Chakravarthy, Mr. Raghu, Ms. Lekha, Mr. Senapathi, Mr. Srinivas (G), Mr. Ravi and Ms. Sriranjani for all their help. They provided lively atmosphere and constant encouragement during my thesis writing process. They have even helped me in making some of the illustrations and printing the thesis. I express my sincere thanks to all M.Sc, M.Sc(Tech), M. Phil, M.Tech & PhD-students for their useful interaction with me. I like to thank all inmates and staff at NRS Hostel for their co-operation.

I express my sincere thanks to all NSC personnel for their unimaginable helping nature and their nice way of collaborative research. I thank the present director Dr. A. Roy and the former director Prof. G.K. Mehta for their invaluable suggestions during my

seminars and for providing all necessary facilities execute experimental work. I would like to thank Dr. Kanjilal, Dr. S.K. Datta, Dr. N.C. Mishra, Dr. Ravikumar, Mr. A. Tripathi for teaching me several important concepts and for their constant support.

I take this opportunity to express my sincere thanks to Mr. Ashok Kothari who is involved in designing and fabricating the gas detector (LAPSDT). I like his way of working and thank him for his sincerity and interest in this work. I thank Mr. E. T. Subramanyam and Mr. Kundan Singh who are involved in the development of automated high energy channeling facility. I thank Mr. Subramanyam for his kind help regarding all computer related works, teaching and for making ERDA simulation program.

I had nice time and useful discussions with Dr. S.K. Srivastava and Dr. D. Bhattacharya. I thank them for their kind support during all experiments at NSC. I cannot forget the benefit (understanding concepts of HRXRD) that I got during a casual discussion with Mr. Srivastava while waiting for someone in an airport. I am thankful to Dr. D. Bhattacharya (Debidi) for her care.

I sincerely thank Mr. S.A. Khan for his kind concern, interest and sincerity towards work in general and my research in particular. He helped me a lot while developing the experimental facilities and during all experiments. I express my sincere thanks to Mr. Sugatan and all members of detector lab for extending their help in making detector windows, grids etc. I would like to thank Mr. Akhil for his special interest in my work and for his immediate help during crucial situations. Also I thank Ms. S. Barua in the same contest for making detector windows during the emergency. I am indebted to Mr. P. Barua for his continuous support during all experiments. I express my deep sense of gratitude to Mr. S.S.K. Sonti for both official and personal helps. He gave several useful ideas during the mechanical design of the experimental facilities. I thank his family for providing homely and lively atmosphere during my stay at NSC.

I thank Mr. F. Singh, Mr. Rakesh Kumar, Mr. S. Nath, Mr. Somen and Mr. Ojha for their support and motivation. I thank Mr. Sarvesh Kumar and Mr. Manvendra Kumar for their help in all experiments at NSC. In the same contest I thank Dr. H.S. Nagaraj, Mr. P.K. Diwan, Ms. Anjana Dogra. It is my pleasure to thank Madhu, Bivash, Satya, Mamata, Rajandra, J.P. Singh, Rajen, Buddha, Vandana, Sara, Sashi, Sankar, Padma, Ajay, Vivake, Kashim, Devarani, Kusam, Kamna and all my friends at NSC for providing nice and enjoyable atmosphere during my stay at NSC. My sincere thanks to Mr. P.N. Prakash, Mr. Koteswar Rao, Mr. Maliyadhri, Mr. Sundara Rao and their families for providing homely atmosphere during my stay at NSC and for their useful suggestions in many regards. Also I thank them for their invaluable suggestions and advices. Finally I thank the Pelletron group at NSC.

I express my deep sense of gratitude to Prof. B.N. Dev, Dr. P V Satyam, Dr. T. Som, Mr. Deepak Goswami and all other members of Ion Beam Lab at IOP, Bhubaneswar for their interest and support. I Sincerely thank Dr. A. Sinha, director IUC-DAEF, Kolkata for allowing us to use the IOP Pelletron. Also I thank him for teaching several concepts during his NSC days. I would like to thank Dr. Vikram Kumar,

Director, SSPL, Delhi for allowing me to utilize their experimental facilities. I thank Dr. R.K. Jain, Dr. S.K. Mehta, Dr. R. Muralidharan, Dr.T. Srinivasan and Dr. U. Tiwari for their sincere involvement in MBE (sample growth) and HRXRD measurements. I thank Dr. F. Eichhorn, Dr. R. Groetzschel, Dr. N. Schell and Dr. B. Schmidt, FZR Rossendorf, Dresden, Germany for performing some of the ion channeling, HRXRD and RTA experiments presented in this thesis. I am grateful to Dr. A. Turos Warszawa, Poland for providing lattice matched samples (P520 & P523).

I convey my sincere thanks to my M.Sc teachers Prof. P.S. Keshava Rao, Dr. P. Appalanaidu, Prof. K. Kameswara Rao and Dr. R. Subramanyam for teaching me the basic concepts of physics and for their encouragement towards my research career. I wish to express my gratitude to my best teacher Sri. R. Kanakarao for laying basics in electronics and physics during my graduation.

I take this opportunity to express my deep sense of gratitude to my loving sister Radha and her family. I feel that she has indirectly sacrificed her education for my growth. I express my sincere thanks with regards to my grand parents (ammumma, tathagaru, nannamma and tathagaru) for their motivation, affection and help in many regard. I am grateful to my ammumma who dose not show tiredness even at this age specially for helping some one.

I am indebted to Savitri Pinni, Sekhar chinnannagaru and their children (Raghavendra & Saratchandra) for all kinds of support not only me but to whole family. I thank them for their constant encouragement and affection. I sincerely thank Sitha pinni, Janaki pinni, Binni pinni, Sessa pinni, Chayapinni (my ideal), Padmasree and their families for their constant support, motivation and affection. I convey my sincere thanks to my peddanannagaru (Sri S. Venkateswrlu), Ramam chinnanna, Abbu atta, Papai atta and their families. Also I thank Latha, Raghu, Manasa Padma, Kala and all my cousins and their families (in case married) for their constant encouragement and motivation. I thank all other relatives and friends. I convey my sincere thanks to Hyma aunty, Ramachandra Rao uncle and their children Chinna and Bajja for timely help and support. I also thank them for providing lively atmosphere during my stay at Hyderabad.

My dearest friends Swami, Ravi, Mahesh, Syam, Venkat, Murthi and Gopi do not allow me to use the words like "thanks" and "sorry" but I cannot reset remembering their all kinds of support at this time. I convey my deep gratitude to these and all other friends.

I don't find adequate words to express my gratitude and indebtedness to my parents. I thank them for providing a joyful life with all freedom and for guiding me to take all future steps in my life and for their sacrifice. They have supported me and my studies in spite of all kinds of problems.

TABLE OF CONTENTS

	Declaration	i
	Certificate	ii
	Acknowledgements	iii
Chapter I	Introduction	1
1.1	Introduction	1
1.2	Ion solid interactions (<i>Basic concepts</i>)	2
1.3	Systems of interest (The motivation)	5
1.4	Ion beam characterization techniques	11
	1.4.1 RBS and ERDA	11
	1.4.1.1 <i>Kinematics of RBS & ERDA</i>	12
	1.4.1.2 <i>Compositional analysis</i>	14
	1.4.1.3 <i>Depth Profiling</i>	15
	1.4.1.4 <i>Large solid angle detection</i>	16
	1.4.1.5 <i>Special features of ERDA</i>	17
	1.4.1.6 <i>ERDA with telescope detectors</i>	17
	1.4.2 Ion Channeling & Blocking	19
	1.4.2.1 <i>The channeling (blocking) effect</i>	19
	1.4.2.3 <i>Channeling theory</i>	21
	1.4.2.3 <i>Channeling half angles and</i> <i>minimum yields ~</i>	24
	1.4.2.3.1 <i>Channeling half angles ($\Psi_{1/2}$)</i>	24
	1.4.2.3.2 <i>Minimum yield (χ_{min})</i>	25
	1.4.2.3.3 <i>Special note for</i>	

	<i>diatomic crystals</i>	25
	1.4.2.4 <i>Applications of channeling</i>	26
	1.4.2.4.1 <i>Point Defects</i>	26
	1.4.2.4.2 <i>Stacking faults</i>	27
	1.4.2.4.3 <i>Distortion effects</i>	28
	1.4.2.4.3 <i>Application to SLS</i>	28
	1.4.3 Ion beam methods to probe strains in SLS	29
1.5	Simultaneous on-line modification and measurement of strain	32
1.6	High Resolution X-Ray Diffraction (HRXRD)	32
1.7	Conclusion	33
1.8	References	33
Chapter II	Experimental	41
2.1	Experimental Facilities	41
	2.1.1 The Pelletron Accelerator Laboratory at NSC	41
	2.1.1.1 <i>The Pelletron accelerator</i>	42
	2.1.1.1.1 <i>Beam energy and current</i>	43
	2.1.1.2 <i>Materials Science Beam Line</i>	44
	2.1.1.2.1 <i>The HV chamber:</i>	45
	2.1.1.2.2 <i>The GM chamber</i>	46
	2.1.1.3 <i>GPSC Beam Line</i>	46
	2.1.2 Experimental facilities at SSPL	47
	2.1.3 Channeling facility at IOP	48
	2.1.3.1 <i>The accelerator</i>	48
	2.1.3.2 <i>Channeling facility</i>	49
	2.1.4 Other experimental facilities	49
2.2	Experimental Details	50
	2.2.1 Sample growth and specifications	
	2.2.2 Material treatment (Irradiation and/or annealing)	50

	2.2.3 RBS/Channeling	51
	2.2.4 HRXRD	52
	2.2.5 ERDA, High energy channeling and blocking	52
2.3	Conclusion	53
2.4	References	53
Chapter III	Development of experimental facilities	54
3.1	Development of LAPSDT	54
	3.1.1 Ionization Chambers	55
	3.1.2 General considerations	58
	3.1.3 Z identification and position sensitivity	58
	3.1.3.1 Z identification	58
	3.1.3.2 X-Position (in the scattering plane)	59
	3.1.3.2 Y-Position (perpendicular to the scattering plane)	59
	3.1.4 Design and Fabrication	60
	3.1.4.1 The Inner-structure	63
	3.1.4.2 Detector chamber	65
	3.1.4.3 The window, intermediate chamber and Gas ckt	67
	3.1.4.5 Electronics ckt and data collection	70
	3.1.5. Results and discussion	71
	3.1.5.1 z-identification	72
	3.1.5.2 Position sensitivity	77
	3.1.5.3 Kinematic corrections and depth profiling	79
3.2	Development of an Automated High Energy Channeling Facility	82
	3.2.1 Development and operation of the facility	83
	3.2.1.1 Beam collimation and Sample alignment	83

	3.2.1.2 Sample holder and degrees of freedom	84
	3.2.1.3 Automation and operation	86
	3.2.1.4 Experimental Procedure and Results	86
3.3	Conclusion	89
3.4	References	90
Chapter IV	Ion Beam Mixing and Strain Engineering.	93
4.1	Introduction	96
4.2	The P523 (A lattice Matched Superlattice System)	
4.3	Application of LAPSDT (Online observation of ion beam mixing using ERDA - LAPSDT)	104
4.4	The MQW5 and 4401 (<i>Strained multi quantum wells</i>)	106
4.5	Single Strained Layer Systems (Thickness and ion fluence dependence)	108
4.6	Conclusions	113
4.7	References	114
Chapter V	High Energy Channeling	117
5.1	Introduction	117
5.2	Experimental	118
5.3	Results and discussion	119
5.4	Conclusions	124
5.5	References	125
Chapter VI	Effects of strains and defects in multilayers on the channeling radiation.	126
6.1	Introduction	126
6.2	CR from Positrons and Electrons.	128
6.3	The model	129

6.4	The motivation (Transition probabilities at the stacking boundary)	131
6.5	Initial occupation probability	136
6.6	Effects of SLS on CR	141
6.7	Expressions for Radiation Intensities	144
6.8	Conclusions	145
6.9	References	147
Chapter VII	Conclusion	149
7.1	Instrumentation	149
7.2	Ion Beam Mixing and Strain Engineering	150
7.3	High Energy Channeling	151
7.4	Channeling Radiation in SLS	152
7.4	Future prospects	153
7.5	References	154
	My CV with List of Publications	

CHAPTER I

INTRODUCTION

*This chapter gives complete introduction to the present subject and survey of the existing work. Various concepts, techniques and studies have been discussed in detail. Ion-solid interactions and the importance of the present subject **have been** highlighted. This will also provide an outline of the complete thesis.*

1.1 INTRODUCTION

The main objective of this thesis is to discuss and highlight the importance of ion beam methods to measure and engineer the strain and other parameters of semiconductor multilayers. It contains the experimental and theoretical work that has been done in this direction. Also described are the experimental facilities that have been designed and fabricated for performing the above mentioned experiments. Other experimental techniques, facilities and theoretical models have also been described in detail.

"Ion beam based research" plays major role in the development of science and technology. Rutherford's α - scattering experiment was the first successful attempt to study the structure of atom. Since then, ion beams have been used as probes to study the structure of atom, nucleus and fundamental particles. Such studies have originated the development of modern science on one hand and technology on the other hand via ion scattering and ion implantation techniques respectively. The ultimate goal of the subject is to understand the basic principles of ion - solid interactions and then to apply those principles in the development of modern technology. It has its roots in almost all areas of science like for example material science, medical and biophysics, atomic physics,

nuclear physics etc. Here we concentrate basically on material science where the major interest in the current state of art lies in the studies of effects of high energy heavy ions called as Swift Heavy Ions (SHI) on material properties. Ion beams are used to characterize materials as well as to modify them. Hence one should be careful enough to avoid any modification while using ion beams as characterizing tools by choosing proper beam parameters and detection systems. Similarly one can combine both these techniques to study the online modifications because the same beam that is causing modification can simultaneously be used as material probe. This unique capability of ion beams opens up the possibility to realize controlled modifications. Although this thesis doesn't contain any online experiment, it shows a way to design and perform such experiments. Necessary equipment has also been developed. One such experiment has been performed as an initial step but it will present only qualitative results. Here both the characterization and modification methods have been exploited to measure and modify the strain and other parameters of semiconductor multilayers (superlattices) for the integration of optoelectronic devices.

1.2 ION SOLID INTERACTIONS (*BASIC CONCEPTS*)

When an energetic ion passes through a material it will either interact with the nuclei or the electronic subsystem of the material or both, depending on its energy [1,2]. As a result, it will lose its energy to the material by two corresponding processes called as nuclear energy loss (S_n) and electronic energy loss (S_e). The loss of energy at low ion energies (<10 KeV/amu) is by elastic collisions referred as nuclear energy loss or nuclear stopping, whereas the energy loss at higher energies (>1 MeV/amu) is by inelastic collisions resulting in excitation or ionization of atom is referred as electronic energy loss or electronic stopping. In a narrow range of energy (in between the above two energies) the contribution of electronic and nuclear process are comparable.

Nuclear stopping dominates in low energy region where the ion undergoes elastic collisions with the atoms of the material. As a result the target atoms are displaced from their sites, creating vacancies and displaced atoms in interstitial sites. Large amounts of

such defects will be introduced into system and will modify some of the important properties of the materials. Hence study of such process will help in engineering the material properties. These ions will be implanted in the materials at certain depth (called range) when they are completely stopped within the material. The range of the ion depends on the ion energy and material properties. Well established theory [1-3] and simulation programs (like TRIM¹ [4]) are available to calculate these stopping powers and ranges for different ion, target combinations. Ion implantation has been exploited extensively in the development of present day's technology [3,5]. Low energy irradiation in multi/bi layer targets causes intermixing of different element at the interface [6]. This will influence the diffusion properties of the materials and will help in making alloys of different elements for various applications. Such process called as ion beam mixing has also been studied and utilized rigorously [6,7]. Chemically immiscible systems can also be mixed with this technique. These elastic collisions are also used to characterize different materials. In fact ion beams were initially used only for characterization purpose. These details are given in section 1.4. The interaction of low energy ions with the matter has been thoroughly studied and applied in the technology development.

The other process, *i.e* the electronic stopping of ions in matter, dominates in the high energy region when the ion velocity is comparable or greater than that of valence electrons of the target material. In the electronic stopping, the incident ions make inelastic collisions with the atoms of the material and the atoms either get excited or get ionized. This high energy (MeV) irradiation of materials causes modification to their properties, which is distinctly different from the above discussed low energy modifications. Therefore, ion beam modification of materials produced by swift heavy ions has become an important area of research in the recent years. This process cause different effects in different materials. It creates columnar defects in high T_c superconducting materials [8], cylindrical tracks in polymers [9], amorphization [10] and re-crystallization [11] in some materials, phase transitions [12], structural changes [13] etc. Ion beam mixing discussed in the low energy region has a new dimension in this energy region with several advantages [14]. This techniques has been applied in the

¹ TRansport of Ions in Matter (TRIM).

bandgap tuning of semiconductor superlattices and other semiconductor materials [15]. The present work also deals similar problem [16,17]. These details along with complete literature survey are given in chapter 4.

There are some important considerations while selecting ion-target combinations for studying the electronic energy loss process. One should see, so that the nuclear stopping is very low and can be neglected when compared to electronic energy loss. Then one can study the pure effects of electronic stopping. The ion energy and film thickness are to be chosen such that the S_e is constant (homogeneous) throughout the film. These measures can easily be taken with the help of simulation software like TRIM.

In fact it is expected that the SHI interact only with the electronic subsystem of the material. So no atom should move in the influence of the SHI irradiation, but the movement of target atoms is evident from above mentioned effects. In this connection SHI irradiation studies attain importance from the fundamental need of understanding this energy transfer mechanism in this energy region. It is believed that the high-energy beam loses its energy to the electronic subsystem of the target material, and then this energy will be transferred to the lattice atoms via the electron phonon coupling. There are two models namely "Coulomb explosion model [18]" and the "Thermal spike model [19]" to explain such energy transfer mechanisms. According to the Coulomb explosion model, a positive ion core along the ionizing path of the energetic beam repels the nearby atoms. This causes a radial motion of the atoms sitting around this core. This model is applicable for the insulators like polymers. Thermal spike model assumes that the inelastic energy loss of the energetic beam produces very high temperature, which exists for a very short time, thereby called as thermal spike. During the spike period the material will melt because these temperatures are very well above the melting temperatures. Diffusion occurs in this molten state but it cannot come back to the equilibrium because of the rapid quenching. Thermal spike is shown to be more responsible for the mixing occurring at the metal-metal and metal - semiconductor interfaces. These two models are described in fig.(1.1) in the form of a table. SHI induced mixing (in various systems like metal-metal, metal-semiconductor and semiconductor-

emiconductor) has been recently studied by several authors [14,15, 20 &21]. The basic **thrust** of such work is to understand the above mentioned energy transfer mechanism as well as to make new materials for novel device applications. Very few such studies have been reported in semiconductor superlattices. Here we studied the effects of SHI in such technologically important structures.

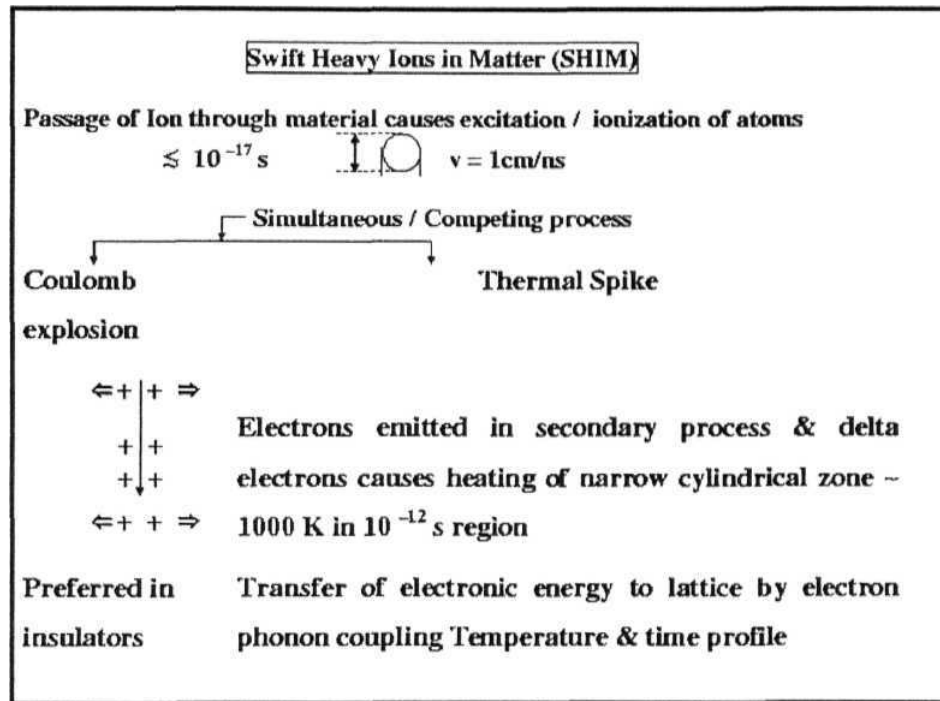


Fig. 1.1: Description of Coulomb explosion and Thermal spike models to understand the ion solid interactions in high energy region.

1.3 SYSTEMS OF *INTEREST* (THE MOTIVATION)

Semiconductor superlattices have potential device applications [22-26] for high performance detectors, high speed and high frequency digital and analogue circuits. The usefulness of these structures is that, they offer precise control over the states and motions of charge carriers in semiconductors, which is possible because of the ability to tailor the band structure of these materials. As a result, the electronic and optoelectronic properties are enhanced manifold. These are basically multilayers with different band gap

on either side of each interface, and therefore called as *heterostructures*. The band structure of these materials depends on the band structure of each layer and the band offsets at each interface. Such structures made of III-V binary, ternary, or tertiary compound semiconductors have more applications in the optoelectronics because of their direct band gap nature. For example, the direct band gap nature of GaAs is shown in fig. 1.2a in comparison with most famous indirect band gap semiconductor Si. The band gap of these materials can be chosen by selectively choosing the composition of different constituent elements as shown in figures 1.2b & c. [5,25]. They show very low electron effective mass (fig. 1.2d) which is revealed itself by very high electron mobility and the ionic component in the crystal binding. Crystal binding is an important difference between these III-V compound semiconductors and the elemental semiconductors. The invention of semiconductor laser and the discovery of the Gunn Effect have mobilized the researchers in this area. The hetero junctions, quantum wells and superlattices are all byproducts of this research. They play major role in the present day's electronics and optoelectronic devices [25,26].

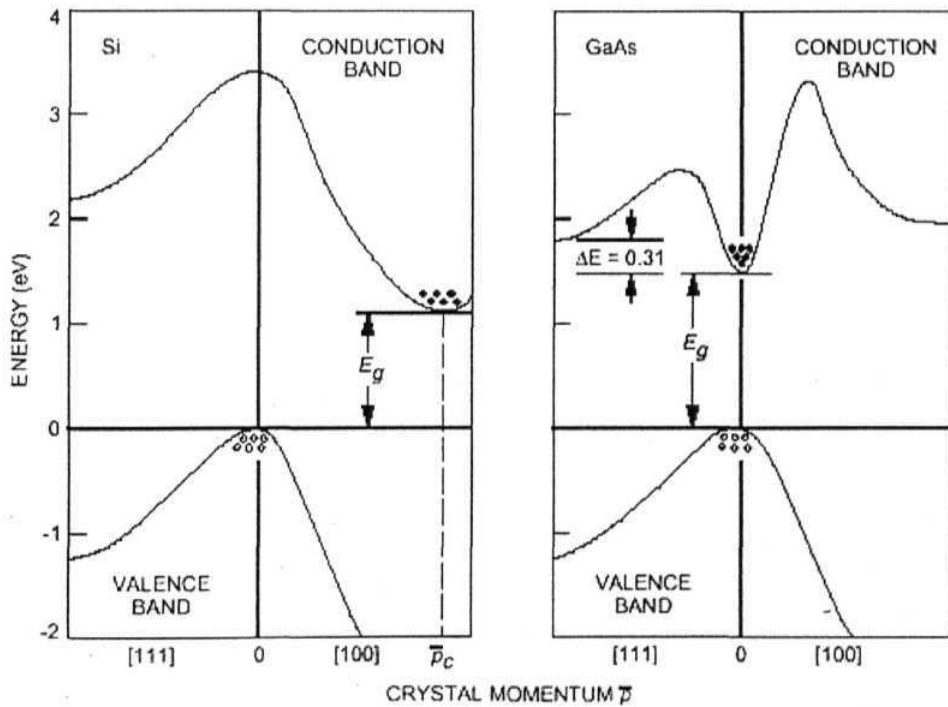


Fig. 1.2a: Simple band structure of Si and GaAS

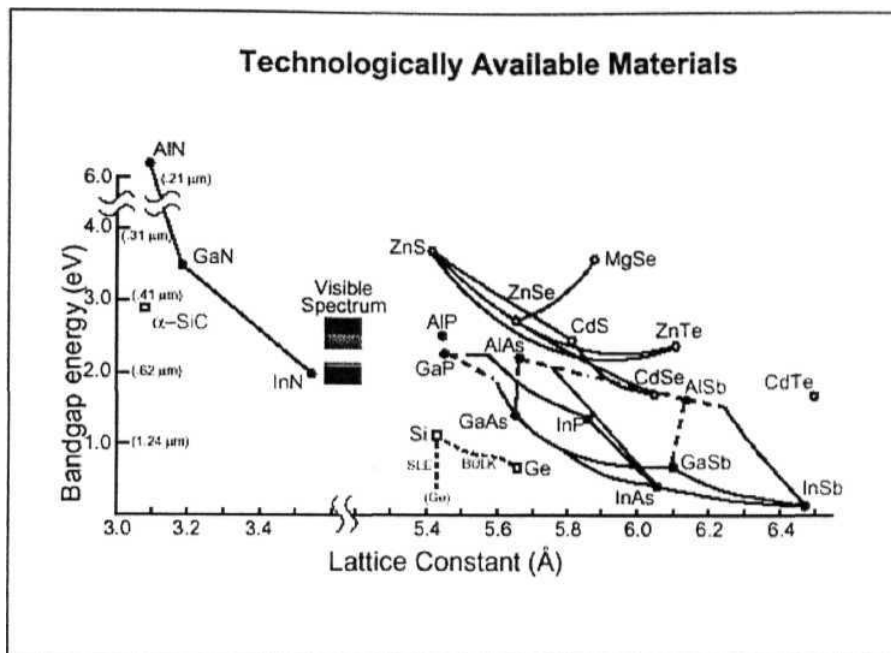


Fig. 1.2b: Band gap Vs Lattice parameter of all available compound semiconductors
(Bandgap Tailoring)

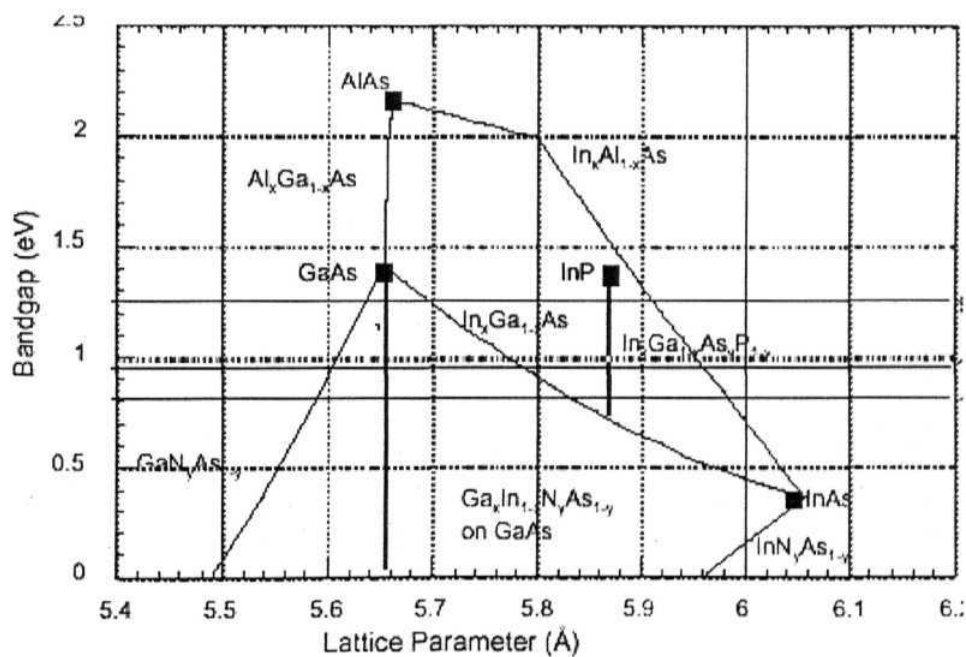


Fig. 1.2c: A part of fig. 1.2b to focus on InGaAs and InGaAsP materials
which are studied in this thesis.

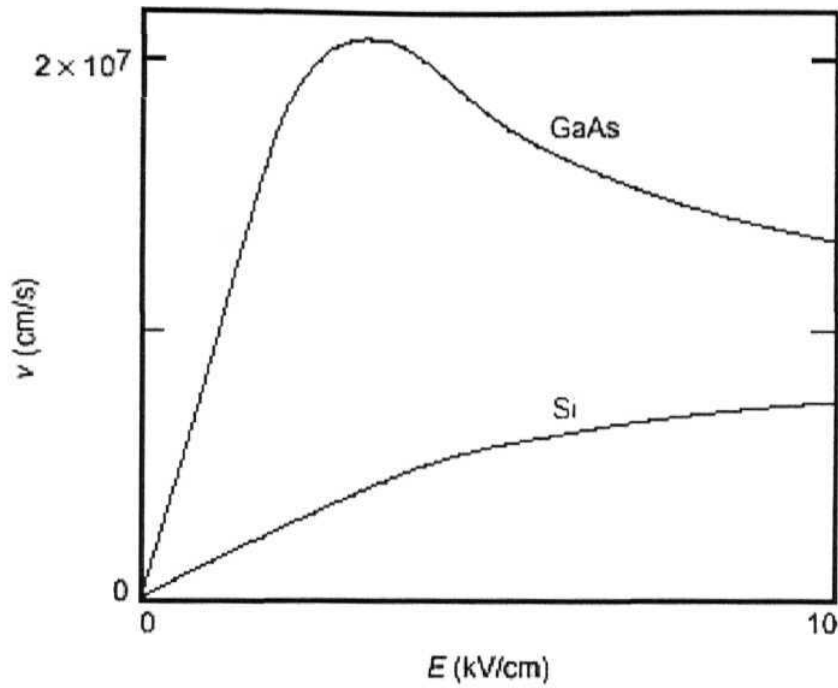


Fig. 1.2d: Electron drift velocity Vs Electric field

Fig. 1.2 (Taken from standard literature and text books)

All layers of a superlattice will have similar crystal structure and lattice parameter. Alternating layers of two materials are grown with equal layer thickness of layers of the same materials. The sum thickness of the bi-layer which is repeated to make a superlattice is called as the period of the superlattice. The name superlattice is referred to this extra manmade symmetry in the growth direction. This symmetry is reflected in many experiments like X-ray diffraction (a superlattice interference pattern is commonly observed for example see Fig. 4.4). Multi-layer with small lattice mismatch leading to compressive or tensile strain in the alternating layers is called Strained Layer Superlattice (SLS). With the advent of epitaxial growth techniques like Molecular Beam Epitaxy (MBE) [27] and Organo Metal Vapor Phase Epitaxy (OMVPE) [28], it is possible to grow crystals with monolayer precision, maintaining the crystalline quality to a very high accuracy. Atoms deposited on a substrate take positions corresponding to the potential

minima of the lattice sites. Hence in the strained-layer epitaxy, despite the difference in substrate and deposit lattice parameters, deposit atoms are constrained to the substrate interatomic spacing in the plane of the interface as shown in fig. 1.3. Corresponding change occurs in the perpendicular lattice parameter due to the Poisson effect (fig1.3). The strain in the epilayer due to the tetragonal distortion improves the device performance and is a parameter for tailoring the device performance [24]. The strain energy increases with increase in thickness of the epilayers and beyond a critical thickness, the strain relaxes to generate misfit dislocations (fig. 1.3) which deteriorate the device properties.

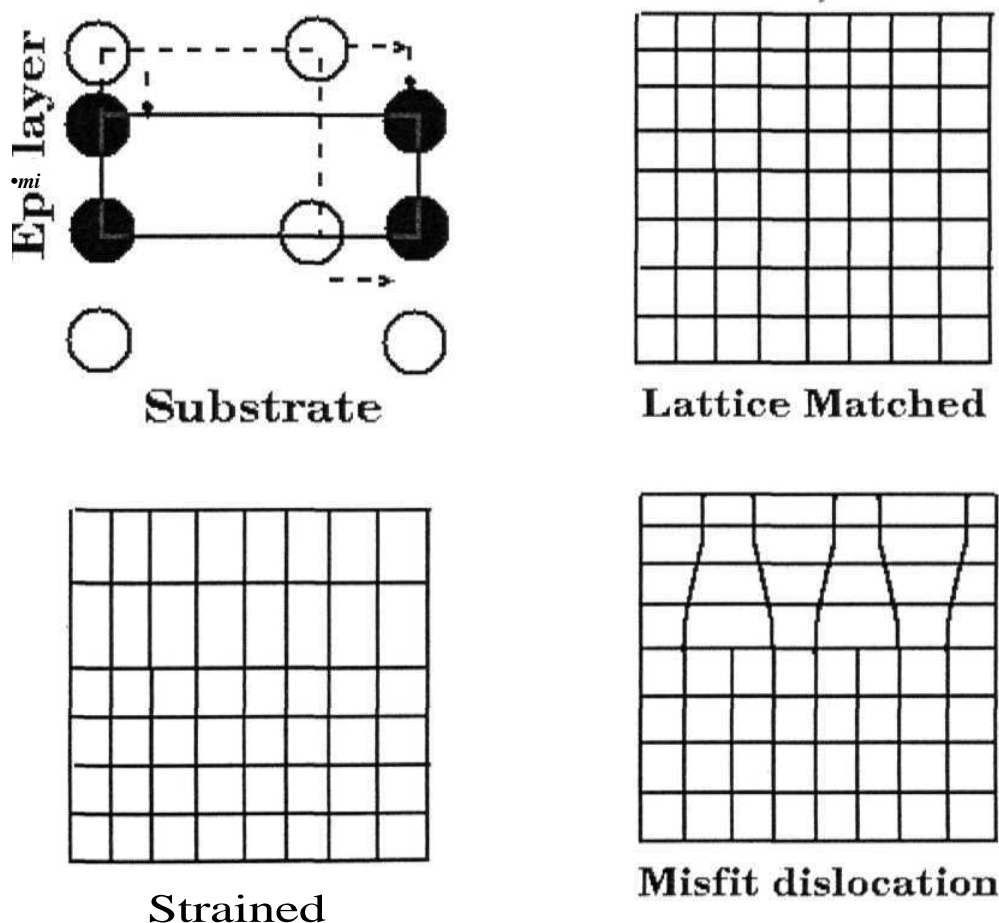


Fig. 1.3: Growth process and conceptual diagrams to describe SLS

Strained layers offer the ability to select an alternative energy band structure for applications to various semiconductor devices which is not possible by lattice matched

systems. Band gap increases with compressive strain, hence it is possible to achieve new range of band gaps. The strain across the interface increases the valence or conduction band offsets which allow more electrons or holes to be accumulated in the two dimensional electron gas. This increases both the speed and current drive of the devices that are made by SLS such as MODFET²s, HBT¹s. The emitter efficiency of HBT can be improved by using strained layer hetero junction as base emitter junction. Presence of strain lifts the cubic symmetry of unit cell which reflects on the band structure of the material. The degeneracy in the valence band at $k=0$ point will be lifted by this effect. Hence heavy hole and light hole bands will be split into two separate bands by decreasing the density of holes at the valence band maximum. This will reduce the required threshold current of strained quantum well lasers. Hence this splitting in the valence band has been used in improving the emission properties of quantum well lasers.

Spatial bandgap tuning of SLS (or any heterostructure) is important because the integration of photonic circuits demand different optical bandgaps for different devices. Meeting such band gap requirements is quite difficult during the growth. Hence the alternative way is to alter the bandgap after growing the structures. Compositional disordering and mixing at the interface by ion implantation and subsequent thermal annealing is normailly employed [29-31]. This intermixing can be achieved by swift heavy ions, which alter the strain [16,17]. It will be useful in engineering the strain at the interface. These details are discussed in detail with specific reference to current state of art in chapter 4.

Both, the lattice matched and coherently grown strained systems have their own applications. The strain produced in SLS is a parameter for tailoring the device performance. Therefore the strain measurements and modification are of great interest. We have studied such effects in strained $\text{In}_x\text{Ga}_{1-x}\text{As}/\text{GaAs}$ and lattice matched $\text{In}_{0.43}\text{Ga}_{0.57}\text{As}/\text{InP}$ systems. All these results will be discussed in detail in the following chapters.

1.4 ION BEAM CHARACTERIZATION TECHNIQUES

The use of ion beam techniques for materials analysis [32-34] is another but an important aspect of ions in materials. Energetic charged particles have been used to probe over a wide range of distances from a Fermi in Nuclear Physics (NP) to orders of Angstroms in Condensed Matter (CM). The atomic structure was probed using alpha particles, early last century and ever since the energetic particles have been used extensively as probes in CM, NP and Atomic Physics. During last 3 to 4 decades even other particles like electrons, positrons, protons and heavy ions have been used for these studies. The properties probed are as wide ranging as electronic process, lattice properties, radiation damage and more recently the strain produced due to lattice mismatch in multi layers and quantum well structures.

Ion beams are used for compositional analysis and the depth profiling of different materials [32-34]. They are used for determining the crystalline quality of single crystals and epitaxial films. Ion beams are used extensively to diagnose the presence and nature of different types of defects and strains. The non-destructive nature of ion beam analysis is a key positive feature as compared to other techniques like SIMS³, TEM² etc. There is a possibility of radiation damage or materials modification (IBM) in the sample by irradiation during the ion beam analysis (IBA) but one can take proper care while choosing ion-target combination to avoid /reduce such effects to a negligible level. One can also use the combination of both IBM and IBA for online monitoring of IBM as discussed in the introduction.

1.4.1 RBS and ERDA

Rutherford Backscattering Spectroscopy (*RBS*) [32-34] and Elastic Recoil Detection Analysis (*ERDA*) [34-38] are two powerful and complementary techniques to determine the thickness, composition, defect densities and strains. These are well established and well used techniques in Ion beam analysis [34]. In RBS, a few MeV He

or other light ions are made incident on the sample and the scattered particles are detected at back angle. The energy of the back scattered particles depends on the mass of the scatterer and the depth at which the scattering took place. Therefore it allows the determination of the masses in the sample and their distribution inside the sample. The scattering yield gives a measure of the atomic concentration of each target element. RBS has poor sensitivity for light elements especially lighter than the substrate. The sensitivity of RBS is overcome by its complimentary technique ERDA where the recoils emerging from a tilted target sample are detected in forward direction at an angle larger than the tilt angle. Instead of light particles, heavier projectiles are employed from heavy ion accelerators. Scattered ions and unwanted heavy recoils will be stopped in a stopping foil placed in front of the detector.

1.4.1.1 Kinematics of RBS & ERDA

RBS and ERDA are governed by simple elastic collisions between the projectile and the target atom. So the kinematics can be obtained using conservation principles (both conservation of energy and momentum). Fig.(1.4) shows the schematic diagram of the basic kinematics involved in these two processes. Part of the incident particle energy will be transferred to the target atom depending on its mass and provides the signature of target atom. The ratio of the scattered/recoiled particle energy to that of the incident particle is defined as kinematic factor. These kinematic factors obtained from conservation principles are given by

$$K_{rbs} = \frac{E_s}{E_p} = \left[\frac{(M_t^2 - M_p^2 \sin^2 \theta)^{1/2} + M_p \cos \theta}{M_p + M_t} \right]^2 \quad 1.1$$

and

$$K_{erda} = \frac{E_r}{E_p} = \frac{4M_p M_t}{(M_p + M_t)^2} \cos^2 \phi \quad 1.2$$

³ Secondary Ion Mass Spectroscopy (SIMS) and Transmission Electron Microscope (TEM)

Where M_1 and M_2 are masses of projectile and target atom; E_p , E_s and E_r are the projectile, scattered and recoiled energies respectively. θ is scattering angle and ϕ is recoil angle which are actually detector angles in respective experiments. Since we know the incident beam parameters and detector angle we can calculate M_2 if we can measure E_s (eq 1.1) or E_r experimentally. Radiation detectors are generally used to measure these energy values [2]. For example such an experiment on an ultra thin film gives different peaks on the energy axis (scatter/recoil) corresponding to different elements in the film. Higher mass will have maximum energy and vice versa. Hence one can identify the constituent elements of a given target material. This capability of RBS/ERDA has been exploited very well by researchers and industries.

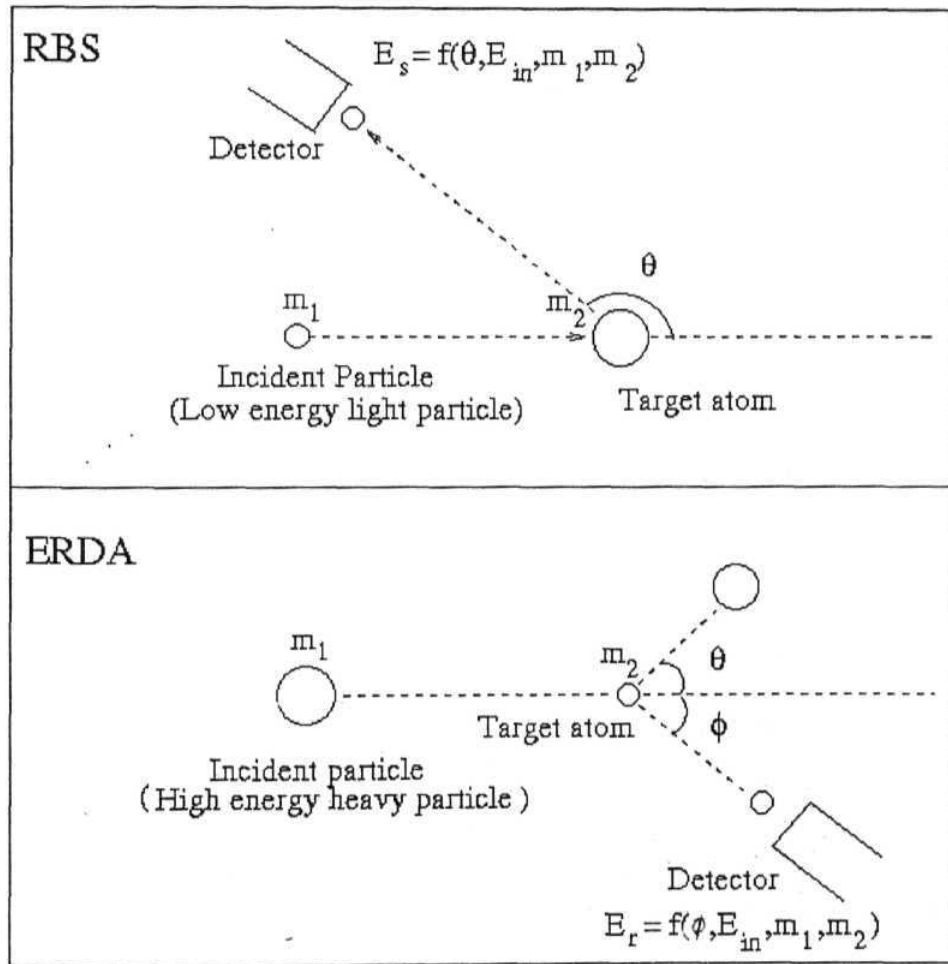


Fig. 1.4: Kinematics of BRS and ERDA

1.4.1.2 Compositional analysis

The identity of target atom is established by the energy of the scattered particle after an elastic collision. The number N_s of target atoms per unit area (areal atomic density) is determined by the probability of a collision between the incident particles and target atoms using the simple formula

Where Y is the yield (total number of detected particles), Ω is detector solid angle⁴, Q is fluence (total number of incident particles per unit area), and σ is scattering cross-section (a function of θ in RBS and ϕ in ERDA). Scattering cross-section is defined as the likelihood of a collision and is given by

$$\sigma(\theta) = \sigma(\phi) = \frac{1}{\Omega} \int_{\Omega} \frac{d\sigma}{d\Omega} d\Omega \quad 1.4$$

where the differential cross-section $d\sigma/d\Omega$ is given by

$$\left(\frac{d\sigma}{d\Omega} \right)_{rbs} = \left(\frac{Z_1 Z_2 e^2}{4E} \right)^2 \frac{4}{\sin^4 \theta} \frac{\left\{ \cos \theta + \left[1 - \left\{ (M_p / M_t) \sin \theta \right\}^2 \right]^{1/2} \right\}}{\left[1 - \left\{ (M_p / M_t) \sin \theta \right\}^2 \right]^{1/2}} \quad 1.5$$

and

$$\left(\frac{d\sigma}{d\Omega} \right)_{erda} = \left[\frac{Z_p Z_t e^2 (M_p + M_t)}{2E_p M_t} \right]^2 \frac{1}{\cos^3 \phi} \quad 1.6$$

The area of the peak corresponding to an element in the (RBS/ERDA) spectrum is a measure of N_s . Absolute concentration of any particular element can be obtained if we can calculate the exact cross-section values or by comparing the result with a standard calibration sample (with known composition). However relative compositions of different elements can easily be obtained and hence the stoichiometry of a sample can be determined using these methods.

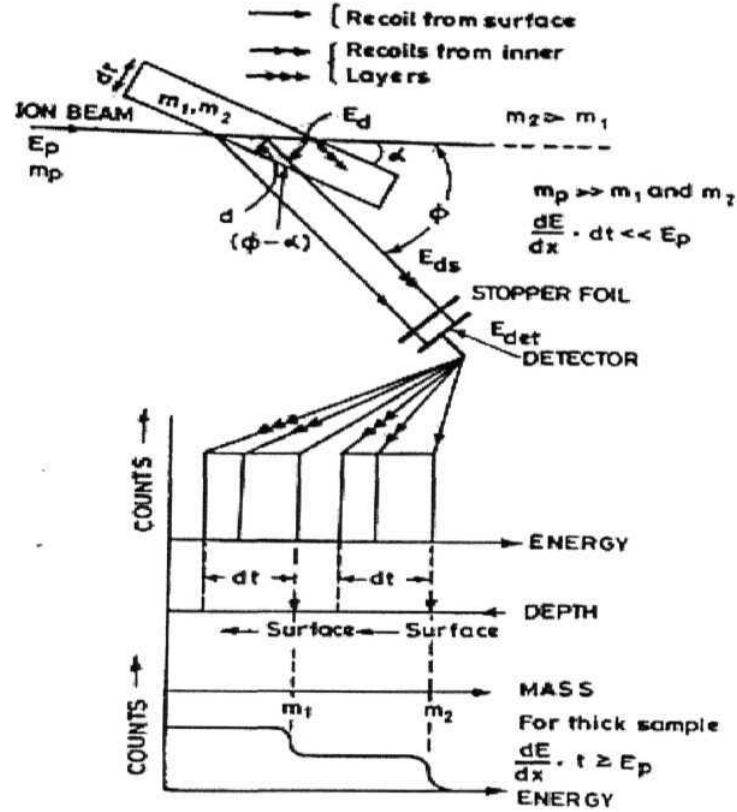


Fig. 1.5: Experimental setup, ERDA kinematics & depth profiling
 in case of thick samples (taken from Ref. [38])

1.4.1.3 Depth Profiling

The above given concepts are applicable only if the film is too thin or the signal is corresponding to near surface region. If scattering takes place underneath the sample surface then scattered energy is less than that of a particle scattered from same element but on the surface. This is because the incident particle loses its energy while traversing inside the sample and similarly the scattered/recoiled particle will also lose its energy while coming out of the sample. Hence detected energy is less than the actual expected value. This is inherently carrying information regarding the depth at which scattering took place. Depth scale can be generated if we know the stopping powers of incident and

⁴ Detector solid angle is defined as a ratio of detector opening area (active) to the distance between the target and detector.

detected particles in the given target material. Fig.(1.5) shows typical experimental geometry of an ERDA experiment used for depth profiling. It also shows the method to generate depth scale of different constituent elements. This will also affect the scattering cross-section because scattering cross-section is a function of projectile energy. Hence one has to consider the corresponding increase in the yield in compositional analysis in case of thick targets. Well established programs like RUMP [39] are available to generate such depth scales. Similar program for ERDA has been developed at NSC and was used for simulating and analyzing ERDA experiments and data respectively. RBS data has been analyzed with RUMP simulation code. Explicit formulas for generating depth scales and for calculating depth resolutions are given in refs. [2-4].

1.4.1.4 Large solid angle detection

Large solid angle detection is desirable so as to improve the sensitivity of the technique. It will improve the statistics and hence the sensitivity. This is very important requirement in ERDA experiments because heavy ions are bombarded on the sample during the ERDA experiment. Large solid angle is used to reduce/avoid the radiation damage by reducing detection time and thereby the irradiation time. However it has an adverse effect in terms of the resolution of the technique. Large solid angle implies a large detector acceptance ($\delta\phi$) allowing an angular spread ($\phi - \delta\phi$ to $\phi + \delta\phi$) instead of a single recoil angle (ϕ). This introduces broadening in the energy signal and hence deteriorates the depth resolution of the measurements. In the case of ERDA the recoil energy being a function of ϕ ($E(\phi) = K\cos^2\phi$) will have a spread $[dE(\phi)/E(\phi)]$ of $-2\tan\phi d\phi$.

This problem can be addressed by using a position sensitive detector which not only detects the energy but also the angular information ($d\phi$) of recoils. The correction to this kinematic broadening known as kinematic correction can be implemented with this information. Detected energy is to be multiplied by $\cos^2\phi$ and then normalized by $\cos^2(\phi \pm \delta\phi)$ to avoid such kinematic errors. Assmann *et al.* [40] demonstrated the use of such a large area position sensitive detector with the position sensitive feature in ERDA.

The advantage of such a scheme was to increase the sensitivity without compromising the depth resolution. It became so popular that other accelerator laboratories including NSC having high energy heavy ions developed similar detectors [41-43]. Such a detector has been fabricated and kinematic corrections have been implemented in this thesis work [43]. Further details and references are given in chapter 3.

1.4.1.5 *Special features of ERDA*

The above mentioned methods are suitable when the elements to be detected (for determination of concentration) are well separated in mass. If there are elements in the sample which have neighboring masses, the recoil/scattering energies overlap and it becomes difficult to distinguish such elements in the sample. It is a severe problem in the case of thick targets as shown in fig.(1.5). In such situation ERDA has an inherent advantage in contrast to RBS. In RBS the scattered incident particle is detected all the time i.e same particle but with different energy is detected corresponding to all constituent elements but in ERDA different particles are detected as a signature of different constituent elements. The target atom itself will be recoiled indicating its presence in the sample. Hence one can selectively detect any required species independently using mass (or Z) separation methods like magnetic spectrometers. One can also separate such recoils by measuring the flight time of recoils because different masses will have different velocities. Similarly one can measure the energy loss (which is proportional to MZ^2/E) in a thin detector of known material to separate such neighboring masses. This concept is used in telescope detectors. This particular feature of detecting different species is an intrinsic advantage of ERDA when compared to RBS and made ERDA more versatile and accurate technique.

1.4.1.6 *ERDA with telescope detectors*

ERDA is made powerful by combining it with other particle identification techniques to discriminate different elements. Most commonly used techniques are time of flight (TOF) [44,45] spectrometer, *DE-E* detector telescope [46,47], magnetic

spectrograph [48,49] and Bragg curve spectrometer (BCS) [50,51]. TOF is best suited for low recoil energies but has the disadvantage of low detection efficiency for hydrogen and other lighter mass elements. TOF setups use micro channel plates for timing signals, which are fragile and require careful handling and good vacuum conditions. BCS uses relatively simple detector electronics but an additional detector is necessary if position sensitivity is desired. Also, detection of H is difficult with this technique. A magnetic spectrograph requires huge magnets and space for the same. It is expensive as well, but it provides the best possible resolution and is a good choice. Considering all this, the use of detector telescopes is an ideal choice for identifying neighboring mass elements with good depth resolution. Such a set up can be designed and fabricated indigenously as per the requirement. As mentioned above, Telescope detectors consist of two detectors. First one is used in transmission mode so that the recoils going through lose a fraction AE of their energy. Rest of the energy $E_{\text{rest}} = E - AE$ is deposited in the second detector, which has such a **thickness** that the recoils get stopped in it. The recoil energies have to be high enough to overcome the detector entrance window and the transmission type AE detector. The energy lost, AE in the first detector, depends on the atomic number and the mass of the recoil. Thus the energy lost by the recoils of different elements having almost identical energies is different and can be used to identify the atomic number (Z) of recoil. Total energy is obtained by adding the energies AE and E_{rest} obtained from the first and second detector after proper calibration of the electronic gains in the two detectors. Plots drawn between AE and E , known as E - AE spectrum will have separate bands for each element. These detectors are called as E - AE telescopic detectors. There are different possible configurations for telescope detectors. Using a transmission type thin solid state detector as AE detector and thick solid state detector as E_{rest} detector is one of the choices. The use of a gaseous detector for AE is another choice coupled to a solid state detector as the E_{rest} detector. The third choice is using the gaseous detector for both the AE and E_{rest} measurements. The main advantage of the gaseous type detectors is that these are insensitive to radiation damage, rugged and can be fabricated indigenously. On the other hand, the solid state detectors are prone to radiation damage, besides being fragile (especially AE detectors) and are expensive. A gaseous Large Area two dimensional

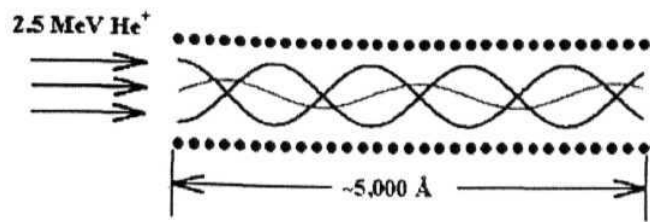
Position Sensitive AE - E Detector Telescope (LAPSDT) has been fabricated as a part of the thesis work [43]. The design and development of this detector are given in chapter 3.

1.4.2 Ion Channeling & Blocking

1.4.2.1 The channeling (blocking) effect

Initially, the scattering process discussed above is believed to be independent of the sample orientation and hence scattering formulae did not consider any of such information. Later on strong orientation effects were observed while performing sputtering studies on a single crystal material [52]. This special effect observed in single crystals is named as channeling effect. When the incident ion beam is directed along a high-symmetry crystal direction, then it will undergo a correlated series of small angle gentle scatterings as shown in fig.(1.6), a phenomenon known as *channeling* [1, 32,33 & 52-56]. The yield of close impact parameter events like RBS, ERDA or Inner Shell excitation is reduced drastically under this channeling condition

Channeling measurements can be made by measuring the incident angle dependence of yield. These angle Vs yield plots, known as angular scans, can be used to map the crystal planes and/or axes. Angular scans define many structural properties and deformations of the crystal. The Full Width at Half Maximum (FWHM) of this scan defines the channeling critical angle below which channeling occurs. χ_{\min} which is the ratio of the backscattered or recoiled yield when aligned (Y_A) to a crystallographic axis to that of the random (Y_R) condition (i.e., $\chi_{\min} = Y_A/Y_R$) is a measure of the crystalline quality of the sample. The use of ion channeling in conjunction with RBS/ERDA provides a measure of the crystalline quality as a function of depth. Channeling is sensitive to lattice defects (or disorder) and has been enormously used to study many types of defects exist in crystals [52,53].



Ion channeling distinguishes between directions in a crystal

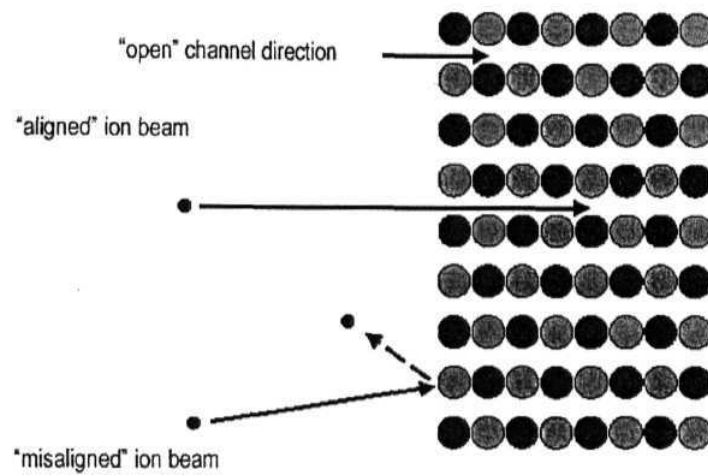


Fig. 1.6a: Channeling phenomenon

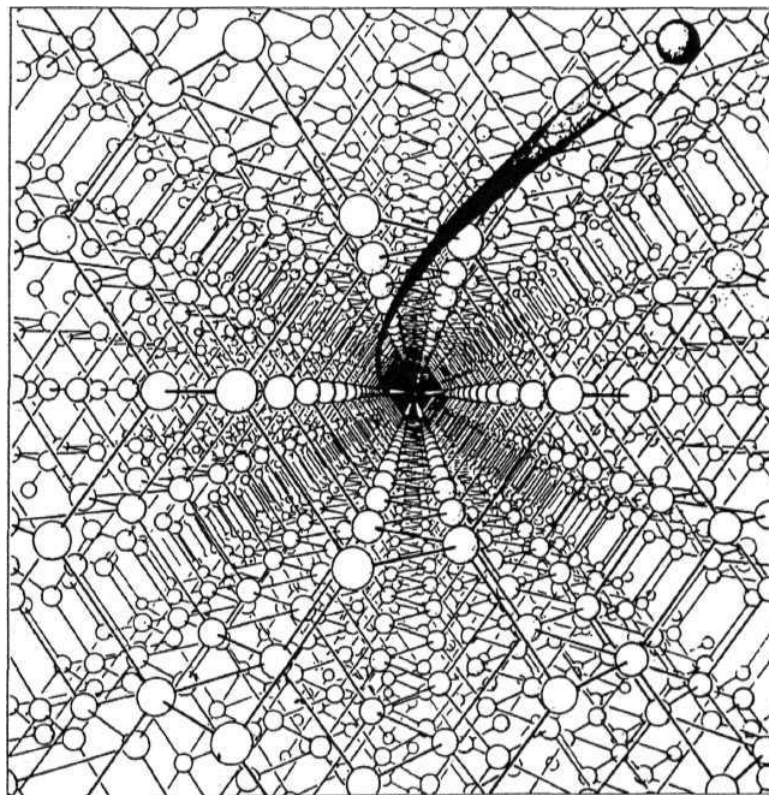


Fig. 1.6b: Axial channeling along Si $\langle 110 \rangle$

Similarly particles that are originated within the crystal and are emerging out will be blocked in the directions of crystal axes or planes a phenomenon is known as blocking (or blocking effect) [54]. Lindhard suggested and proposed [56] that the blocking effect is a time reversal of channeling effect and all results obtained from both the techniques should be identical. Scattered particles in RBS and recoils in ERDA are originated within the crystal and will experience blocking effect. Hence recoil/scattering yield from such targets is not isotropic in the space and patterns equivalent to those in transmission channeling can be seen using a two dimensional position sensitive detector. Blocking effect has long been used in nuclear lifetime measurements [57]. Karyaman [58] first demonstrated the explicit use of Blocking/ERDA in material characterization. ERDA/blocking has recently been used to monitor the online radiation damage [59] and has major applications in performing controlled modification experiments.

1.4.2.3 *Channeling theory*

When single crystals are bombarded with charged particles along one of their major crystallographic directions or planes, they travel longer distances in the crystal than their ranges predicted by simple stopping power theories like Bethe-Bloch formula [56,1,2]. When a charged particle moves along some directions (around axes or planes), under certain conditions it may not be able to feel the interaction due to individual atoms sitting along particular axial or planar direction, so that the moving particle experiences only continuum strings or planes. The condition for this to happen has been derived by Lindhard [56] and Erginsoy [60] in an analysis based on the idea that the particle velocity component parallel to the axial or planar direction is such that the time of flight to cross one lattice spacing is less than the collision time with any individual target atom. This implies that before the particles feels presence of one atom, it is already in the field of next atom along the same direction. It will see only *continuum potential* instead of individual atom field. This model is called *Lindhard's continuum model*

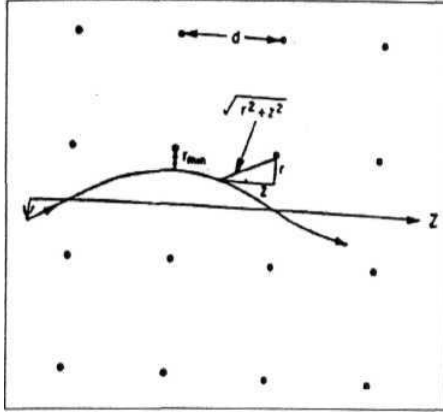


Fig. 1.7a: Axial case

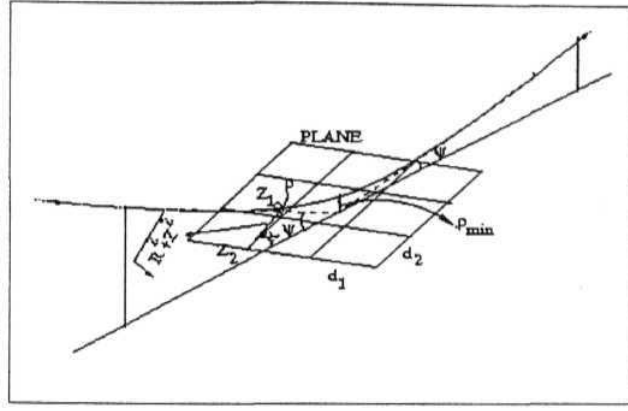


Fig. 1.7b: Planar case

Fig. 1.7: Channeling conditions & Continuum model (geometry)

Mathematically the above-mentioned continuum condition can be written as

$$\frac{r_{\min}}{v \sin \psi} > \frac{d}{v \cos \psi} \quad 1.7$$

Where ψ is the incident angle that the incident particle moving with the velocity v makes with the channel axis, r_{\min} is the minimum distance of approach to the string and d is the interatomic spacing along the axis. This is depicted in fig.(1.7) for both axial and planar cases. According to the continuum approximation, r_{\min} is determined by equating the repulsive interaction due to the continuum string with the transverse kinetic energy, the effect of other strings being negligible when the ion is approaching one of them. The continuum potential $U(r)$ is obtained by averaging the interatomic potential along the string within the framework of simple superposition principle and one gets,

$$U(r) = \int_{-\infty}^{\infty} \frac{dz}{d} V(\sqrt{z^2 + r^2}) \quad 1.8$$

where r is the distance from the strings and $V(R)$ is the interaction potential. For Lindhard standard potential

$$V_{Li}(R) = Z_1 Z_2 e^2 \left[\frac{1}{R} - \frac{1}{\sqrt{R^2 + C^2 a^2}} \right] \quad 1.9$$

Where R is the interatomic distance, $C = (3)^{1/2}$ is the Lindhard constant and a is the Thomas-Fermi screening radius. Substituting this form of interatomic potential in eq. (1.8) one gets

$$U(r) = \frac{Z_1 Z_2 e^2}{d} \ln \left[\left(\frac{Ca}{r} \right)^2 + 1 \right] \quad 1.10$$

The accurate value of r_{min} can be obtained under the small r conditions of the above equation because the particle will be able to go much closer to the string. This equation together with the eq (1.7) gives the range of validity of continuum approximation as follows.

$$\psi < \psi_1 = \sqrt{2Z_1 Z_2 e^2 / dE} \quad \text{for energies } E > E_1 = 2Z_1 Z_2 e^2 d / a^2 \quad 1.11$$

and

$$\psi < \psi_2 = \sqrt{Ca\psi_1 / d\sqrt{2}} \quad \text{for lower energies } E < E_1 \quad 1.12$$

Ψ_1 and Ψ_2 are then the critical angles for channeling in these energy regions. For the planar case, the continuum potential can be obtained by averaging over the particular plane and the corresponding critical angle can be derived as

$$\psi_p = \sqrt{2\pi N_p Z_1 Z_2 e^2 a / E} \quad 1.13$$

Apart from the Lindhard interatomic potential many other interatomic potentials were derived by several authors [61-63]. Suitable interatomic potentials are used depending on the problem and experimental conditions. Quantum mechanical approach with relativistic considerations is necessary for describing the channeling of light energetic particles like electrons and positrons [64-68]. Chapter 6 deals with such theory of light relativistic

particle channeling and the corresponding radiation called channeling radiation. This theory has implications to the effects of strains in semiconductor multi-layers. However the present theory is applicable to all experimental work that is presented here in this thesis.

1.4.2.3 Channeling half angles and minimum yields

1.4.2.3.1 Channeling half angles ($\Psi_{1/2}$)

Critical angles discussed above cannot be directly measured experimentally. It is because the above mentioned theories assume perfect crystal structures and they do not consider the thermal vibrations of the lattice atoms. In addition to this, the effect of the screening offered by the electron cloud to the projectile has also not been considered. Channeling half angle ($\Psi_{1/2}$) is actually measured during the experiment. $\Psi_{1/2}$ is defined as the FWHM of the channeling angular scans. Relations between this $\Psi_{1/2}$ and the above discussed critical angles are given in standard refs. like [33,34 & 69,70] as follows. Monte Carlo simulations are also available [70,71] to estimate these important parameters.

For axial case (if $\Psi_1 > a/d$)

$$\psi_{\frac{1}{2}} = 0.8 F_{RS}(\xi) \psi_1 \quad 1.14$$

Where $\xi = 1.2 u_1/a$ with the thermal vibration amplitude u_1 . F_{RS} is square root of adimensional string potential using Moliere's screening function. u_1 and ξ Vs F_{RS} values are given in a Gemmel's famous review article [54] for different ion-target combinations.

For axial case (if $\Psi_1 < a/d$) (neglecting the thermal vibrations)

$$\psi_{\frac{1}{2}} = 7.57 \left[\frac{a}{d} \psi_1 \right]^{\frac{1}{2}} \quad 1.15$$

For planar case

$$\psi_{\frac{1}{2}} = 0.72 F_{PS}(\xi, \eta) \psi_p \quad 1.16$$

where $\xi = 1.6 u_1/a$, and $\eta = (\text{inter planar spacing } d_p)/a$ and the $F_{PS}(\xi, \eta)$, the square root of adimensional planar potential using Moliere's screening function, values are available in the review article [54]. These half angle values are comparable with the actual experimental results.

1.4.2.3.2 *Minimum yield (χ_{min})*

Being a measure of the crystalline quality χ_{min} is an important quantity to estimate and compare with the experiment. Best fit expressions to χ_{min} are given as follows (either obtained from continuum theory or obtained empirically).

$$(\chi_{min})_{axial} = 18.8 N d u_1^2 (1 + \xi^{-2})^{\frac{1}{2}} \text{ if } \Psi_{1/2} > u_1/d \quad 1.17$$

$$= 18.8 N d u_1^2 \text{ if } \Psi_{1/2} << u_1/d \quad 1.18$$

and

$$(\chi_{min})_{planar} = \frac{2a}{d_p} \quad 1.19$$

where $\xi = 126 u_1 / (\Psi_{1/2} d)$; $\Psi_{1/2}$ given in degrees.

1.4.2.3.3 *Special note for diatomic crystals*

All the above mentioned formulae are used for diatomic crystals (GaAs.) in the present work. In this case of diatomic crystal one has to use the average atomic numbers and lattice spacing along the rows and planes of interest ($\langle 110 \rangle$ in our case). Suitable multiplication factors are given in ref. [54] to obtain d or d_p from crystal lattice parameter. In these structures some of the rows will have mixed effects with mixed atoms

on the axes or planes. On the other hand they may be mono atomic in which case each of the mono atomic axis or plane has separate critical angle.

1.4.2.4 *Applications of channeling*

The above discussed theory is valid only if the crystal is perfect one. In fact, no crystal is perfect in real life. Some intrinsic defects are always present in actual crystals. In addition to this some defects are generated using ion implantation / irradiation performed for modern semiconductor device applications. The isolated potential introduced by any defects (or defect clusters) present in crystal violates the continuum potential offered by perfect crystal planes or axes and there by cause dechanneling. Hence understanding of this dechanneling mechanism is essential prerequisite to characterize these defects. It is important to know the sensitivity of the channeled particles (channelons) to different types of defects present in the solids. For example if the projectile directly hits the defect encountered along its trajectory (or scatters in the potential by this defect) then the trajectory is modified and particle gets dechanneled. Such effects are called obstruction type [64]. Examples are stacking faults, interstitial atoms, grains or twin boundaries. On the other hand if the defect gives raise to distortion in a certain region of the crystal, disturbing the regularity of the material in that region then the particle trajectory modification appears on the extent of distortion, which depends on the distance from the core of the defect [72]. Such dechanneling is called as distortion type. Most important example is the dislocation. These extended defects are well characterized by dechanneling studies [73]. Suitable theory is developed to estimate the type and densities of different defects from the dechanneling data [63-75]. Identification of different defects and mapping their coordinates within the crystal is also possible by these techniques [55].

1.4.2.4.1 Point Defects

Simple RBS analysis gives the depth distribution of different elements in a given target material. This information can be used to identify the presence of any foreign

atoms. This technique combined with the channeling has been used to map the location of these defects [33,34,55]. When the impurity is situated on the regular site then it will not have any effect on the channeling. However when it is located at an interstitial site then it may obstruct the channeled particles in some crystallographic directions. Thus by measuring the minimum yield in different orientations one determines the coordinates of the defect. The theoretical description of these defects is based on the assumption that the dechanneling is caused by Rutherford scattering of projectile with the impurity atoms. The dechanneling probability (cross-section) from these theories has the $E^{-1/2}$ dependence [1,76]. Hence by measuring the energy dependence of dechanneling cross-section, one confirms the presence of interstitials. This knowledge combined with the RBS data gives information on type and concentration of point defects present in a crystal. Their depth distribution and in fact the location is uniquely determined. Hence channeling technique combined with RBS has important applications in the development of the modern advanced materials.

1.4.2.4.2 Stacking faults

A stacking fault is another good example of obstruction without any distortion. At the stacking fault the potential valleys present on one side are obstructed by the potential hills present on the other side. When a channelon hits a stacking fault, its transverse energy is changed by ΔV and there is a critical value of ΔV corresponding to two critical positions in the channel, for which the change in transverse energy is sufficient to get dechanneled. The dechanneling probability is then the probability of channelons occupying a position between these two critical positions. The total dechanneling probability is then obtained by taking into the account of all possible values of the transverse energy. Dechanneling probability obtained from these calculations is found to be independent of the incident energy [73]. Hence once again by performing the energy dependence experiments one can verify the presence of stacking fault in any material. Similar theory is developed for the dechanneling of light relativistic particles also [64]. Several experiments have been performed to characterize such obstruction effects on the channeling [77].

1.4.2.4.3 Distortion effects

The most important example of defects that produce the distortion in the channels is the dislocation. Around the dislocation, the atomic rows and planes exhibit curvature, which will alter the trajectory of the channelon. As is well known from the dislocation theory [78], this distortion is maximum near the dislocation core and decreases as one moves away from the core. Thus one can think of a cylindrical region around the dislocation axis, the so called "dechanneling cylinder" [72,79] within the distortion is large enough for most of the particles to get dechanneled. In the region outside this cylinder the distortion is not enough for dechanneling to occur, although even here the amplitude of the channelons changes. The dechanneling cross-section is linear with E and for higher energies and/or heavy ions this is proportional to $E^{1/2}$ [1]. Hence once again by performing the energy dependent studies one can characterize dislocations. These concepts are in fact directly applicable to recently observed nanotube channeling [80]. This is very recent and interesting phenomenon which can be explained with the concepts proposed in late seventies [72]. Quantum mechanical calculations are made for the case of light relativistic particles [65,66].

1.4.2.4.3 Application to SLS

The strain in SLS has a significant role in tuning the important devices properties for example like bandgap, band offsets etc.. Hence it is important to measure the accurate value of the strain. On the other hand misfit dislocations generated beyond the critical thickness deteriorate the device performance. Presence of any such dislocations / obstructions can be identified by the dechanneling studies discussed above. Simple RBS can be applied to measure the exact thickness and elemental composition of different layers of SLS. The strain induced tilt in the off-normal axis can also be measured by channeling experiments. Hence RBS/Channeling can be readily applied to characterize these advanced materials [81,82]. These details are discussed in the following section.

1.4.3 Ion beam methods to probe strains in SLS

Osborn [83] gave the first theoretical approach to understand the electronic properties of SLS. Matthews *et al.* [84] and People *et al.* [85] developed two different theories to estimate the critical thickness and to understand the strain relieving phenomenon. The results of these theories are not very much consistent with each other. These phenomena are not well understood so far. Very recently Wang *et al* [86] pointed out the lack of experimental techniques to study SLS. Several optical techniques [87,88] exist to characterize SLS but ion beam techniques give direct, simple and material independent results [89]. Lot of work has been done in this field [89-97]. Kozanecki et al [94] discussed the difficulty in measuring low strains using low energy channeling. Moreover Hashimoto et al [98-100] have shown that the beamsteering effect misleads the final measurements in this low energy region. Nolte et al [101] succeeded to prove the advantage of high energy channeling/blocking -ERDA to probe strains.

Ion channeling technique has emerged as a sensitive tool to measure the strains in SLS. There are three classes of channeling measurements to determine the strain. They are dechanneling studies and a special case of dechanneling studies called as catastrophic dechanneling resonance (CDR) [102]. CDR is the most sensitive to strain, typically, strain values as low as 0.02% can be measured by carrying out CDR. CDR occurs when half wavelength $k/2$ of oscillatory motion of a planar channeled ion beam matches the path length per layer (s , also called the period of superlattice) of SLS which leads to sudden increase in the dechanneling after a certain depth. Study of this resonance gives the information on the strain present in SLS. At shallow depths, the channeled yield is similar to that for a bulk crystal, whereas after penetrating a few layers, almost all of the beam is dechanneled due to the resonance condition. Although it is a very sensitive technique but is a complicated one. In the present conditions it is difficult to perform such experiments with the infrastructure available in India. The third and simple technique is based on the channeling angular scans obtained from RBS/Channeling performed along off normal axes. This technique has been used in this work and will be described below.

Apart from these three techniques, a more sensitive method based on channeling radiation has been proposed recently to measure lattice strains [103].

Ion channeling experiments along the off-normal directions in SLS are sensitive to lattice strains because there exists a small misalignment of the channeling direction at each interface. Hence strain measurements by ion - channeling technique in multilayered structures are based on the tetragonal distortion induced in the layers, which results in the shift ($\Delta\theta$) of the dip of the channeling angular scan measured around off-normal axis. The two components of strain in tetragonal distortion are defined as

$$\epsilon_{\perp,\parallel} = \frac{a_L^{\perp,\parallel} - a_L}{a_L} = \frac{\Delta a_L^{\perp,\parallel}}{a_L} \quad 1.20$$

The suffix L indicates that the lattice parameter corresponds to the layer, which is grown in a thick substrate (L is omitted in the following text because only layer constants are used in what follows) and the superscripts distinguish between the parallel and perpendicular lattice constants. Then the tetragonal distortion ϵ_t is defined as $\epsilon_{\parallel} - \epsilon_{\perp}$. The off normal axis ($\langle 110 \rangle$ for $\langle 100 \rangle$ growth), being parallel to the diagonal of the cubic cell makes an angle θ with the sample plane. This angle can be defined in terms of lattice parameters as $\tan \theta = a_{\perp}/a_{\parallel}$. Any small change in these lattice parameters due to the strain causes a change in θ , which can be obtained by differentiating the above equation on both sides.

$$\sec^2 \theta d\theta = \frac{a_{\parallel} da_{\perp} - a_{\perp} da_{\parallel}}{a_{\parallel}^2} = \frac{a_{\perp}}{a_{\parallel}} \epsilon_t = \tan \theta \epsilon_t \quad 1.21$$

$$\Rightarrow \epsilon_t = \frac{\Delta \theta}{\sin \theta \cos \theta} \quad 1.22$$

Hence, one can estimate the strain value by mapping the off normal axis using the channeling techniques as shown in fig. 1.8. The difference between the positions of dips obtained from layer and the substrate around off normal axis gives the input $\Delta\theta$ for the above equation. The FWHM of this curve is directly related to the channeling critical angle, which varies inversely as square root of incident energy. Hence the angular scans will be sharp in high energy channeling thereby the strain resolution and the sensitivity

of the method are improved [100,101]. If the energy is too low then the results are mislead by steering effect due to the broad critical angles [98-100]. Hence high energy channeling measurements are recommended for strain measurements.

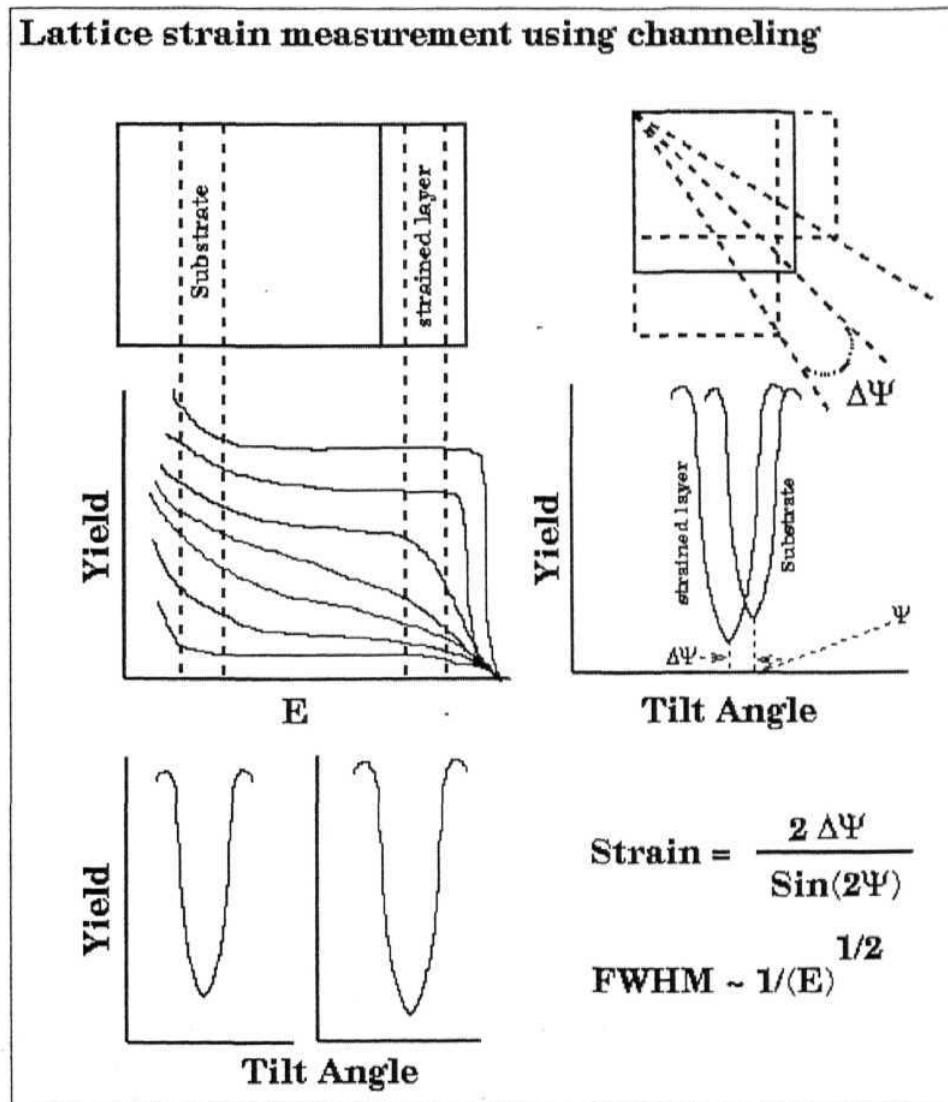


Fig. 1.8: procedure of strain measurements using ion channeling.

1.5 SIMULTANEOUS ON-LINE MODIFICATION AND MEASUREMENT OF STRAIN

The modifications in the interface have been shown in several works [104-106]. It is expected that the strain in the SLS can be altered by SHI. One such work is reported [29], where the PL peak position is shown to be shifting by SHI irradiation. It is inferred from the previous discussion that SHI can be used for measuring the strain as well as for altering the same. Normally, the fluence required for modification is an order of magnitude higher than the fluence required for the strain measurements; it is therefore, possible to measure the strain as a function of the ion fluence. Thus SHI allows on-line measurement of modification of strain. Possibilities of on-line monitoring of ion induced modifications have been demonstrated using blocking/ERDA in recent years [40]. Possibility of controlled modification using the online measurements is discussed in this thesis.

1.6 HIGH RESOLUTION X-RAY DIFFRACTION (HRXRD)

In the present work, HRXRD is used to measure the strain and quality of the samples as a complimentary technique to channeling measurements. HRXRD alone is used to study the ion beam mixing effects in some cases. In fact it is an accurate and non-destructive technique [100,107] for characterizing epitaxial films, multi layers and the interdiffusion. The strain present in the system modifies the interplanar spacing, hence HRXRD is sensitive to this tetragonal distortion. In optimum conditions it is capable of measuring the strain with a sensitivity of about 10^{-5} and a depth sensitivity of 0.1nm for highly perfect and uniform structures whereas, for single layers the minimum thickness needed for depth analysis is ~10nm. For example Figs. (4.4), shows an HRXRD pattern measured from a superlattice and Fig. (4.9) corresponds to single strained layer. The sharp and intense peak in the center corresponding to Bragg angle (for the substrate material and for particular reflection) is known as the substrate peak. The width of the peak determines the angular resolution of the measurement. A broad peak appearing on the left side to the substrate peak in fig. 4.9 corresponds to the layer i.e the thin strained

layer grown on GaAs substrate and hence is called as layer peak. The tetragonal distortion due to the presence of strain in this layer, modifies the interplanar spacing and thereby the Bragg reflection angle. Hence the layer peak got separated from the substrate peak. It appears on the left side for the compressive strain and on the right side for the tensile strain. The peak is broad and the intensity is low because it corresponds to a thin layer. The layer thickness and the composition can be estimated using the simulation programs. Figs. 4.4 shows the patterns obtained for a superlattice. The system of equi-spaced low intensity peaks around the substrate peak is due to the interference between the reflections emerging from different layers. These are called satellite peaks, a good number of satellite orders appear if the interfaces are sufficiently sharp. Here the center of the satellite system matches with the substrate peak for lattice matched samples. Hence the shift ($\Delta 0$) in the layer peak position (or the center of the satellite system) with respect to that of the substrate peak is a measure of the strain (ϵ_{\perp}). It can be easily estimated by differentiating the Bragg's law ($2d \sin\theta = n\lambda$), as $\Delta d_{\perp} / d = -\Delta\theta \cot\theta$. The superlattice period (s) of multilayers can be calculated from the interference pattern. If θ_1, θ_2 are the angular positions of two consecutive satellite orders then $s = \lambda / 2(\sin\theta_1 - \sin\theta_2)$. The reduction of the satellite intensities after irradiation represents the interdiffusion. The measured strain, composition and thickness help in understanding the mixing effects. Hence HRXRD is a suitable technique for characterizing these materials and also to study the mixing effects.

1.7 CONCLUSION

We conclude this chapter with an outline of the complete thesis work. Next chapter provides the information of the different experimental facilities/techniques that have been used in this work. Typical experimental specifications are also given. Chapter 3 presents the development of experimental facilities that have been developed as a part of this thesis work. Performance of these facilities is shown in the chapter. Results of ion beam mixing experiments to engineer the strain in SLS are given in chapter 4 with detailed discussions. Performance of the automated high energy channeling facility developed at NSC (as a part of the thesis work) and results obtained are discussed in

chapter 5. Apart from this experimental work, some theoretical models are proposed for understanding the effects of strains and defects on light relativistic particle (positron/electron) channeling and consequent channeling radiation. Channeling radiation is very sensitive to the strain/defects present in the crystal structure. However these experiments cannot be performed in India in present situation. These theoretical models are given in chapter 6. Last chapter is devoted for overall conclusions obtained from all results. Possibilities of the further work in this area are also discussed in this chapter. Hence in a sentence the complete work done under the title "Ion beam characterization and engineering of strain in semiconductor multi-layers" is presented in this thesis with suitable introduction and discussions.

1.8 REFERENCES

1. A.P. Pathak, *Rad. Eff.* 61, 1 (1982).
2. Radiation Detection and Measurement, G.K. Knoll, *Wiley and sons*, New York (1986).
3. The stopping and ranges of ions in solids, Vol. 1, J.F. Ziegler, J.P. Biersack, U. Littmark, *Pergamon publishers* (New York), 1985.
4. J.F. Ziegler, J.P. Biersack and U. Littmark, *IBM research report* RC9250 (1982).
5. Physics of Semiconductor Devices, SM Sze, *Wiley publishers*, New York (1981).
6. S.K. Ghose, D.K. Goswami, B. Rout, B.N. Dev, G. Kuri and G. Materlik, *Appl. Phys. Lett.* 79, 467 (2001) and *refs. therein*.
7. M. Milosavljevic, S.Dhar, P. Schaaf, N. Bibic, M.Han, K.-P. Lieb, *Appl. Phys. A* 71, 43(2000)
8. L. Civale, A.D. Marwick, T.K. Worthington, M.A. Kirk, J.R. Thomson, L. Krusin-Elbaum, Y. Sun, J.R. Clem and F. Holtzberg, *Phys. Rev. Lett.* 67, 648 (1991).
9. R.L. Fleischer, P.B. Price, R.M. Walker, *J. Appl Phys.* 36, 4645 (1965).
10. H. Trinkds, *Mat. Sc. Form* 248-249, 3 (1997); B. Breger, *Nucl. Instrum. Meth.* 146, 426 (1999).
11. G.S. Viridi, B.C. Pathak, D.K. Avasthi, D. Kanjilal, *Nucl. Instrum. Meth.* 181, 189 (2002).

12. U. Tiwari, N. Sen, A.K. Banddopadhyay, D. Kanjilal, P. Sen, *Euro. Phys. Lett.* 25, 705 (1994).
13. H.C. Barshilia, S. Sah, B.R. Mehta, *Thin Solid Films* 285, 265 (1995).
14. S.K. Srivastava, Ph. D Thesis submitted to Jawharlal Nehru University (Nuclear Science Centre), New Delhi (2002).
15. W. Xia, S.N. Hsu, C.C. Han, S.A. Papert, B.Zhu, C. Cozzolino, P.K.L. Yu and S.S. Lau, *Nucl. lustrum. Meth.* B59/60, 491 (1991).
16. Pathak A.P, Nageswara Rao S.V.S, Siddiqui A.M, Lakshmi G.B.V.S, Srivastava S.K, Ghosh S, Bhattacharya D, Avasthi D.K, Goswami D.K., Satyam P.V, Dev B.N and Turos A, *Nucl. Insrt. Meth.* B193, 319 (2002).
17. Ion irradiation effects and ion beam studies of semiconductor multilayers, Nageswara Rao S.V.S, Pathak A.P, Avasthi D.K, Muralidharan R, Tiwari U, Srinivasan T, Metha S.K, Jain R.K, Eichhom F, Groetzschel R and Schell N, *submitted to World Scientific, presented in international conference PSI 2002 at Puri, India, March,(2002).*
18. R.L. Fleisher, P.B. Prile and R.M. Walker, Nuclear tracks in solids, *Univ. of California Press, California* (1975).
19. Z.G. Wang, Ch. Dufo ur, E. Paumier and M. Toulemonde, *J. Phys.* C6, 6733 (1994)
20. W. Assmann, M. Dobler, D.K. Avasthi, S.Kruiser, H.D. Mieskes, H. Nolte, *Nucl lustrum. Meth.* B146, 271 (1998).
21. C. Dufor, Ph. Bauer, G. Marchal, J. Grilhe, C. Jaquen, J. Pacaud, J.C. Jousset, *Euro Phys. Lett.* 21, 671 (1993).
22. M.S. Shur, T.A. Fjeldly and A.D. Bykhovski, *J. Appl. Phys.* 85, 3009 (1999).
23. T. Ashely, C.T. Elliott, N.T. Gordon, R.S. Hall, A.D. Johnson and G.J. Pryce, *Appl. Phys. Lett.* 64, 118 (1994).
24. Semiconductors and Semimetals, Vol (1-3), Vol(26) & Vol (32, 33), *Academic Press, New York* (1991).
25. Physics of Semiconductors and Their Heterostructures, J. Singh, *McGraw-Hill International* (1993)

26. Fundamentals of Semiconductor Physics and devices, Rolf Enderlein and Norman J.M. Horing, *World Scientific, Singapore (1997)*.
27. K.G. Gunther, *Natureforsch* 134, 1081, 1985.
28. Organometallic Vapour - Phase Epitaxi, Theory and Practice, G.B. Stringfellow, *Acad. Press.*, New York (1999).
29. S. Charbonneau, P.J. Poole, P.G. Piva, M. Buchanan, R.D. Goldberg and I.V. Mitchell, *Nucl. Instrum. Meth.* B106,457 (1995).
30. J.Z. Wan, D.A. Thompson and J.G. Simmons, *Nucl. Instrum. Meth.* B106, 461 (1995).
31. V. Hofsaef, J. Kuhn, C. Kaden, V. Harle, H. Bolay, F. Scholz, H. Schweizer, H. Hillmer, R. Losch and W. Schlapp, *Nucl. Instrum. Meth.* B106, 471 (1995).
32. L.C. Feldman and J.W. Mayer, Fundamentals of Surface and Thin film Analysis, *North-Holland*, New York, (1986)
33. W.K.Chu, J.W.Mayer, M.A.Nicolet, Backscattering spectrometry, *Acad. Press*, New York, (1978).
34. Handbook of Modern Ion Beam Analysis, M. Bozoian, J.R. Tesmer, M. Nastasi (Eds.), *Material Research Society*, Pittsburgh, (1995)
35. L'Ecuyer, J., Brassard, C, Cardinal, C. and Terreault, B., *Nucl. Instrum. Method*, B149, 271 (1978).
36. D.K. Avasthi, *Nucl. Instrum. Meth.* B136-188, 729 (1998).
37. D. K. Avasthi, *Bullten of Materials Science* 19, 3, 1996.
38. D.K. Avasthi and W. Assmann, *Current science* 80, 1532 (2001).
39. L. R. Doolittle, *Nucl. Instrum. Meth.* B9, 334 (1985); B15, 227 (1986); *PhD Thesis*, (Cornell University, Ithaca, New York (1978).
40. Assmann, W., Huber, H., Steinhausen, Ch., Dobler, M., Gltickler, H. and Weidinger, A., *Nucl. Instrum. Meth.* B89, 480 (1994).
41. Davies, J. A., Foster, J. S. and Walka, S. S., *Nucl. Instrum. Meth.* B136-138, 594 (1998).
42. Timmers, H., Ophel, T. R. and Elliman, R. G., *Nucl. Instrum. Meth.* B156, 236 (1999).

43. Development of a Large Area two dimensional Position Sensitive AE-E Detector Telescope, S.V.S. Nageswara Rao et. al. *NSC (New Delhi) annual report*, 63, (2001-2002); Effect of field homogenization on position sensitivity of LAPSDT, S.A. Khan, S.V.S. Nageswara Rao et. al., *NSC (New Delhi) annual report*, 65, (2001-2002); Submitted an abstract to ICACS 20, Puri, India.
44. Whitlow, H. J., Possnert, G. and Petersson, C. S., *Nucl. Instrum. Meth.* B27, 448 (1987).
45. Groleau, R., Gujrathi, S. C. and Martin, J. P., *Nucl Instrum. Meth.* 218, 11 (1983).
46. Avasthi, D. K., Kabiraj, D., Bhagwat, A., Mehta, G. K., Vankar, V. D. and Ogale, S. B., *Nucl. Instrum. Meth.* B93, 480 (1994).
47. S. Ghosh, D.K. Avasthi, T.Som, A. Tripathi, S.K. Srivastava, S.V.S. Nageswara Rao, F. Gruner and Walter Assmann, *Nucl. Instrum. Meth.* B190(1-4), 169 (2002).
48. Boerma, D. O., Labohm, F. and Reinders, J. A., *Nucl. Instrum. Meth.* B68, 291 (1990).
49. Dollinger, G., Frey, C. M., Bergmaier, A. and Fastermann, T., *Nucl Instrum. Meth.* B129, 603(1998).
50. Tripathi, A., Mandal, S., Kataria, D. O., Avasthi, D. K. and Datta, S. K., *Nucl Instrum. Meth.* B129, 423 (1997).
51. Behrisch, R., Grotzschel, R., Hentschel, E. and Assmann, W., *Nucl. Instrum. Meth.* 668,245(1992).
52. P.K. Rol, J.M. Fluit, F.P. Viehbock and M. De Jong, Page 257, *Proc. 4th inter. Conf. on Ionization phenomena in gases*, Ed.: N.R. Nilsson, *North Holand*, Amsterdam (1960)
53. Yu. Kagan, Yu. V. Kononets and Zh. Eksp, *Soviet Phys. JEPT31*, 124 (1970).
54. D.S. Gemmel, *Rev. of Mod. Phys.* 46,129 (1974).
55. L.C. Feldman, J.W. Mayer and S.T. Picraus, *Material Analysis by Ion Channeling*, *Academic Press*, New York (1982).
56. J. Lindhard, *Mat. Fys. Medd. Dan. Vid. Selsk.* 34, 1 (1965).
57. D.S. Gemmel and R.E. Holland, *Phys. Rev. Lett.* 14, 945 (1965).

58. S.A. Karamyan, *Nucl. Inst. and Meth.* B51, 354 (1990).
59. D.K. Avasthi, W. Assmann, H. Huber, H.D. Mieskes, H. Nolet, *Nucl. Instr. Meth.* B142, 117 (1998), and references therein.
60. C. Erginsoy, *Phys. Lett.* 15, 360 (1965)
61. Interatomic potentials, *Acad. Press.*, New York (1972).
62. A.P. Pathak, *J. Phys.* C8, L439 (1975).
63. A.P. Pathak, *Rad. Eff.* 30, 193 (1976); 43, 55 (1979)
64. L. N. S. Prakash Goteti and Anand P. Pathak, *J. Phys.* C 9, 1709 (1997).
65. L. N. S. Prakash Goteti and Anand P. Pathak, *Phys. Rev.* B58, 5243 (1998); B59, 8516(1999).
66. L. N. S. Prakash Goteti, "Quantum models for effects of extended defects on ion-channeling", *Ph.D Thesis, University of Hyderabad (1999)*.
67. F. Grasso, M. LO Savio and E. Rimini, *Rad. Eff* 12, 149 (1972).
68. A.P. Pathak, L.N.S. Prakash Goteti and S.V.S. Nageswara Rao, *Nucl. Instrum. Meth.* B193, 188(2002).
69. Ion Beam Hand Book for Material Analysis, J.W. Mayer and E. Rimini, *Academic Press, New York, (1978)*
70. Channeling (Theory, Observation and Applications), Ed. D.V. Morgan, *John Wiley Inc., Great Britain, (1973)*
71. J.H. Barrett, *Phys. Rev.* 166, 219 (1968); 3, 1527 (1971) and refs. therein.
72. A.P. Pathak, *Phys. Rev.* B13, 4688 (1976); B15, 3309 (1977).
73. A.P. Pathak, *Phys. Rev.* B13, 461 (1976).
74. A. P. Pathak, *Phys. Lett.* A 55, 104 (1976); 57, 467 (1976).
75. A.P. Pathak, V. Harikumar, *Nucl. Instrum. Meth.* B99, 499 (1995).
76. J.J. Quillico and J.C. Jousset, *Phys. Rev.* B11, 1791 (1975).
77. H. Park, R.H. Patnell, R.L. Swent, J.D. Kephart, B.L. Berman, S. Datz and R.W. Fearick, *J. Appl. Phys.* 55, 358 (1984) and refs. therein.
78. Dislocations, J. Fiedel, *Pergamon, New York (1964)*.
79. Y. Quere, *Phys. Stat. Sol.* 30, 713 (1968).
80. V.V. Klimov and V.S. Letokhov, *Phys. Lett.* A222, 424 (1996) and refs. therein.

81. Effects of defects and strain on ion channeling, *Azher M. Siddiqui, Ph. D., University of Hyderabad, Hyderabad* (2001).
82. Azher M. Siddiqui, Anand B. Pathak, B. Sundaravel, Amal K. Das, K. Sekar, B.N. Dev, B.M. Arora, *Nucl. Instr. and Meth.* B142, 389 (1998).
83. G.C. Osbourn, *J. Appl. Phys.* 53, 1586 (1982).
84. J.W. Matthews and A.F. Blakeslee, *J. Cryst. Growth*, 27, 118 (1974); 32, 265 (1974).
85. R. People and J.C. Bean, *Appl. Phys. Lett.* 47, 322 (1985); 49, 229 (1985).
86. P.Y. Wang, J.F. Chen, J.S. Wang, N.C. Chen and Y.S. Chen, *J. Appl. Phys.* 85, 2985 (1999).
87. U.D. Venkateswara!, T. Burnett, L.J. Cui, M.Li, B.A. Weinstein, H.M. Kim, C.R. Wie, K. Elcess, C.G. Fonstad, and C. Mallhiot, *Phys. Rev.* B42, 3100 (1990).
88. M. Constant, N. Matrullo, A. Lorriaux and L. Boussekey, *J. Raman. Spec.*, 21, 225 (1996).
89. W.K. Chu, C.K. Pan and C.A. Chang, *Phys. Rev.* B28, 4033 (1983).
90. S.T. Picraux, L.R. Dawson, G.C. Osbourn, R.M. Biefeld and W.K. Chu., *Appl. Phys., Lett.* 43, 930 (1983); 43, 1020 (1983).
91. S.T. Picraux, L.R. Dawson, G.C. Osbourn, and W.K. Chu., *Appl. Phys., Lett.* 218, 57(1983).
92. S.T. Picraux, L.R. Dawson, J.Y. Tsao, B.L. Doyle and S.R. Lee, *Nucl. Instrum. Meth.* B33, 891 (1988).
93. W.K. Chu, J.A. Ellison, S.T. Picraux, R.M. Biefeld and G.C. Osbourn, *Nucl. Instrum. Meth.* B 218, 81 (1983).
94. A. Kozanecki, J. Kaczanowski, B.J. Sealy and W.P. Gillin, *Nucl. Instrum. Meth.* 8118, 640(1996).
95. P.W.L. Van Dijk, L.J. van IJzendoorn, M.J.A. de Vogit, *Nucl. Instrum. Meth.* B118, 97, (1996).
96. K.M. Yu and K.T. Chan, *Appl. Phys. Lett.* 56, 45, (1990).
97. A.V. Drigo, M. Mazzer and F. Romanato, *Nucl. Instrum. Meth.* B63, 30 (1992).
98. Shin. Hashimoto, Y.-Q. Feng, Gibson, L.J. Schowalter and B.D. Hunt, *Nucl. Instrum. Meth.* B13, 45 (1986).

99. A.P. Pathak, S.V.S. Nageswara Rao, Azher M. Siddiqui, *Nucl. Instr. and Meth.* B161-163, 487 (2000).
100. Azher M. Siddiqui, S.V.S. Nageswara Rao, Anand P. Pathak, V. N. Kulkarni, R. Kesav Murthy, Eric Williams, Daryush Ila, Claudiu Muntele, K.S. Chandrasekaran and B. M. Arora, *J. Appl. Phys.* 90, 2824 (2001).
101. H. Nolte, W. Assmann, H. Huber, S.A. Karamian, and H.D. Mieskes, *Nucl. Instrum. and Meth.* B136, 587 (1998).
102. W.K. Chu, J.A. Ellison, S.T. Picraux, R.M. Biefeld and G.C. Osbourn, *Phys. Rev. Lett.* 52(2), 125 (1984).
103. H. Park, R.H. Patnell, R.L. Swent, J.D. Kephart, B.L. Berman, S. Datz and R.W. Fearick, *J. Appl. Phys.* 55, 358 (1984).
104. A.Paul , A.Gupta, S.M.Chaudhuri, D.M.Phase, S.Ghosh and D.K.Avasthi, *Nucl. Instr. Meth.* B156, 158 (1999).
105. A.Gupta, S.Pandita, D.K.Avasthi, G.S.Lodha, R.V.Nandedkar, *Nucl. Instr. and Meth.* B146, 265 (1998).
106. B.N. Dev, *Nucl. Instr. and Meth.* B156, 258 (2002) and refs. therein
107. C. R. Wie, *Mater. Sci. Eng., R.* 13, 1 (1994).

CHAPTER II

EXPERIMENTAL

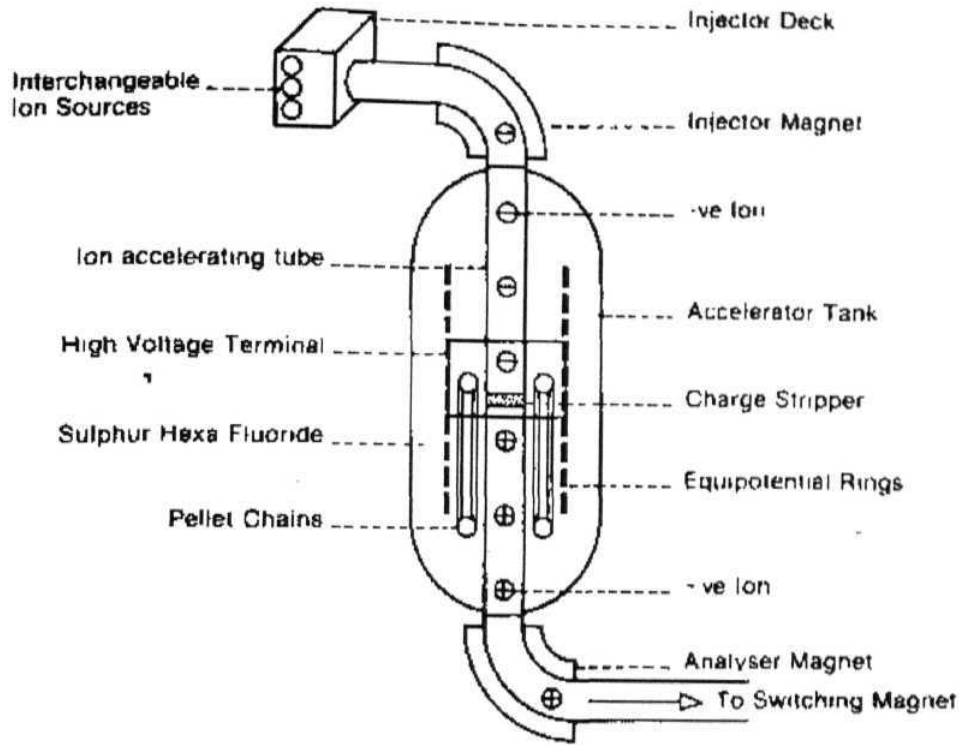
This chapter gives complete details (section 1) of different experimental facilities (/instruments) that have been used in this thesis work. Experimental details (section 2) regarding the sample growth, irradiation and characterization are described. Sample identities (IDs) and other nomenclature have been defined in this chapter. This information will be used throughout the thesis.

2.1 EXPERIMENTAL FACILITIES

Several experimental facilities and techniques have been employed to execute this thesis work. Major part of the work was done in the Pelletron accelerator laboratory of Nuclear Science Centre, New Delhi (*an inter university research facility of UGC*). This section will provide the details of all these experimental facilities while the next section will discuss the typical specifications of the experiments that have been performed.

2.1.1 The Pelletron Accelerator Laboratory at NSC

Nuclear Science Centre (NSC) has many research facilities including the Pelletron accelerator [1-3]. Any ion of choice (if it can attain negative charge) can be accelerated to higher energy using this 15 MV Pelletron accelerator. Here we describe some of the specifications of the accelerator and facilities that were actually used in this work. These are only brief descriptions and further details can be obtained from ref. [1-3].



A schematic figure showing the principle of acceleration of ions in Pelletron

Fig. (2.1) Schematic diagram of the NSC accelerator

2.1.1.] The Pelletron accelerator

Fig.(2.1)* shows a schematic diagram of the NSC Pelletron accelerator. This illustration will also describe the principle of acceleration and different steps involved in the process. This is basically a heavy ion tandem type of electrostatic accelerator. A SNICS (Source of Negative Ions by Cesium Sputtering) source will produce required negative ions. These ions are then pre-accelerated to $\sim 400\text{KeV}$ within the ion source and are injected into strong electrical field inside the accelerator tank which is filled with SF_6 insulating gas. However beam passes through a UHV beam line called as accelerator tube. At the center of the tank is a terminal shell which is maintained at required high voltage ($\leq 15\text{ MV}$). This terminal voltage is buildup based on the principle of Van-de Graff accelerator. Here a chain of metal pellets is used instead of a belt for carrying the

charge to terminal and hence it is called as Pelletron. The negative ions on traversing through the accelerating tubes from the column top of the tank to the positive terminal get accelerated. There is a stripper foil (either thin carbon film or gas stripper) placed at the terminal. Energetic negative ions are stripped while passing through this foil. The stripper potential is set so that it can collect all stripped electrons within required time span. Hence negative ions are transformed into positive ions at the terminal. These positive ions are then repelled away from the positively charged terminal and are accelerated to ground potential to the bottom of the tank. In this manner same terminal potential is used twice to accelerate the ions. On exiting from the tank, the ions are bent into horizontal plane by analyzing magnet, which also selects a particular beam of ion and charge state. The switching magnet diverts the high energy ion beams into a pre-selected beam line of various beam lines (experimental areas) existing in the beam hall. The entire machine is computer controlled and is operated from the control room.

2.1.1.1.1 Beam energy and current

One unit charge traveling in a field of one volt potential will gain energy of one eV. Hence 1MV potential can produce 1MeV of energy. Electrostatic accelerators work on this basic principle of acceleration. Here in the NSC Pelletron, the acceleration process involves two intermediate steps as described above. In the first step a singly charged negative ion will be accelerated in the field of terminal voltage (V) and will attain an energy V ($=1 \times V$). Then if the particle attains a charge state q after passing through the stripper foil, it will be accelerated once again to energy qV under the same terminal potential. Hence in total the particle attains an energy of $(1+q)V$. Hence terminal potential is setup based on the required beam energy and available charge states. In general most abandoned charge state is chosen so as to have stable beam. Beam current depends on the nature of the ion species charge state, energy, stripper foil and other beam tuning parameters. Gas stripper will provide a stable current. Required (within the limits *) current can be obtained through proper beam tuning process.

obtained from www.nsc.ernet.in This site gives complete details regarding the NSC facility

Two of the seven beam lines were used in this work. These are namely materials science beam line (15°) and GPSC (General Purpose Scattering Chamber) beam line (45°). A brief description of these beam lines and associated experimental facilities is given below.

2.1.1.2 Materials Science Beam Line

This beam line is used for carrying out Swift Heavy Ion (SHI) based materials research. Several users from different universities work in the area of materials characterization and engineering with SHI at this facility. Fig.(2.2) shows a schematic diagram of the beam line and associated facilities. There are three experimental chambers on this beam line namely High Vacuum (HV) chamber, Ultra High Vacuum (UHV) chamber and Goniometer (GM) Chamber. The UHV chamber is meant for surface and interfacial studies. It is equipped with several characterization instruments like STM, RGA etc. However this has not been used in the present work while the other two chambers have been extensively used. A brief description of these two chambers is given below.

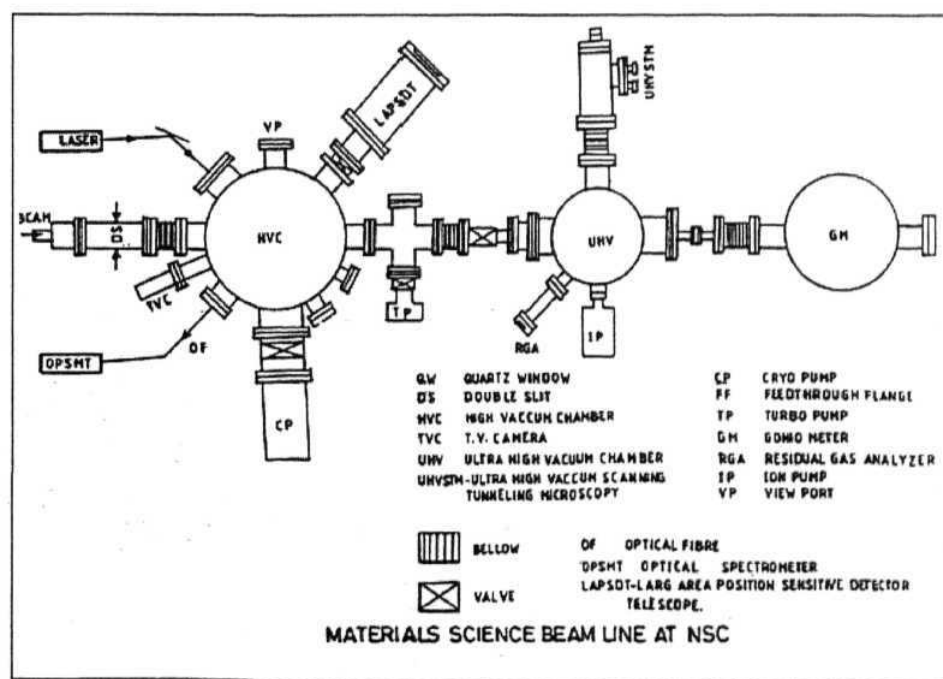


Fig. (2.2) Materials Science Beam line at NSC

2.1.1.2.1 The HV chamber:

This chamber is generally used for irradiation and ERDA experiments. This chamber is equipped with a large solid angle telescopic detector for ERDA and related 3n-line measurements. This chamber has two sector plates for detector mounting. One of them can be rotated from outside the chamber with the help of a stepper motor within the vacuum. However here in this present work, we have used this chamber only for irradiation purpose. A clean vacuum of the order of 10^{-7} mbar can be obtained using a diffusion pumping system fitted with LN2 trap and a Cryopump. A remote controlled LN2 cooled target holder can be positioned perpendicular to the beam line. Many samples can be mounted on the sample ladder for irradiation/ERDA experiments, required sample can be brought into the beam position using a bellow sealed linear movement of the target ladder (maximum possible movement is 140mm) without breaking the vacuum. This target ladder can also be rotated by 360° . The double O-ring sealing mechanism on the vacuum jacket allows the rotation of the sample holder even at LN2 temperature without breaking the vacuum. Irradiation is generally performed in a typical vacuum of the order of low 10^{-6} mbar. A sample can be irradiated homogeneously with the help of an electromagnetic scanner over a specified sample area (of max. $15 \times 15 \text{ mm}^2$). Apart from the facility to irradiate the materials with an appropriate fluence, various on-line and in situ measurements can also be performed. In the present work, all irradiations have been performed in this chamber only.

The Double Slit (DS) installed in front of the HV chamber (fig. 2.2) is used for cutting the beam. A fine (1mm) beam spot is used for ERDA experiments. This DS in combination with the other DS installed recently in front of the GM chamber is used for obtaining collimated fine beam required for channeling experiments in GM chamber.

2.1.1.2.2 The GM chamber:

A three axes goniometer has been installed in a high vacuum chamber (of 50 cm diameter) dedicated for channeling, blocking, X-ray reflectivity and X-ray fluorescence experiments. A clean vacuum of the order of 10^{-7} m bars is maintained using turbo molecular pump. Ion channeling facility has been established by using a UHV compatible 3-axes goniometer (HV). The UHV sample manipulator provides three rotational and three translational motions. The sample can be rotated by a complete cycle (360°) around the axis of the goniometer (θ or R1) with a precision of 0.018° , 180° around the axis of the incident ion-beam (ϕ or R2) with a precision of 0.0125° and can be tilted around the vertical axis perpendicular to both R1 and R2 with a precision of 0.0071° . The goniometer has been mounted from the base plate of a chamber having an inner diameter of 50 cm and eleven ports having four view ports. The facility has been fully automated for performing channeling/blocking experiments as a part of this thesis work.

2.1.1.3 GPSC Beam Line:

This beam line has one experimental chamber (GPSC) and is extensively used for both materials science and nuclear physics experiments. This is a large diameter (1.5m) chamber and is generally used for ERDA experiments using detector telescope systems. A time of flight set up is available for electronic sputtering and desorption studies, which can be installed at the end of GPSC as and when needed. This 1.5 m diameter scattering chamber provides versatile flexibility for planning special geometry experiments. It is widely used for characterization experiments by elastic recoil detection technique besides for the nuclear physics experiments. It has a remote control sample ladder and two detector arms. Irradiation experiments can also be performed using a hexagonal faced sample ladder, in which around 45 samples of 10 mm^2 size can be mounted. Also this target ladder can be changed without breaking the vacuum. Ion beam scanning in an area of $15 \times 15 \text{ mm}^2$ is possible. In this chamber, we have performed ERDA experiments using LAPSDT which was mounted on the 35° port.

2.1.2 Experimental facilities at SSPL

Some of the samples have been grown at SSPL using the MBE facility *Riber 2300 R&D machine*. The growth rate can be kept as low as 1 \AA/s so as to grow layered structures of quantum wells and superlattices with good crystalline quality, uniform chemical composition and sharp rectangular interfaces. Substrate surface is generally prepared using 3:1:1 ($\text{H}_2\text{SO}_4:\text{H}_2\text{O}_2:\text{HO}_2$) incase where the epi-ready wafers are not available. The growth specifications and other details can be found in ref. [4,5]. These samples are then characterized by HRXRD before and after irradiation/annealing. Here we give a brief description of the HRXRD facility.

HRXRD experiments have been performed using the X'Pert Materials Research Diffractometer (MRD) at SSPL Delhi, with $\text{Cu K}\alpha$ radiation set in point focus mode. Primary optics consists of a Bartels 4 crystal (220) Ge monochromator $\text{K}\alpha_1$ radiation with angular spread of about 12° ^{arc/s} in the scattering plane. All measurements are performed in $\omega - 2\theta$ mode, after tilt and azimuthal optimizations of the sample on the Eulerian cradle. This MRD consists of a goniometer which is controlled by two position controls which are able to drive ω and 2θ in steps of 0.0001° with a reproducibility of $\pm 0.0001^\circ$. The MRD cradle has five motorized movements 1) the Φ rotation (360° , step size 0.02°) with a reproducibility of $\pm 0.01^\circ$ and a slew speed of $70^\circ/\text{Sec}$. b) a tilt Ψ (180° , step size 0.01°) with a reproducibility of $\pm 0.01^\circ$ and a slew speed of $2^\circ/\text{Sec}$. c) X/Y translation for wafer mapping ($\pm 50 \text{ mm}$) with a step size of 0.01 mm and a precision of $10 \text{ }\mu\text{m}$. d) Z- translation ($\pm 5 \text{ mm}$) with a step size of 0.001 mm and a precision of $1 \mu\text{m}$ and e) Sample oscillation around any point on X and Y table perpendicular to diffraction plane. The cradle can be used as a programmable automatic sample changer for multiple samples that have different shapes. The diameter of the X-ray beam can be defined using the parallel plate collimators. This setup runs on windows based software supplied by Philips Company. Simulation software (MADMX) is also available for simulation and data analysis.

ION SCATTERING FACILITY AT
INSTITUTE OF PHYSICS, BHUBANESWAR, INDIA

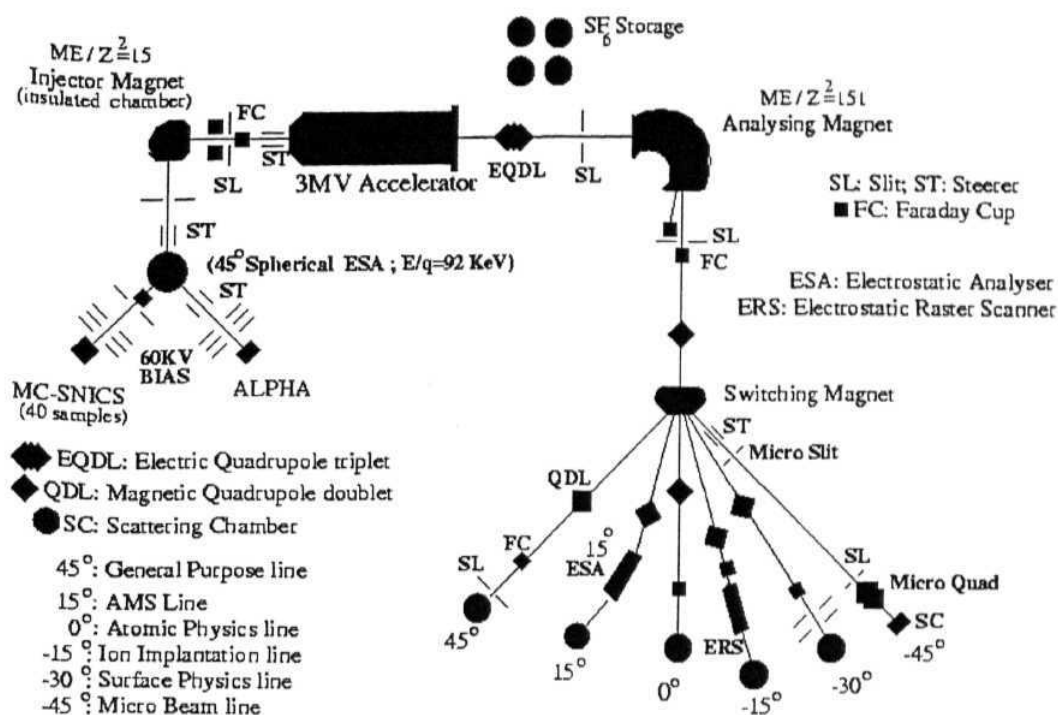


Fig. (2.3): Schematic diagram of the Accelerator facility at IOPB.

2.1.3 Channeling facility at IOP

2.1.3.1 The accelerator

This is a 3 MV Tandem type electrostatic Pelletron accelerator. The operation of this accelerator is same as that of NSC Pelletron accelerator. The only difference is the maximum achievable terminal potential. This accelerator uses two ion sources namely Alphatross and SNICS for producing *He* (or any gaseous) negative ions and negative ions of other elements (from solid targets) respectively. Fig.(2.3) shows the schematic diagram of the accelerator and associated beam lines.

2.1.3.2 Channeling facility

RBS and channeling experiments have been carried out in the general purpose scattering chamber. This scattering chamber is equipped with a goniometer with five degrees of freedom of which three (x, y, z) are translational and the other two (θ, Φ) are rotational. On the goniometer, the θ precision is of 0.1° and the Φ rotation has a precision of 0.3° . The beam is collimated by a pair of collimators of diameter 15 mm, separated by a distance of 0.5m. Scattered particles are generally detected using an SSBD positioned at back angles (150° to 170°). Initial alignment is done using laser beam. Complete details are available in ref.[6,7].

2.1.4 Other experimental facilities

One sample was obtained from Warsaw, Poland. This sample was grown using the MOCVD (Metal Organic Chemical Vapor Deposition) facility at Warsaw, Poland. This sample has been annealed before and after irradiation using the RTA facility at Rossendorf (FZR). These sample along with some other samples were characterized using synchrotron based HRXRD at ROBL, Grenoble. ROBL stands for ROssendorf Beam Line[®]. It is meant for the synchrotron radiation for the research center of Rossendorf (FZR). The plant is at the European Source of Synchrotron Radiation Facility (ESRF) in Grenoble, France. It has two experimental stations of which one (MRH) is meant for the materials research. HRXRD experiments have been performed using this radiation at MRH. This uses a goniometer with 6 independent axes of rotation with precision better than 0.0001° . This also has three translational motions ($z = 1\mu$ step and X, Y with 10μ step). High load scintillation detectors or energy dispersive PIN diode (with energy resolution better than 200 eV and sensitive area of 7mm^2) detectors are generally used. 2D Position Sensitive Detectors are also available with the facility.

obtained from www.iopb.res.in. This site gives complete details regarding IOP facilities.

2.2 EXPERIMENTAL DETAILS

2.2.1 Sample growth and specifications

Necessary multilayer or single layer samples were grown or obtained from different labs in India and abroad. Following table (table 2.2.1) shows the sample specifications, growth technique and their source. Sample *IDs* given in this table are used throughout the thesis.

Table 2.2.1: Sample specifications and IDs

<i>Sample ID</i>	<i>Specification</i>	<i>Growth technique</i>	<i>Source</i>
4201	$\text{In}_{0.1}\text{Ga}_{0.9}\text{As}(100 \text{ \AA})/\text{GaAs}$	MBE	SSPL, Delhi
2701	$\text{In}_{0.1}\text{Ga}_{0.9}\text{As}(150 \text{ \AA})/\text{GaAs}$	"	"
2601	$\text{In}_{0.1}\text{Ga}_{0.9}\text{As}(250 \text{ \AA})/\text{GaAs}$	"	"
4101	$\text{In}_{0.1}\text{Ga}_{0.9}\text{As}(400 \text{ \AA})/\text{GaAs}$	"	"
4401	$\text{In}_{0.14}\text{Ga}_{0.86}\text{As}(75 \text{ \AA})/\text{GaAs}(\sim 200 \text{ \AA}) \dots \times 10 / \text{GaAs}$	"	"
MQW5	$\text{In}_{0.12}\text{Ga}_{0.88}\text{As}(75 \text{ \AA})/\text{GaAs}(150 \text{ \AA}) \dots \times 20 / \text{GaAs}$	"	"
P520 & P523	$\text{In}_{0.47}\text{Ga}_{0.53}\text{As}(150 \text{ \AA})/\text{InP}(150 \text{ \AA}) \dots \times 10 / \text{InP}$ (Lattice matched)	MOCVD	Warsaw, Poland

Reasonably good crystalline and interface quality has been observed and strain values were measured for all samples using one or more characterization techniques like low / high energy channeling, HRXRD as discussed in the following chapters.

2.2.2 Material treatment (Irradiation and/or annealing)

Each sample was cut into two or three counter parts with one part kept unirradiated. The other parts were irradiated by energetic Ag ions delivered from the

© Complete details are available at www.fz-rossendorf.de

15MV Pelletron accelerator at NSC. The irradiation details are given in table 2.2.2. Then each of the (both pristine and irradiated) P523 samples was again cut into two parts and one part was annealed (Rapid Thermal Annealing (RTA)) at 450°C for 90 S .in N₂ atmosphere using the RTA facility at Dresden, Germany. Annealed samples are referred with a tag "RTA" at the end of the sample name. The letter "U" at the end of samples ID indicates that the sample is unirradiated one.

Table 2.2.2: Irradiation details

Sample ID	Irradiation Details		New name
	Energy (MeV)	Fluence (ions/cm ²)	
4201	150	1 X 10 ¹³	4201113
2701	150	1 X 10 ¹³	2701113
2601	150	5 X 10 ¹² , 1 X 10 ¹³ & 2 X 10 ¹³	2601512, 2601113 & 2601213
4101	150	1 X 10 ¹³	4101113
4401	200	5 X 10 ¹²	4401 I
MQW5	130	5 X 10 ¹²	MWQ5I
P523	130	5 X 10 ¹² & 5 X 10 ¹³	P523I & I2

2.2.3 RBS/Channeling

RBS / channeling on some of the pristine and irradiated samples were performed using 3.5 MeV He⁺⁺ ions delivered from 3MV Tandem accelerator at IOP, Bhubaneswar. A Silicon Surface Barrier Detector (SSBD) positioned at 150° (Scattering angle) was used to detect scattered particles. Target tilt was kept around 45° so as to align the incident beam to off normal (<110> direction) axis. Incident beam was collimated using a pair of collimators placed in the beam line. Samples were initially aligned using LASER beam.

2.2.4 HRXRD

High Resolution X-ray Diffraction (*HRXRD*) measurements are performed on all pristine, annealed, irradiated and irradiated+annealed samples to study their layered structure, interface quality and to measure the strain. *HRXRD* is very sensitive to the lattice strain and is capable of detecting the strains with a sensitivity of about 10^{-5} . Two sets of samples were studied near the reflection $\langle 004 \rangle$ (GaAs) (for MQW5) and $\langle 006 \rangle$ (InP) (for P523) at ROBL Material Research Station, Grenoble using the synchrotron radiation. The wavelength of radiation was determined to be 0.15362nm from the angular position of Bragg lines. The other samples were characterized by *Cu Ka* radiation near $\langle 004 \rangle$ (GaAs) reflection at SSPL, Delhi, using the X'Pert Materials research diffractometer. Typically for $\langle 004 \rangle$ reflection of GaAs with *Cu Ka* X-rays, the extinction and absorption lengths are 1.5 μ and 30 μ respectively [8]. Therefore all the layers of the all samples are adequately scanned.

2.2.5 ERDA, High energy channeling and blocking

Two experimental facilities namely a Large Area two dimensional Position Sensitive AE-E Detector Telescope (LAPSDT) and an automated high energy channeling facility have been developed as a part of the thesis work. Design and development details of these facilities are discussed in the next chapter. These facilities were used to perform ERDA and high energy channeling experiments at NSC. Some of the ERDA experiments are performed using 150 MeV Ag with a recoil angle of 35° in GPSC and some are performed using 200 MeV Ag with a recoil angle of 55° in Goniometer chamber (GM). The target was 12° was for 4101 & 25° for all other samples.

40 MeV Si ions delivered from the 15 MV Pelletron accelerator of NSC have been used as incident beam in high energy channeling/blocking experiments. A pair of double slits separated from each other by roughly around 4m was employed to define the incident angle and also to get the fine and parallel beam. Two SSB Detectors were placed at 60° and 110° for alignment and data collection respectively. Forward angle was used

for alignment process so as to reduce the irradiation time while back angle was used to improve the energy resolution. Channeling studies have been performed on the strained In_{0.1}Ga_{0.9}As layer grown on GaAs substrate at SSPL, Delhi using Molecular Beam Epitaxy (MBE). Three samples with different layer thickness (100 Å⁰, 250 Å⁰ & 400 Å⁰) have been investigated in this study. The target tilt was around 45°

2.3 CONCLUSION

An overall description of all facilities that have been used in this work is given with experimental specifications. Further details are given in respective chapters as and when required. Some of the above mentioned details may be repeated in the following chapters just for the sake of completeness of those chapters.

2.4 REFERENCES

1. D. Kanjilal, S. Chopra, M.M. Narayanan, I.S. Iyer, V. Jha, R. Jhoshi and S.K. Datta, *Nucl. lustrum. Meth.* A238, 97 (1993).
2. D.K. Avasthi, *Nucl. lustrum. Meth.* B136-138, 729 (1998).
3. J.P. Singh, R. Singh, S. Ghosh, A. Tripathi, D. Kabiraj, S. Guptha, T. Som, Ravi Kumar, S.K. Arora, A. Ashokan, D.K. Avasthi, D. Kanjilal, N.C. Mishra and G.K. Mehta, *Nucl lustrum. Meth.* B156, 206 (1999) *and refs. there in.*
4. R.K. Jain, *Physics of Semiconductor devices* Vol. 1, Ed. V. Kumar and S.K. Agrawal, *Narosa Publishing house*, New Delhi, page 120 {1998}.
5. T. Srinivasan, R. Muralidharan, S.K. Mehta, B.P. Jain, S.N. Singh, R.K. Jain and V. Kumar, *Vacuum* 60, 425 (2001).
6. K. Sekhar, P.V. Satyam, G. Kuri, D.P. Mahopatra, and B.N. Dev, *Nucl. lustrum. Meth.* B73,63(1993).
7. Azher M. Siddiqui, Anand P. Pathak, B. Sundarvel, Amal K. Das, K. Sekhar, B.N. Dev and B.M. Arora, *Nucl. lustrum. Meth.* B142, 389 (1998).
8. C.R. Wie, *Mater. Sci. Eng.*, 13, 1 (1994).

CHAPTER III

DEVELOPMENT OF EXPERIMENTAL FACILITIES

Two major experimental facilities i.e a Large Area two dimensional Position Sensitive AE-E Detector Telescope (LAPSDT) and an automated high energy channeling facility have been developed as a part of the thesis. All these details are given in this chapter in two separate sections. The first section is devoted to describe the design, development and the performance of the LAPSDT and the second section describes the automated high energy channeling facility along with the necessary introduction and examples.

3.1 DEVELOPMENT OF LAPSDT:

This detector is basically a gas ionization chamber with telescopic features and two-dimensional position sensitivity [1]. It is mainly intended to detect heavy recoils in high energy *ERDA* experiments at NSC, New Delhi. Large solid angle is chosen so as to minimize the detection time which in turn will reduce any possible radiation damage during the measurement. The consequent kinematic broadening (due to large detector acceptance) can be taken care by recording the position information. Kinematic corrections are implemented in both single and multilayered samples. Two-dimensional position sensitivity has also been obtained [1]. Channeling/Blocking - *ERDA*, Transverse heating/cooling, on-line radiation damage / modifications and sputtering and many such studies can be performed using this detector.

This detector has been designed keeping the constantly increasing demand for gaseous detectors [2-8] in heavy ion physics, especially for detecting heavy recoils. Initially semiconductor detectors showed good performance [3] but they are expensive. More importantly, they are often spoiled in heavy ion detection and produce unreliable results due to various problems like pulse height effects. Another advantage with gas filled detectors is that the effective length of a gas detector can be tuned accordingly during the operation just by simply changing the gas pressure which is not possible in any other type of detectors. This feature is important in the multi anode telescopic detectors which are capable of detecting both high and low mass elements simultaneously. Hence gas filled detectors are most suitable for this purpose and many laboratories involved in such research, have also opted similar detector systems [4-8], These are stable in operation and inexpensive to operate and maintain, hence many researchers are currently working to improve the performance of such detectors [4-6,1].

Any radiation detector works based on the basic principles of ion matter interactions. Energetic ions interact with gas medium primarily in two modes *i.e* the excitation and the ionization of the gas molecules. Although the measurement of excitation to detect the particle energy is used in some special cases, the detection of ionization is simple and most widely used in the particle detection [3]. Gas ionization chambers are particle detectors in which ionization is measured and an equivalent electrical signal is drawn. A detailed introduction to ionization chambers is given in the next section and then the following sections are devoted to describe the design and performance of the detector.

3.1.1 Ionization Chambers

An ionization chamber is simply an enclosure containing a gas and two or more electrodes. A thin window foil isolates the gas filled detector from the vacuum chamber. Energetic particles entering the detector chamber ionize the gas molecules and these ions and electrons, called ion pairs are collected on the electrodes with suitable electric field. Such an energetic particle loses a quantum of energy little more than the ionization

energy of the gas in creating each ion pair. Hence if the particle is fully stopped within the gas medium i.e if it deposits its total energy to the gas then the total number of ion pairs detected is proportional to the particle energy, Such ion pairs are the basic constituents of the electrical signal developed by the ionization chamber as a measure of the incident particle energy. As many other detectors, ionization chambers can also be used in both DC current mode and the pulse mode. DC current mode is used for dose measurements whereas the pulse mode is necessary for the energy measurements and then to perform the spectroscopic studies.

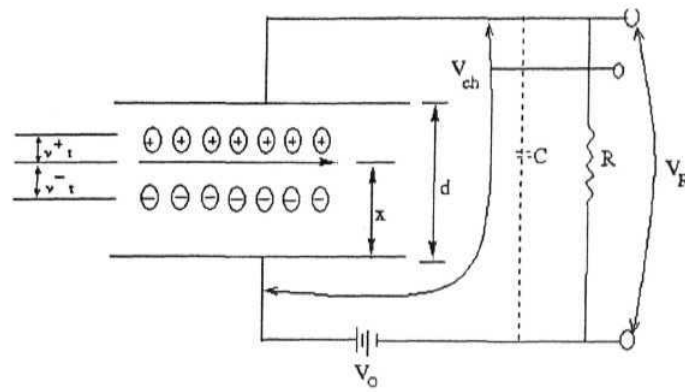


*Fig. 3.1: Equivalent circuit of a two parallel plate ionization chamber
(operated in pulse mode)*

In this work the detector has been operated only in the pulse mode all the time and only this mode will be described here. Figure 3.1 shows the equivalent circuit (*ckt*) of a two parallel plate ionization chamber operated in pulse mode. The ion chamber works like a capacitor and no net current flows in the absence of any ionization. The electrodes are charged up to the bias voltage (V_0) and no voltage is developed at the load resistance (R). When an ion pair is generated by an ionizing radiation then the drift of such an ion pair under the influence of the applied electric field reduces the effective voltage developed on the chamber capacitor. Hence such a drift induces a current flow in the *ckt* and a voltage then appears at R which is equal to the amount by which the chamber voltage has dropped. This voltage reaches its maximum when all charges are collected on the electrodes and then will drop to zero slowly on a time scale determined by the time

constant of the external ckt. A triangular pulse whose amplitude is proportional to the incident particle energy is produced at R if the time constant is more than the collection time.

In general the mobility of electrons in a gas is 1000 times more than that of the positive ions and hence the collection time for ions is 1000 times more than that of the electrons. The collection time of the ions is of the order of milliseconds and hence the detection of ions will restrict the pulse rate. Hence most of the detectors are used only in the electron sensitive mode with a time constant which is intermediate to that of electrons and ions collection times, so as to detect higher rate interactions. However such choice needs further improvements because the signal depends on the position where ion pair is generated. If the total effective charge ultimately transferred by an ion pair is q then the part transported by an electron may range from zero to q , depending on the point of its generation. Detailed mathematical expressions are not given here which are available in fundamental text books in this area [3]. This geometrical dependence of pulse height can be eliminated up to a considerable extent by using a Frisch Grid [3, 9] which is at an intermediate potential. Here the collector (anode) is screened electrically from the entire volume in which the particle tracks are formed. In this three electrode chamber called as girded chamber, electrons are first accelerated by the grid which is placed very near to the anode. Although these electrons develop a very small amount of voltage on the grid, they pass through the grid and produce an effective voltage on the anode which is independent of the position of its origin. Mathematical expressions can be found in refs. [2, 3].

Such a girded ionization chamber is fabricated to detect high rate heavy elastic recoils with good energy resolution. Telescopic features combined with position sensitivity enhance the applications and performance of this detector and results in accurate data collection needed in our experiments.

3.1.2 General considerations

First requirement is to stop the incident ion completely within the gas and then to collect the total ion pairs that are produced. This requirement determines the sizes of all electrodes and the operating pressure. Some general considerations are necessary to reduce any loss in the collection of ion pairs and also to avoid the secondary ionization process (delta rays). If electronegative molecules such as oxygen are present then the ionization electrons may become attached to them to form slow moving negative ions [2, 3]. Another loss is caused by recombination in which the ionization electron gets recombined with the parent ion to form a neutral atom [2, 3]. Hence we have to choose a suitable bias voltage and a pure gas which is less electronegative and provides high mobility to ion pairs. Recombination loss is more if the gas pressure is more hence it is advisable to work with low gas pressures. The drift velocity of an electron (or an ion) is a function of reduced field strength defined as X/p [10], where X is the electric field strength and p is the gas pressure. X/p value is to be chosen so as to have maximum possible drift velocity at its saturated value so that a small variation in the X/p value is affordable. Also it should not exceed a value beyond which delta rays are generated due to the secondary ionizations. Optimum value of X/p found from literature [2-4 & 9-11] is around 1 V/an/mb.

A continuous flow of pure isobutane gas was used as ionizing medium with an optimum field determined experimentally by optimizing the signal to noise ratio. Most of the time, the detector is operated under very low pressures (10mbar to 60 mbar).

3.1.3 Z identification and position sensitivity

3.1.3.1 Z identification

As discussed earlier in previous chapter, ERDA combined with telescope detector allows us to separate the near Z atoms in both low and high mass regions [12]. Telescope detector is a combination of two detectors namely AE and E_{rest} detectors. AE is a very

ch_{in} detector in which the incident particle loses only a very small amount of its energy (AE) and will pass through. This particle then will be stopped completely within the E_{rest} detector. Separate bands corresponding to different elements can be observed in the graph (E-AE spectrum) drawn between E (=AE+E_{rest}) and AE (=KMZ²/E) [12]. These telescopic features can be obtained in an ionization chamber simply by dividing the anode into two parts [4-8]. Such anode is called as split anode. In this work the anode is split into three parts so as to have flexibility on the effective lengths of AE and E_{rest} anodes.

3.1.3.2 X-Position (in the scattering plane)

X-position coordinate can be obtained by dividing the cathode into two equal parts, say cathode left (CL) and cathode right (CR), such that the particle traverses more area of the CL when compared to CR if the particle enters on the left side and vice versa. Many researchers worked in this area to optimize a proper shape which can give linear and reliable position coordinate. Such studies were initiated with a cathode which was divided into two parts through one of its diagonals [13]. Later on many such geometrical combinations have been tried to establish the Backgammon shape [4-11] in which the cathode is divided in saw tooth shape as shown in fig. (3.2). We have also opted the same method to generate the X-Position coordinate [$X = (CL - CR) / (CL + CR)$]. Later on we have shifted the Backgammon structure to one of the anodes to improve the performance [5] as explained in the following sections.

3.1.3.2 Y-Position (perpendicular to the scattering plane)

Cathode signal depends on the distance at which the ion pair is originated because no grid is used to screen the ions. However the total energy of the incident particle can be measured from the anode. Hence Y-Position signal can directly be derived from the cathode signal just by normalizing it with anode signal ($Y = C/E$).

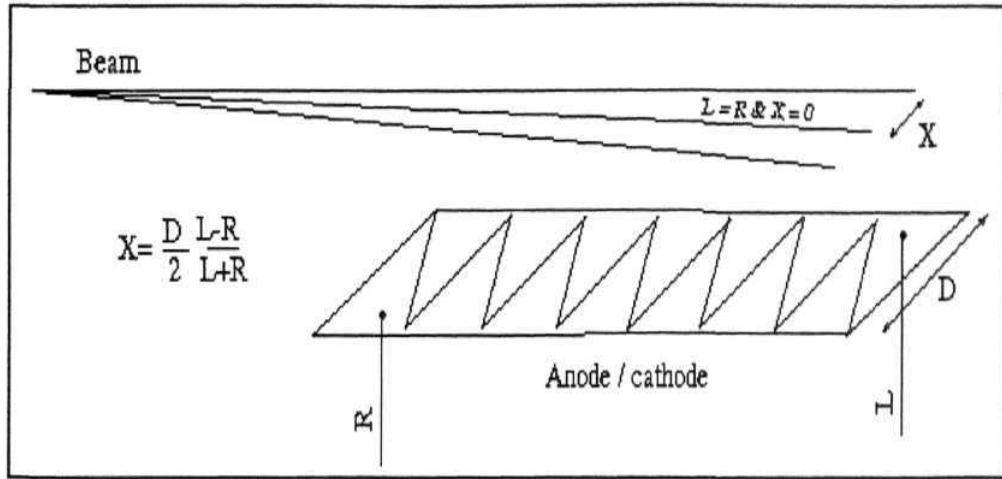
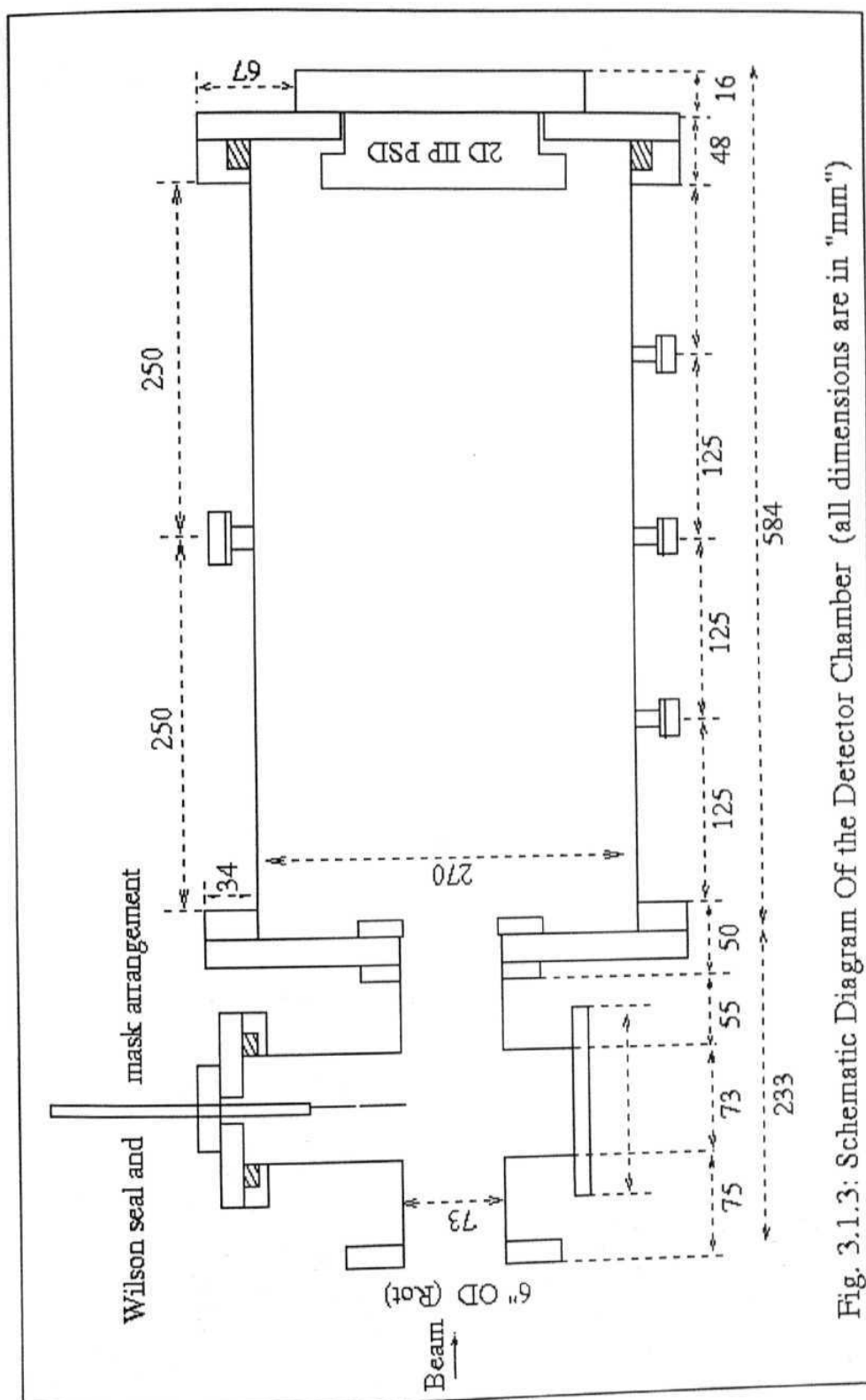
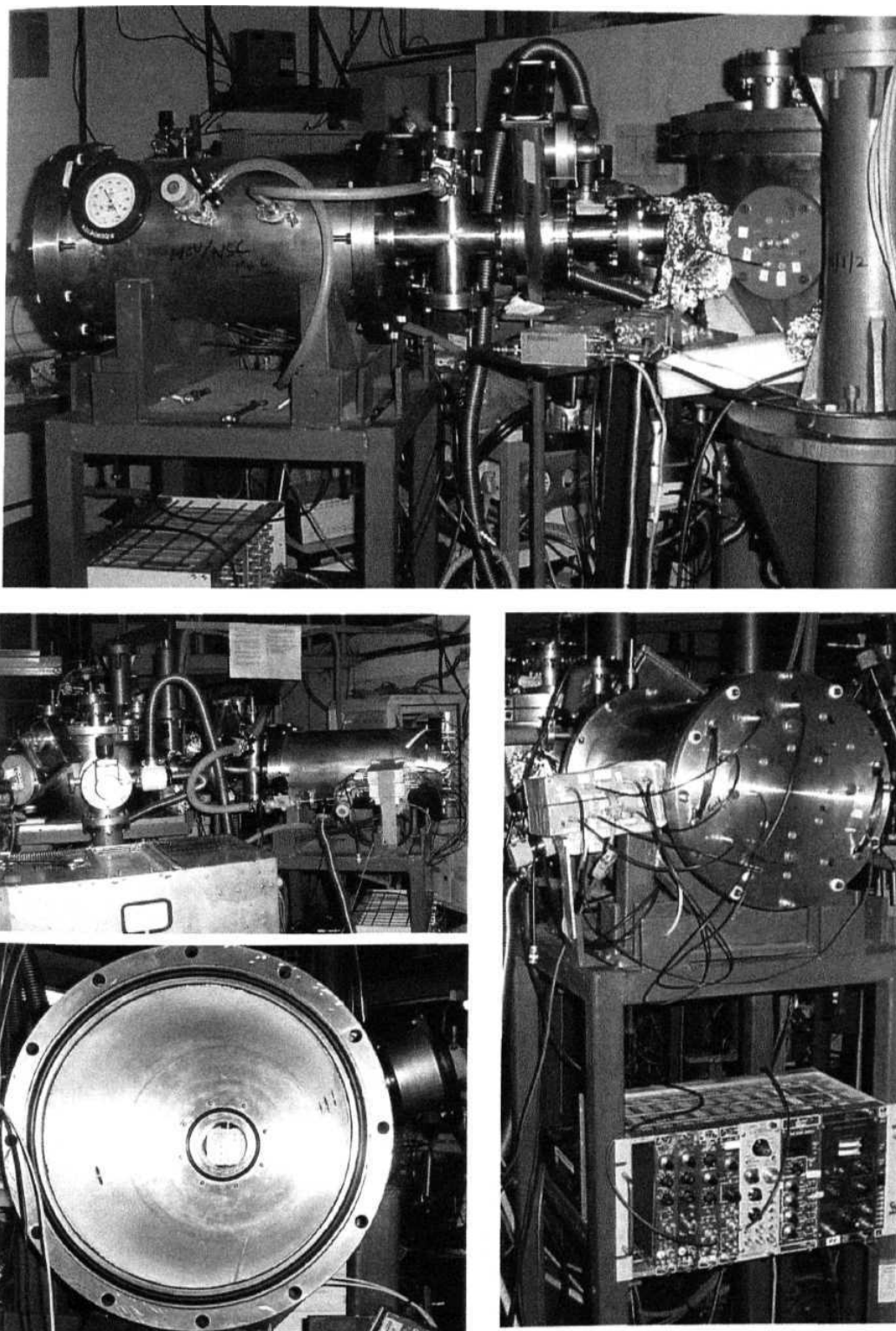


Fig. 3.2: Backgammon shape /Saw tooth shape for X-position measurements.

3.1.4 Design and Fabrication

The detector has been designed to suit our experimental requirements along with the general requirements of all experiments that are likely to be performed in the laboratory. Importance is also given for the mechanical design. The design of the detector is more versatile and flexible. Hence the detector can be readily tuned to any experimental conditions. Also it is easy to incorporate any improvements/modifications in the design because it is more flexible with sufficient number of rotatable flanges and feed-throughs. The detector can be moved as a whole, with its height adjustable stand along with its dedicated electronics. Fig. (3.3) shows the schematic diagram of the detector chamber and Fig. (3.4) shows the images of this detector installed on the 55° port of the goniometer chamber. This detector is installed and tested on two experimental chambers namely **GPSC** and **Goniometer chamber** at NSC, New Delhi and then it was used in several experiments.





*Fig. 3.4: Images of LAPSDT mounted on the 55° port of Goniometer chamber
(3 side views, Electronics modules and inside view)*

3.1.4.1 The Inner-structure

The basic model for complete inner-structure is shown in Fig.(3.5), The inner-structure is made very rigid so as to avoid unnecessary noise generated by loose contacts. Moreover necessary care is taken to have proper shielding and isolation (using Perspex screws, bolts and supports). This detector has been designed to detect up to the lightest semiconductor (B) of highest possible recoil energy (30 MeV) at NSC without using any semiconductor detector. Hence the plate (anode and cathode) length is estimated to stop $30\text{ MeV } B$ within isobutane gas of reasonable pressure i.e 80mb. Since most of the time the recoils are much heavier, it allows us to work with very low pressures like 10mb. Hence it is very easy to handle with very thin ($\sim 1.5\text{ }\mu\text{m}$) window foils also. The maximum possible detector opening or the detector acceptance angle is decided by the inner diameter of the 55 degree port of the goniometer chamber. The distance between plates and the plate width are estimated by considering the fact that the beam entering the detector through the cone defined by the solid angle should always be confined within the plates. A geometrical representation of the above required information is provided in fig.(3.6). These calculated values are listed below.

Cathode/anode/grid length	470 mm
Cathode/anode/grid width	160 mm
Separation between plates	160 mm

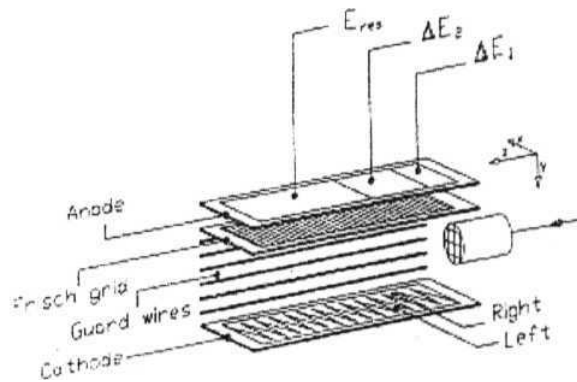


Fig. 3.5: Schematic diagram of the inner structure of an ionization chamber.

potential gradient improves the 2D patterns obtained using AE2 Backgammon, which otherwise is to be corrected by software as done in other labs. Figures (3.8 & 3.9) show the images of the inner-structure (viewed from different angles).

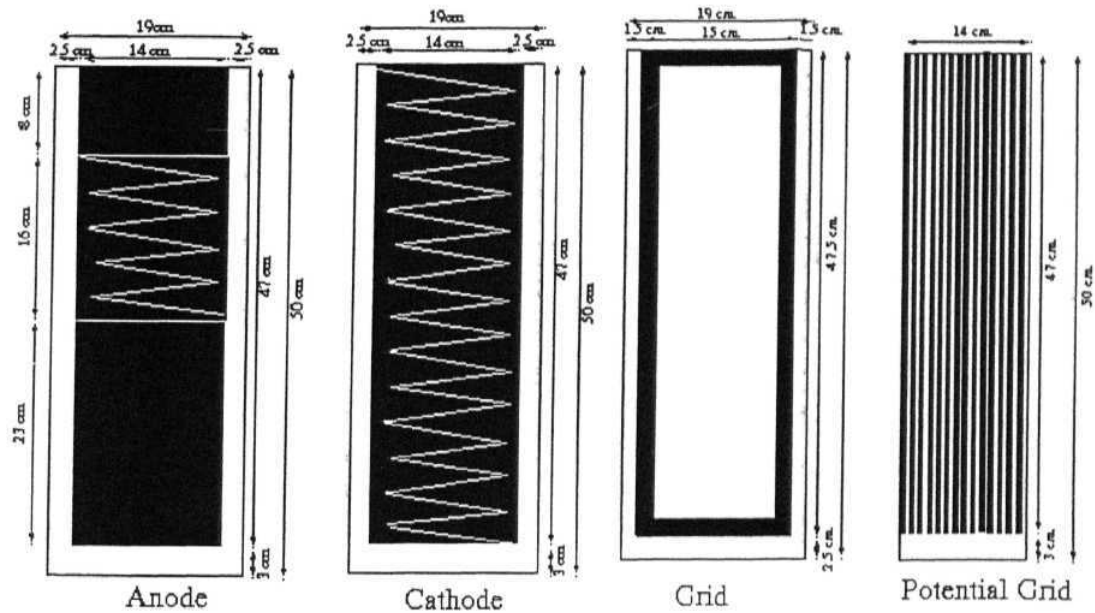


Fig. 3.7: Schematic diagram showing the structure and dimensions of different plates (like anode/cathode/grid & PD) of LAPSDT

3.J.4.2 Detector chamber

A leak proof chamber has been made using SS (stain less steel) pipe to enclose the inner-structure. From the above information the detector length and diameter are estimated using simple geometrical formulae.

Detector length	500 mm
Detector diameter	270 mm

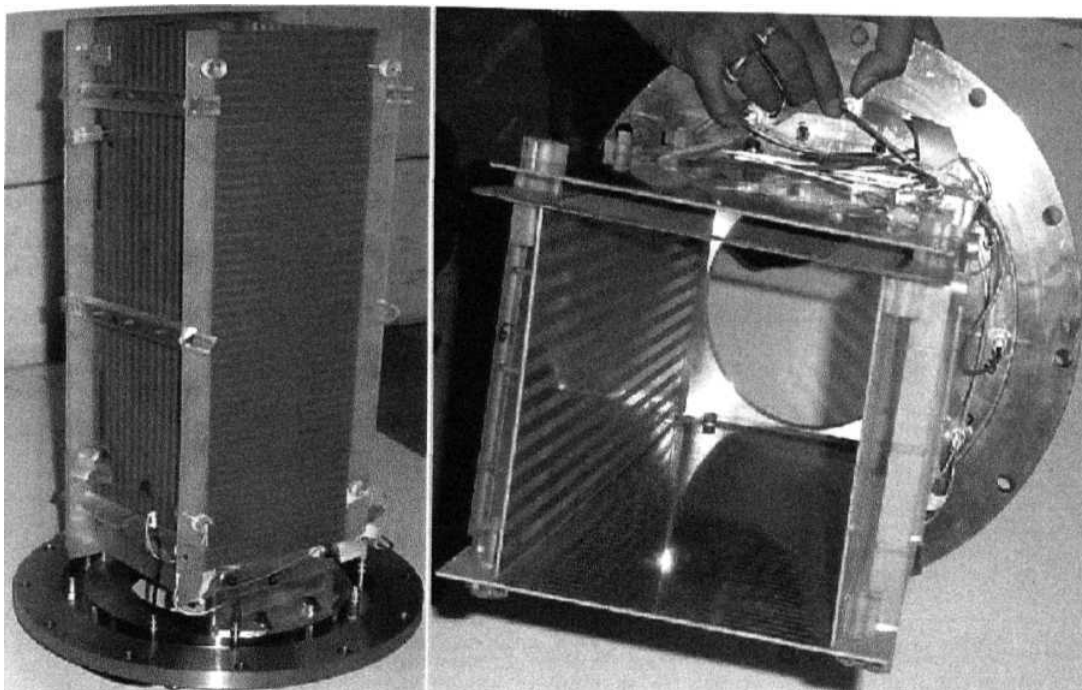


Fig. 3.8: Photograph of the inner structure (Side view and front view) showing the overall interior design.

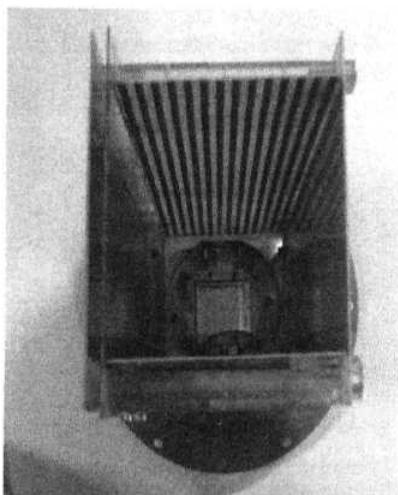


Fig. 3.9a

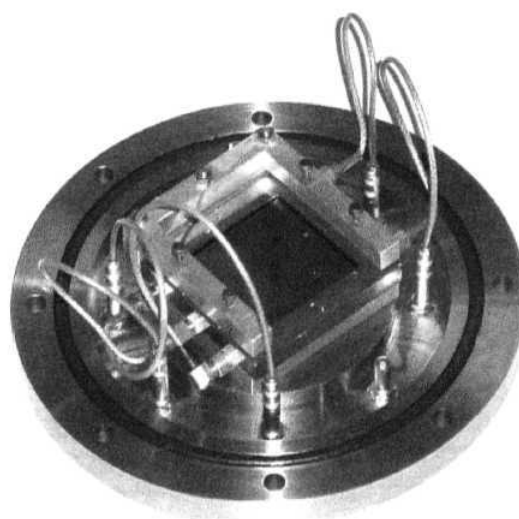


Fig. 3.9b

Fig. 3.9: Ion implanted 2D position sensitive (semiconductor) detector mounted on the "end flange " of the LAPSDT. (a) with inner structure (b) without inner structure

3.1.4.3 The window, intermediate chamber and Gas ckt

67

An intermediate chamber is needed to control the gas flow during the pumping/venting/gas filling process. This chamber will also serve as an adaptor if the chamber port and the detector opening port are not compatible. Different adaptors have been used while mounting the detector on different ports of GPSC and Goniometer chamber. However since the detector has basically been designed for 55° port of the Goniometer chamber, we have fabricated a permanent intermediate chamber for this particular case. It is made using a "cross shown in fig.(3.11)" with Wilson screw facility such that it can be used for inserting or removing (or to rotate) mask (made of PCB plate)/source during the calibration in vacuum. One of the pictures presented in fig (3.4) shows an internal view of the detector chamber. It shows the window mount place and a mask mounted on the cross. The gas is directly inputted from the isobutane cylinder and is kept in continuous flow using a rotary pump. Gas ckt used to control gas flow is shown in fig.(3.12) and images can be seen in fig.(3.4).

Cross and its associated flanges (1,2,3 & 5 are in same order below)

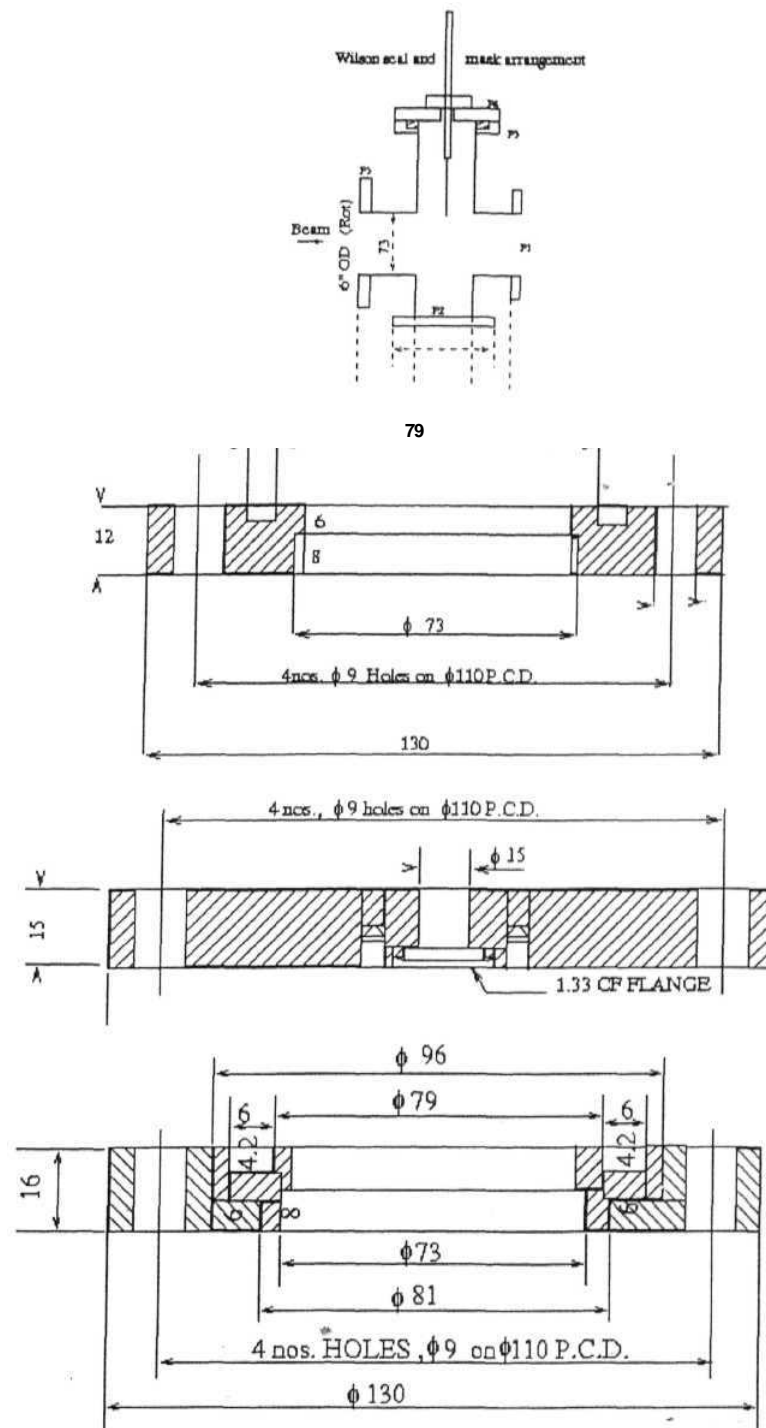


Fig.3.11: Design of the intermediate chamber (cross) and associated flanges

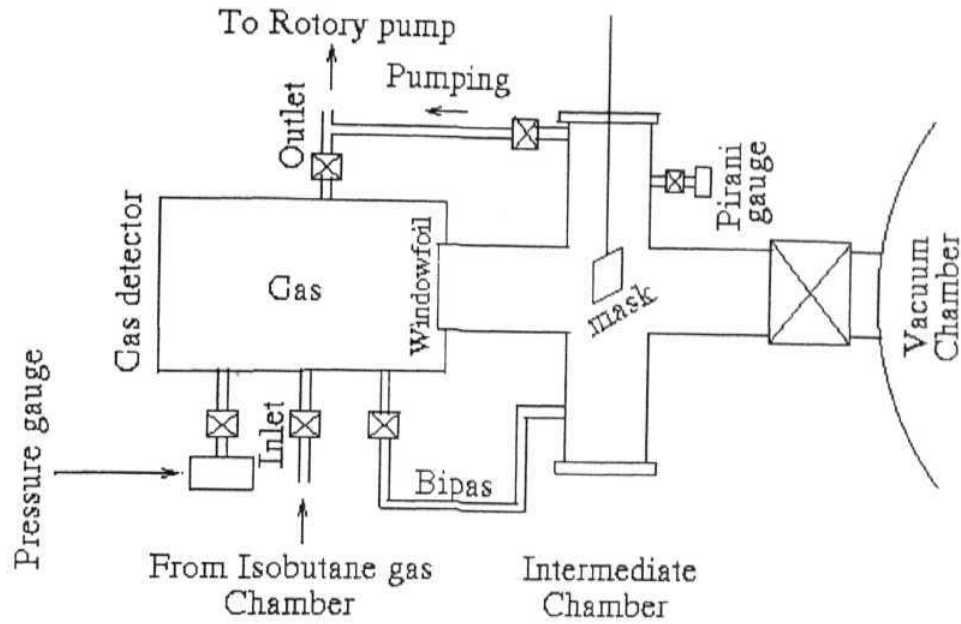


Fig. 3.12: Gas Circuit.

3.1.4.5 Electronics ckt and data collection

Figure (3.13) shows the complete schematic diagram of the electronic ckt used for collecting the data and a photo of the detector with electronic modules is shown in fig. (3.4). All the detector plates are biased through pre-amps (two sets of home made 4-channel pre-amp of type 142 IH / Ortec 142IH) and the signals have also been collected from the same connections. Then these signals are amplified using shaping (Gaussian) amplifiers (EG&G Ortec). The bias voltage and shaping time for different signals have been optimized experimentally using both source (Am/Cf) and beam. Timing Single Channel analyzer (TSCA) and Gate and Delay Generator (GDG) have been used to obtain the gate signal from AEi signal and all the other signals are brought into gate using delays (amp internal delay / a delay amplifier). CAMAC (Computer Automation and Control) based data acquisition system is used to collect the data in event by event mode (list mode). All the channels of the ADC (AD811) are triggered by a single strobe generated using TSCA/GDG. Hence every trigger will send a packet of data of all signals corresponding to same event to the computer. A linux based data acquisition software

(FREEDOM [14]) has been used to collect and analyze the data. A simulation program called SERDA (Simulation ERDA) to simulate ERDA has also been developed as a part of this FREEDOM software. We provide some of the examples in the following section to describe the performance of this detector along with simulations.

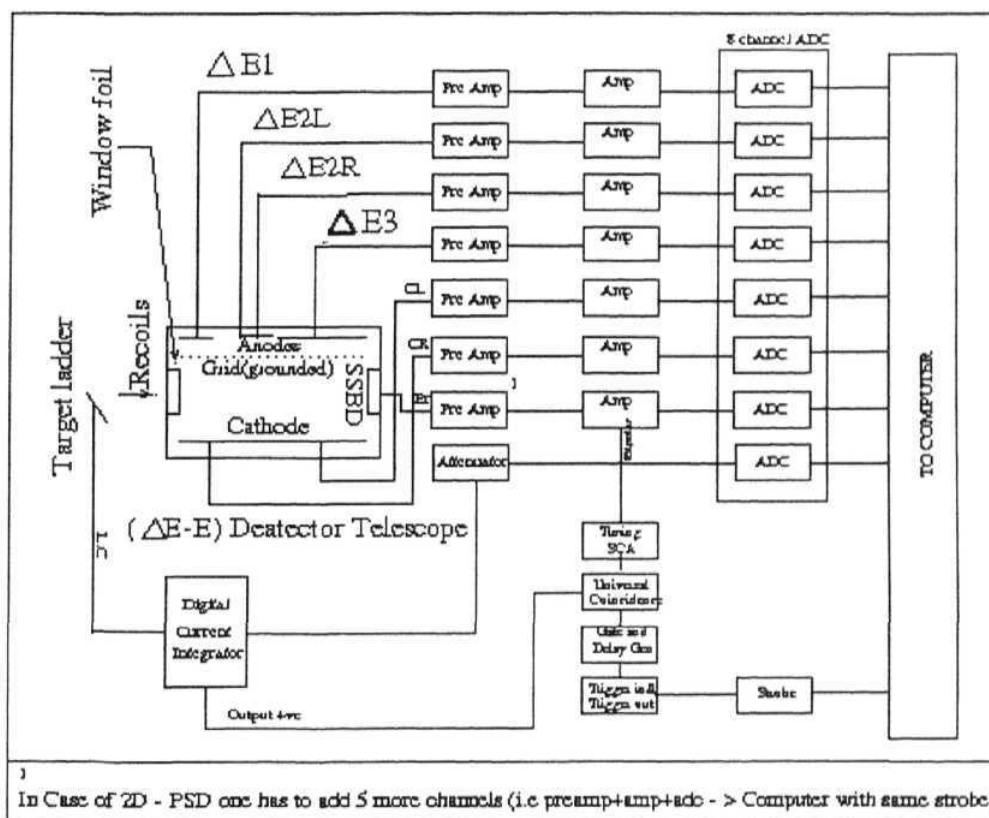


Fig. 3.13: Electronic ckt. (used to collect the LAPSDT data in event mode.)

3.1.5. Results and discussion

Here we present some of the results to show the detector performance. Some of the experiments are performed using 150 MeV Ag with a recoil angle of 35° in GPSC and some are performed using 200 MeV Ag with a recoil angle of 55° in Goniometer chamber (GM). We refer these experiments with the name of chamber (say GPSC/GM). GPSC experiments were performed with Backgammon structure on the cathode while

GM experiments were performed with the Backgammon on the ΔE_2 anode.

3.1.5.1 *z-identification*

Example 1 (Calibration Sample): The inset of the figure (3.14a) shows the structure of the calibration sample prepared for the LAPSDT based ERDA experiments. This sample was grown by electron gun evaporation technique in the high vacuum chamber at the target laboratory of NSC. Elements in the different layers were chosen so as to have reference AE-E bands in different mass regions (From Li to Ni). Generally $\Delta E-E_{\text{rest}}$ and $AE - E_{\text{total}}$ spectra are measured to identify different constituent elements of the target material. Fig. (3.14a and b) show measured $\Delta E-E_{\text{rest}}$ and $AE - E_{\text{total}}$ spectra respectively during the ERDA experiment in GM chamber on the calibration sample. The inset of the fig.(3.14b) shows the simulation spectra obtained from SERDA program for the same experimental conditions. Clear separation between different constituent elements could be observed from these spectra and bands are in agreement with the simulation spectra shown in the inset. Kinematic broadening in this data will mislead the depth analysis hence depth profiling, thickness and composition analysis are given in section 3.1.5.3 with kinematic corrections. Both the axes of all the spectra shown in this section are given in channel numbers instead of MeV. Direct relation between energy and these channel numbers has been obtained from the calibration data and the simulation program. Calibration data is either obtained from the above mentioned calibration sample / thin Al foil / thin C foil or from the standard radiation sources $\{Am \ \& \ Cf\}$. These calibrations are used during the analysis process but all spectra (including the position spectra) presented here are given in terms of channel numbers. Through simulations have been performed before planning each ERDA experiment and they have also been used in the analysis work. However, hereafter simulations spectra are not shown while presenting the experimental data.

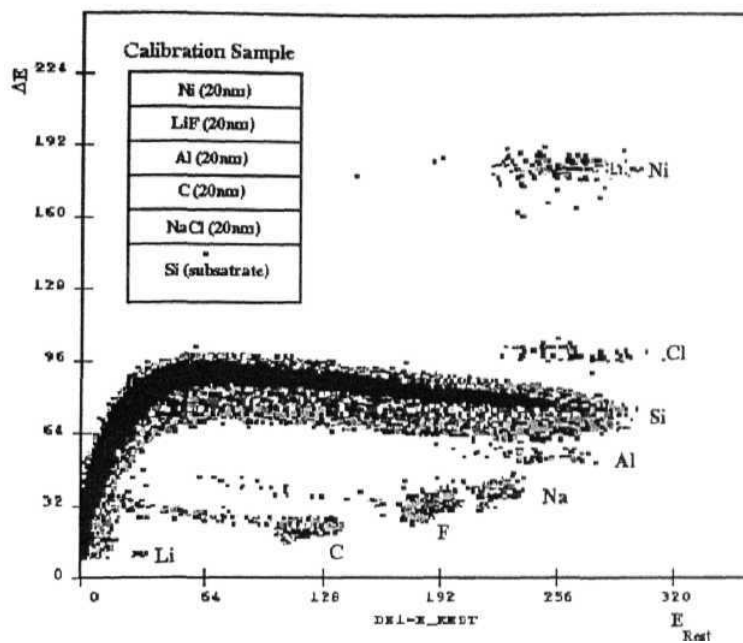


Fig. 3.14a

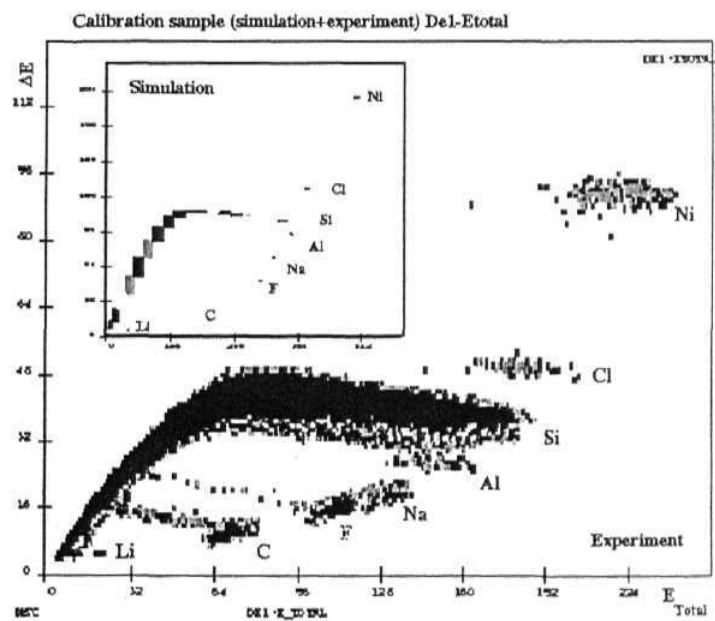
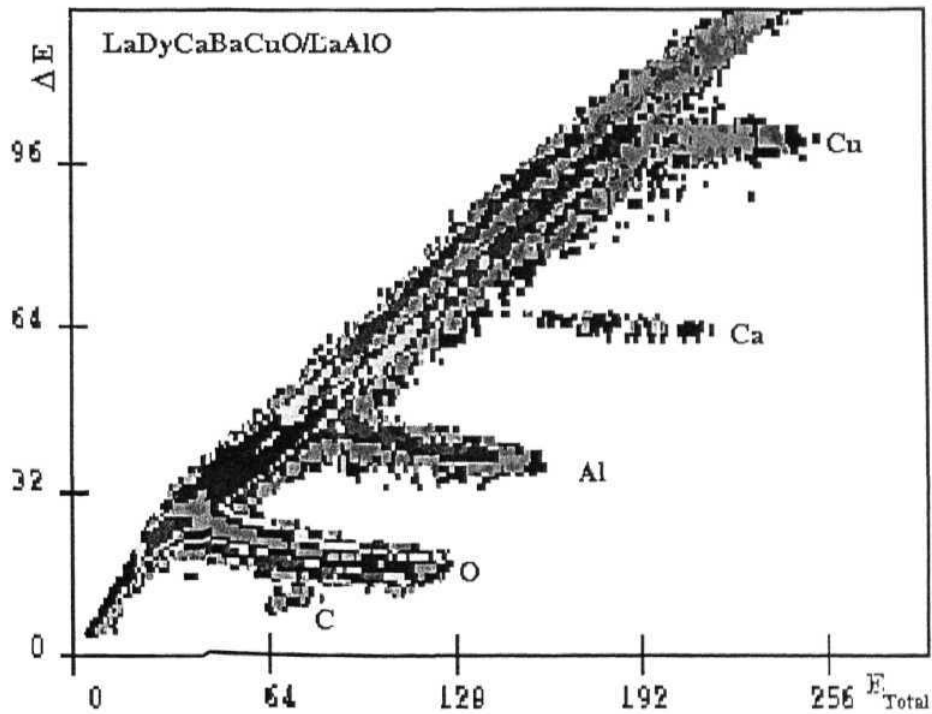


Fig. 3.14b

Fig. 3.14: a) $\Delta E_j - E_{res}$ spectrum obtained from Calibration sample (inset - sample structure). b) $\Delta E \setminus -E_{total}$ of the same sample (inset - simulation)

Example 2 (ERDA on a superconductor to monitor oxygen variation): This experiment has been performed to measure the ion fluence dependence on the evolution of oxygen (ratio of O to Cu content in the film) from a superconducting sample (LaDyCaBaCuO / LaAlO₃). Hence gas pressure and other parameters were setup to detect lighter elements like O. The results of this experiment are not discussed here because they are out of scope of this thesis work. However E - AE spectra obtained in this experiment is shown in fig.(3.15) as an example to describe the z-sensitivity of the detector. This spectrum is obtained in an ERDA experiment performed in GM chamber. O, Al Ca and Cu bands are shown in this figure. Also observed is the band corresponding to common impurity “C”.



*Fig. 3.15: $\Delta E_1 \sim E_{total}$ spectrum obtained from the superconducting sample
LaDyCaBaCuO / LaAlO₃*

Example 3 (thin CuO film on Glass substrate) ERDA has been performed on this sample in GPSC so as to see the bands 'corresponding to different elements and bands related to common impurity elements (because Glass contains almost all light elements). This spectrum is measured in the forward angle (35°) and contains a band corresponding to scattering events also. All the spectra that have been measured in GPSC are containing

the scattering events. The inset of the Fig.(3.16a) shows the E-AE spectra obtained from CuO/Glass sample while the actual figure is showing the projections of O,Cu & Si bands from both the film and substrate. From this figure it is clear that this could not have been separated in the normal ERDA without telescopic detector. Bands corresponding to lower elements are not clear in this spectrum. Hence similar spectra were measured using very low gas pressure (25mb where as the earlier spectrum was measured with 49mb) ΔE_3 . ΔE_2 spectrum shown in fig.(3.16b) shows clear separation between the light elements. It shows separate bands for C, O, Na, Mg & Si and proves the existence of these elements in the sample.

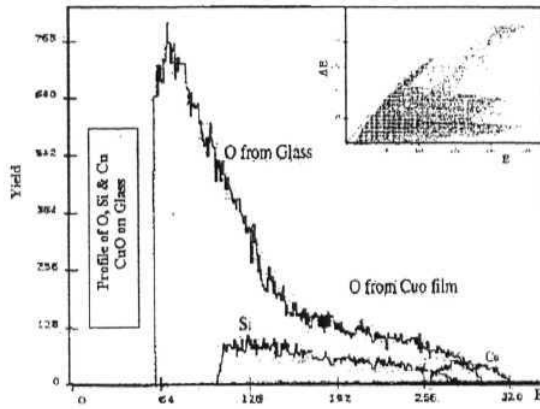


Fig. 3.16a

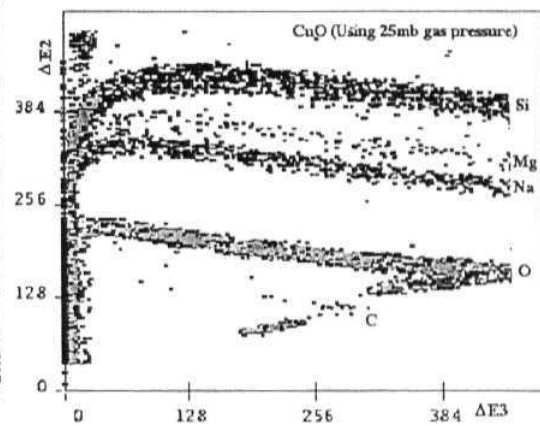


Fig. 3.16b

Fig. 3.16: a) Projections of O,Cu & Si bands from the E-AE spectrum shown in the inset (Showing the depth profiling of these elements from both the film & substrate).

b) ΔE_3 - ΔE_2 spectrum obtained from the sample with low gas pressure (25) - More z-resolution in the lower mass region.

Example 4 (InGaAs/InP superlattice grown on InP [P520]): Ion beam mixing effects in such lattice matched superlattice (P523) have been studied in detail in this thesis. Ion beam induced strains have been measured using ion beam and X-ray methods. These results are discussed in the next chapter. Here we discuss the simple ERDA spectrum measured using LAPSDT. The structure of this MOCVD grown sample has been discussed in the previous chapter and a schematic diagram is shown as in inset in the left

bottom corner of the fig.(3.1.17). The other inset of the same figure shows the ΔE_3 - ΔE_2 spectrum obtained using low pressure (25) in the GPSC. This spectrum indicates the existence of some impurity elements (like O, C, Na / Mg etc) in this MOCVD grown sample. May be this is a reason for having some what diffused/smeared out interfaces when compared to P523. Although these two samples have same thickness and composition in each layer the interface in P523 are found to sharper than that of P520. The actual figure shows the projection of Phosphorus (P) band. This sample contains P_{λ} in the alternating layers InP and hence corresponding peaks are observed in the projection of P band. This proves that the detector's depth resolution is better than 150 \AA and it has further been improved after implementing the kinematic corrections. All these examples witness considerably good performance of the detector in terms of elemental identification. The other features of the detector like position sensitivity have been described in the following sections.

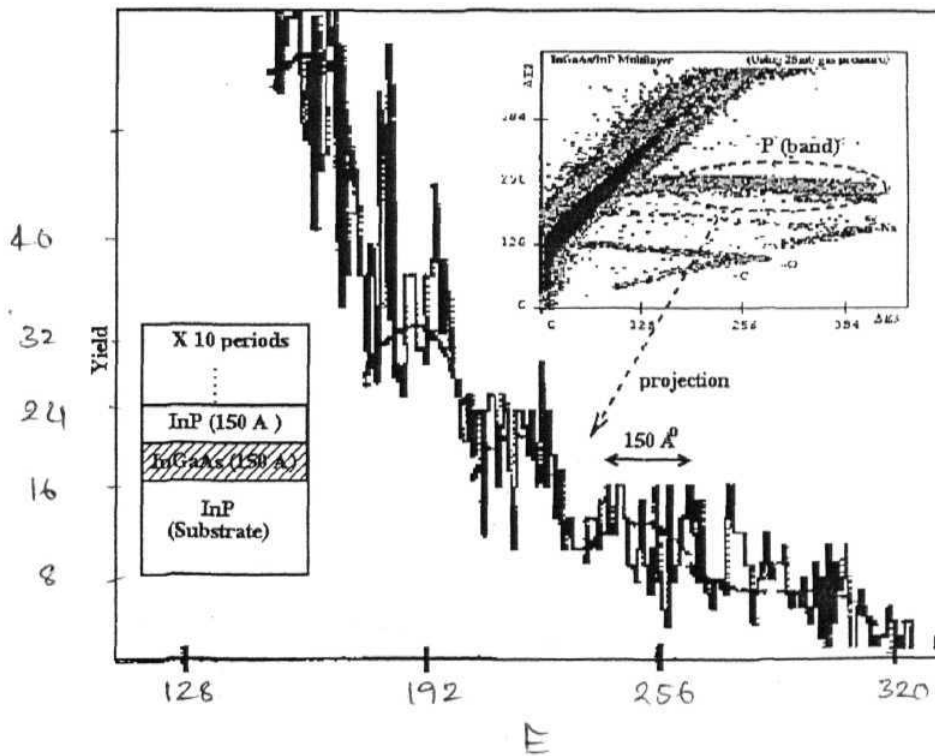


Fig. 3.17: Projection of P band from the AE3-AE2 shown in the upper inset.

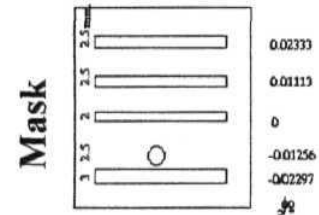
Lower inset shows the sample structure.

3.1.5.2 Position sensitivity

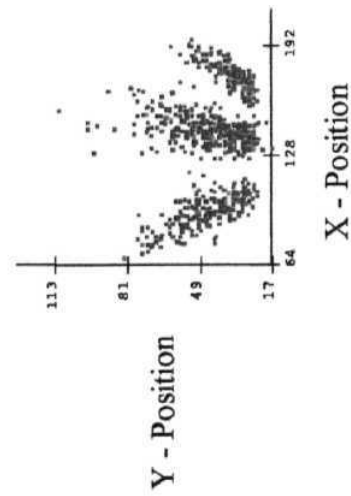
Position information is obtained and plotted using the methods and formulae mentioned in the section 3.1.3. Two dimensional position sensitivity of the detector has been tested using a mask placed in the intermediate chamber (cross). Fig. (3.18a) shows the measured X-position spectrum when a mask shown in the inset was placed in front of the detector window. Fig. (3.18b) is the same spectrum when the mask was swapped (rotated by 180°). This swapping is reflected in the position spectrum. The width and the height of the various peaks depend on the dimensions of the corresponding slit. In addition to this the height of the peak depends on the recoil angle because the recoil cross-section is a function of recoil angle. This fact can also be observed from fig.(3.18). This figure also shows the relation between X-position and the recoil angle (Φ) or $\delta\Phi$ (wrt 55°). This calibration can directly be used for kinematic corrections. All these spectra were measured with the Backgammon on the cathode in GPSC. The improvement in the position signals after changing the Backgammon structure to the $\Delta E2$ anode and the further improvement due to the potential gradient are shown in figure (3.19). This figure shows the 2D spectra measured using mask with four vertical slits and one hole. The importance of uniform and homogeneous electric field between the detector plates is clearly highlighted in this figure. Here the potential gradient circuit has improved the linearity of the 2D patterns obtained using $\Delta E2$ Backgammon. This non-linearity of the 2D spectrum has been corrected by software in other labs. Here we got perfect linear 2D patterns directly from the experiment with no further treatment. Position resolution of the detector is found to be better than $2mm$ from this data. We have used this position information for implementing the kinematic corrections. A direct calibration for the X-position spectrum to $\delta\Phi$ has been obtained from the above mentioned data and has been used for kinematic corrections.

2D Position Spectra Obtained from Mask Using LAPSDT.

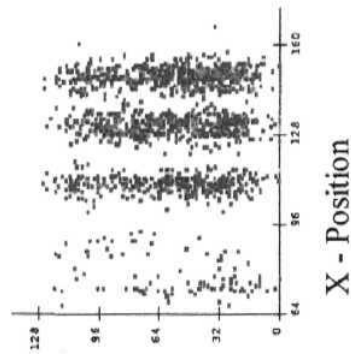
- A- Potential Gradient Off
- B- Potential Gradient On
- C- Mask Swapped



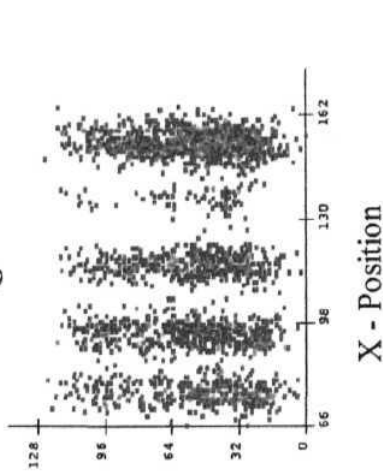
2D Patterns: A



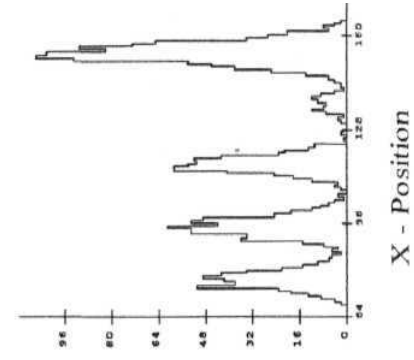
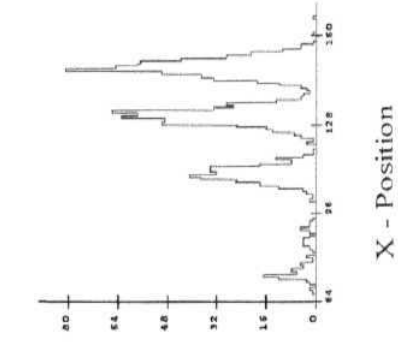
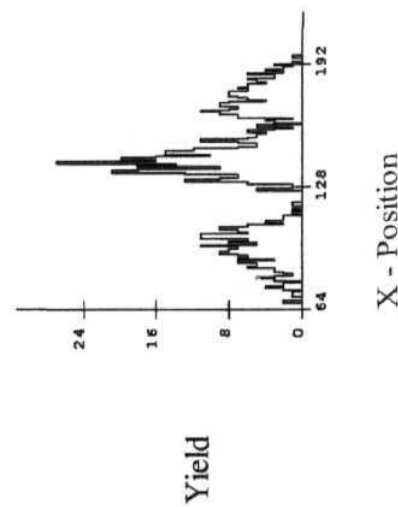
B



C



Projection on X-Axis



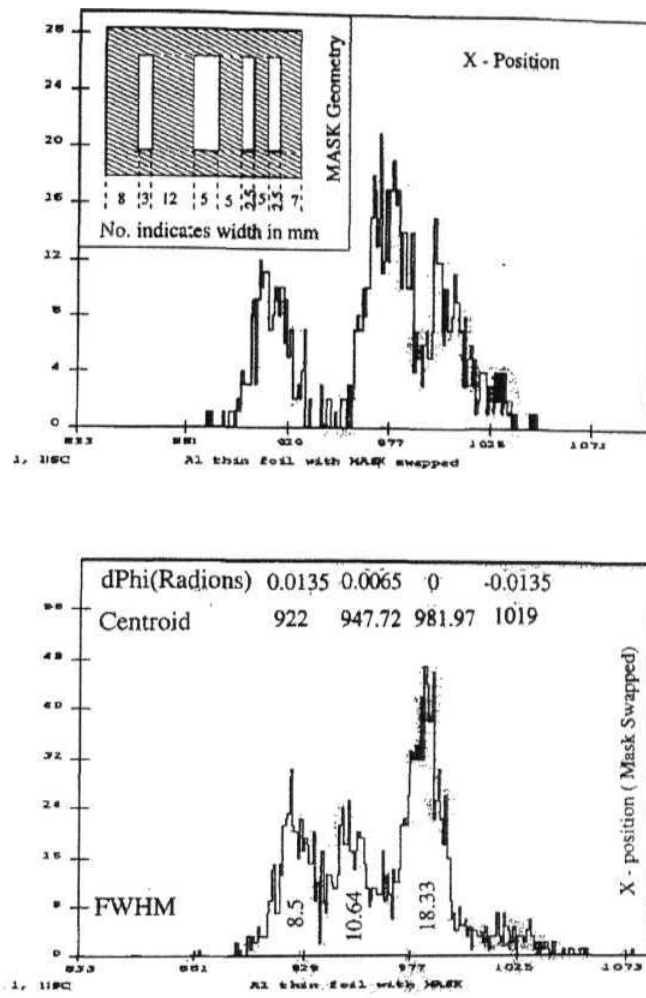


Fig. 3.18: X-Position (a) Top one: with mask and (b) Lower one: when mask swapped

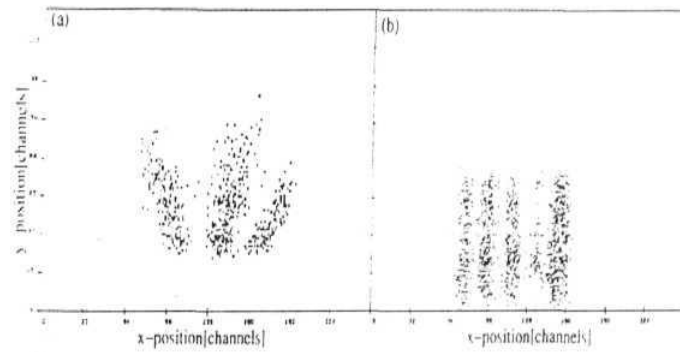


Fig. 3.19 (a): The image of the mask when potential gradient was not used. (b): The image of the same mask when the potential gradient was used for field homogenization.

3.1.5.3 Kinematic corrections & depth profiling:

The necessity of the kinematic corrections with large solid angle detection has been discussed in the previous chapter and in some of the previous sections of this chapter. The present detector has a large acceptance angle ($\delta\Phi \sim 2^\circ$ to 4°) and hence will detect the recoils with recoil angle ranging from $\Phi - \delta\Phi$ to $\Phi + \delta\Phi$ instead of a single recoil angle Φ . The recoil energy ($E = K\cos^2(\Phi)$) is a function of the recoil angle and hence the recoil energy spectrum will be broadened due to this large acceptance angle. This kinematic spread ($dE/E = -2 \tan\Phi d\Phi$) in the energy spectrum will deteriorate the depth resolution of the technique. Hence kinematic corrections are necessary to improve the depth resolution. We can either use the above mentioned formula or even a simpler formula given below for correcting these kinematic effects if we can record the position information. Kinematic corrections have been implemented for all the experiments performed in GM chamber.

$$E_\phi = E_{\phi \pm d\phi} \left(\frac{\cos^2(\phi)}{\cos^2(\phi \pm d\phi)} \right) = E_{\text{detected}} \left(\frac{\cos^2(\phi)}{\cos^2(\phi + d\phi)} \right) \quad (3.1)$$

Where $d\phi$ is measured experimentally from the position information. Hence for the experiments performed in GM chamber ($\Phi=55^\circ$) we can simplify the above equation as

$$E_\phi = E_{\text{detected}} \left(\frac{0.3289899}{\cos^2(0.9594 + d\phi^c)} \right) \quad (3.2)$$

Example 1 (Calibration sample): The calibration sample considered as a first example for z - identification in section 3.1.5.1 has been considered once again in this section. The above mentioned corrections have been implemented in the E_{total} . In addition to this, we have implemented corresponding correction in AE_1 signal also. AE_1 is inversely proportional to E_{total} because the stopping power of any ion in the gas/any medium is inversely proportional to its initial energy. We have derived and used the following formula to implement the correction in ΔE_1 signal for the first time.

$$\Delta E_1(\phi) = \frac{K}{E_{total}(\phi)} \quad (3.3)$$

$$(\Delta E_1)_\phi = (\Delta E_1)_{\phi \pm d\phi} \left(\frac{\cos^2(\phi \pm d\phi)}{\cos^2(\phi)} \right) = (\Delta E_1)_{detected} \left(\frac{\cos^2(\phi \pm d\phi)}{\cos^2(\phi)} \right) \quad (3.4)$$

For the present case

$$(\Delta E_1)_\phi = E_{detected} \left(\frac{\cos^2(0.9594 + d\phi^c)}{0.3289899} \right) \quad (3.5)$$

ΔE_1 - E_{total} spectra have been obtained after implementing the corrections in E_{total} and both in E_{total} and ΔE_1 . Fig. (3.20) shows the projections of three different bands (Cu, Si & c) on the E_{total} axis. These results confirm the improvements in the separation of bands / depth resolution obtained after implementing the kinematic corrections.

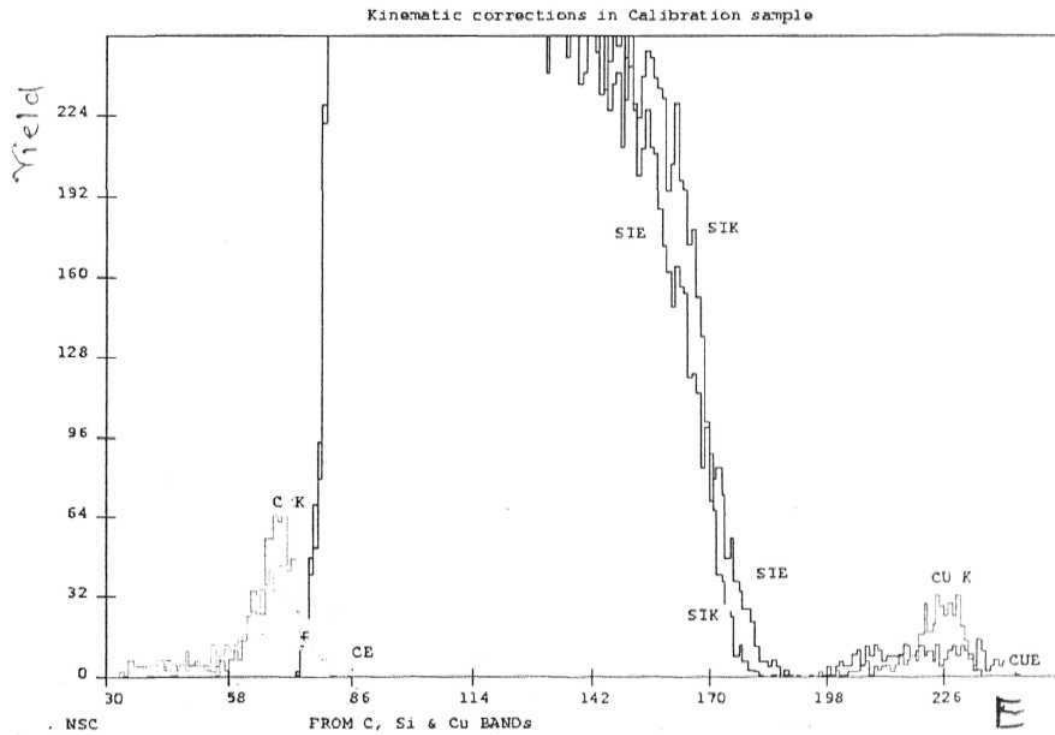
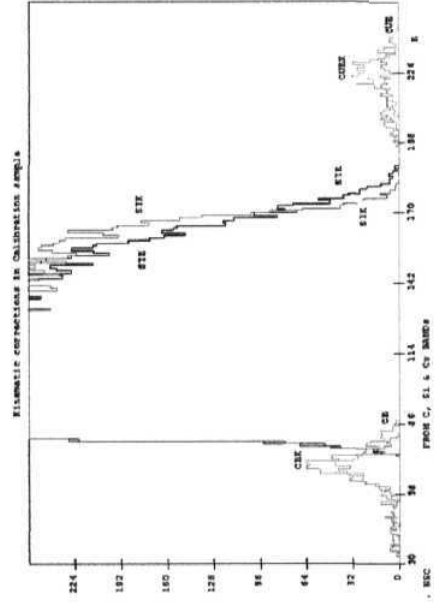


Fig. 3.20: Projections of uncorrected and corrected C (CE & CK), Cu (CUE & CUK) and Si (SIE & SIK) bands obtained from Calibration sample. (axes X: E_{total} , Y: Yield).

Example 2 InGaAs/GaAs sample: This sample has been used in different experiments

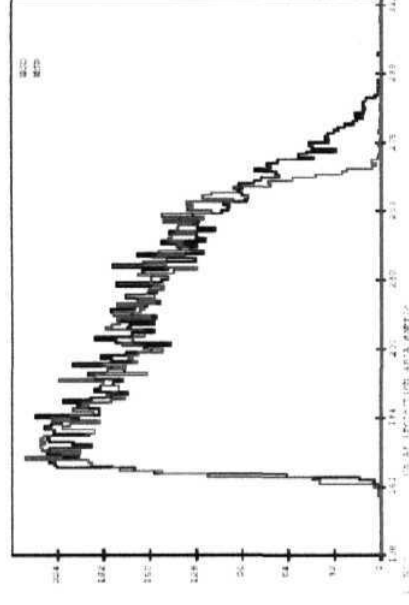


Calibration Sample

Kinematic Corrections
Resolution improved
From 14% to 3.7%

Kinematic Corrections

In_{0.1}Ga_{0.9}As(400Å)/GaAs



presented in chapters 4 & 5. This is a single In_{0.1}Ga_{0.9}As (400Å⁰) layer grown on GaAs substrate. Ga and As bands could not be separated because these elements are coming from depth also. "In" band could be separated in ΔE_1 - E_{total} spectrum shown in fig.(3.21). Kinematic corrections have been used from the mask data presented in the previous chapter. $d\Phi$ ($= mX_{\text{pos}} + c$) is directly obtained ($m= 0.0000937$ & $c= -0.00609$) from the calibration data obtained from the mask as shown in fig.(3.18). Figure (3.22) shows the projection of Ga/As band on the E_{total} axis of both corrected and uncorrected data. The depth resolution has been improved to 3.4% from 14% after implementing the kinematic corrections.

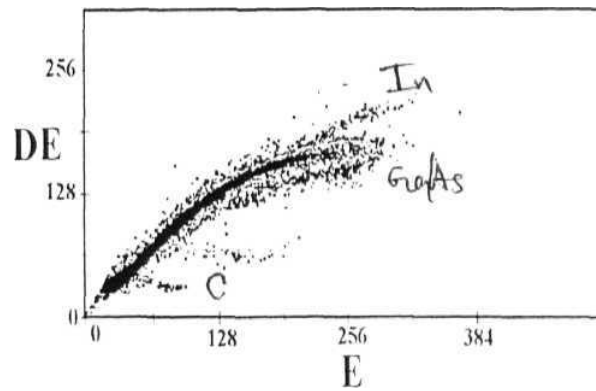


Fig. 3.21: AE - E Spectrum obtained from 400Å In_{0.1}Ga_{0.9}As/GaAs Sample

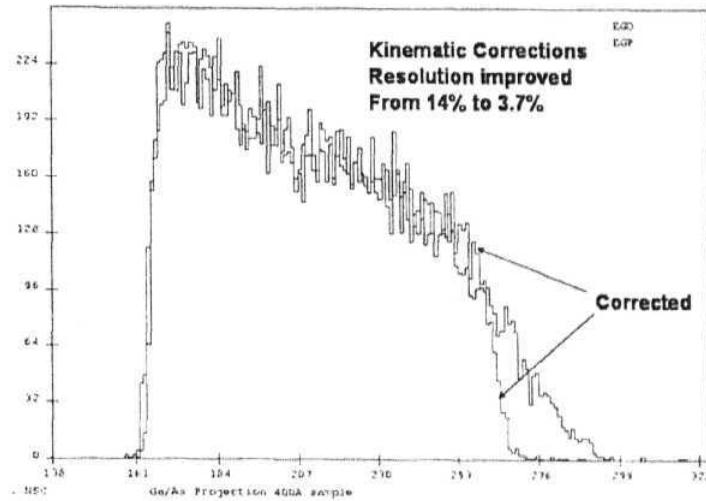


Fig. 3.22: Projection of Ga/As band of fig. 3.21 on Energy axis.
(axes X: Energy & Y: Yield)

3.2 DEVELOPMENT OF AN AUTOMATED HIGH ENERGY CHANNELING FACILITY

The importance and applications of ion channeling technique have been discussed in previous chapters. Moreover the technical importance of strain measurements/modification in SLS and the objective of this thesis work have also been emphasized in the first chapter. High energy channeling is necessary for strain measurements. Further details will be presented in the 5th chapter. Here we discuss only the development part of the facility with brief introduction. Presently there are two channeling facilities are available for material analysis in India. One at the *IIT Kanpur* is not suitable for strain measurements due to non availability of sufficient high energy ions [15, 16]. The other facility at *IOP Bhubaneswar* with 3.5 MeV He is suitable in this sense [17] but there are some problems in measuring very low strains [18] due to the limitations on the step size of various rotations of the goniometer (for example 0 step is 0.1°). In addition to this the goniometer is manually operated. Many channeling experiments [19] have been performed on this system but it may not suit for measuring exact values in the case of low strains. Hence we have developed an automated high energy channeling facility for performing strain measurements [20]. However other usual channeling experiments can also be performed as well.

In ion channeling one can find the axis direction by experimentally plotting the scattered/recoiled yield versus the sample tilt angle (called angular scan). Strain measurements are based on the determination of the direction of the off-normal axis of strained layer, which is shifted with respect to that of substrate. This small shift ($\Delta\psi$) between epilayer and the substrate gives a measure of strain ($\Delta\psi/\sin\psi\cos\psi$). Hence the accuracy of the strain measurement by RBS/channeling depends on the sharpness of the angular scan. The FWHM of this curve is directly related to the channeling critical angle which has one over square root relation to the incident energy. Hence the angular scans will be sharp in high energy channeling thereby the strain resolution and the sensitivity of the method are improved [15, 16]. If the energy is too low then the results are mislead by

steering effect due to the broad critical angles [15-17]. In high energy case, heavy ions can be used for a reasonably high scattering cross-section and also to avoid the possible nuclear reactions. However there are two major difficulties with high energy heavy ion channeling. First of all the alignment becomes difficult due to small critical angle. The other difficulty is to minimize the radiation damage. One can address to both of these problems up to a considerable extent by using an automated program for aligning the sample and also for collecting necessary spectra on an integrated control and data acquisition system. Radiation damage can be minimized by keeping low fluence. The use of LAPSDT in conjunction with ERDA for performing channeling/blocking-ERDA experiments will improve the measurement quality because of the higher recoil cross-sections and Z - identification. Presently the system is ready for such an experiment but the present experiments are performed with small usual SSBDs (Surface barrier detector) only. Irradiation time has been greatly reduced by using the currently developed automated system and also by using a separate detector at forward angles for alignment process. Following sections describe the development, operation and results obtained using this facility and further details regarding the strain measurements are presented in chapter 5.

3.2.1 Development and operation of the facility

An automated high energy channeling facility has been developed at Nuclear Science Center, New Delhi, using the existing goniometer (HV) and other facilities in the materials science beam line.

3.2.1.1 Beam collimation and Sample alignment

Figure 2.3 shows a schematic diagram of the material science beam line. There is a double slit existing in front of the high vacuum chamber for ERDA experiments. We use this slit in conjunction with the newly installed (in front of the goniometer chamber) double slit to get fine collimated and parallel beam. The double slit shown in fig.(3.23a) has been designed and fabricated at NSC workshop as a part of the development of channeling facility. The internal structure of the slit is shown in fig.(3.23b). Tantalum sheet mounted at the inner end of the Wilson based screw can be

moved from outside for cutting the beam. Four such sheets were there to cut the beam from all four sides. These two slits (HV & GM) which are separated each other by roughly around 4m can form a well defined collimated (parallel) beam which is an important requirement for channeling experiments. The angle of incidence can also be kept constant with the use of these well separated slits. Necessary arrangements have been made for laser alignment. The sample will first be aligned with a fine collimated laser beam before starting the actual channeling experiment.

3.2.1.2 Sample holder and degrees of freedom

A sample holder (shown in the inset of fig. 3.24) has been made using G10 with spring ball locking system. A metal (AP) sheet pasted on this G10 sample holder will give target current and the whole sample holder is electrically isolated from the body of the experimental chamber because it is made of G10. This will reduce the possibility of having short ckt problems in the target current measurements. The goniometer sample ladder has six degrees of freedom of which three are translational and the other three are rotational (R1, R2 & tilt). The axis of rotation of R1 ($\theta = 360^\circ$, with step 0.018°) is in the vertical plane and is perpendicular to scattering plane while that of R2 ($\Phi = 200^\circ$, with step 0.0125°) is parallel to beam direction. The axis of rotation of tilt (7° , with step 0.001°) lies in the scattering plane and is perpendicular to beam directions. These details are depicted in fig.(3.24). This figure also shows a photograph of the goniometer sample ladder with a sample mounted on it. All these rotations can be controlled remotely using the stepper motor controls provided with the goniometer. Suitable software and hardware have been developed to control this precision goniometer using the CAMAC based data acquisition system.

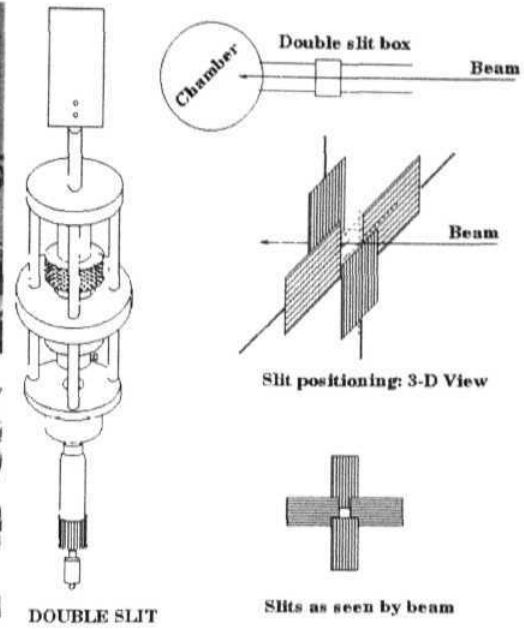
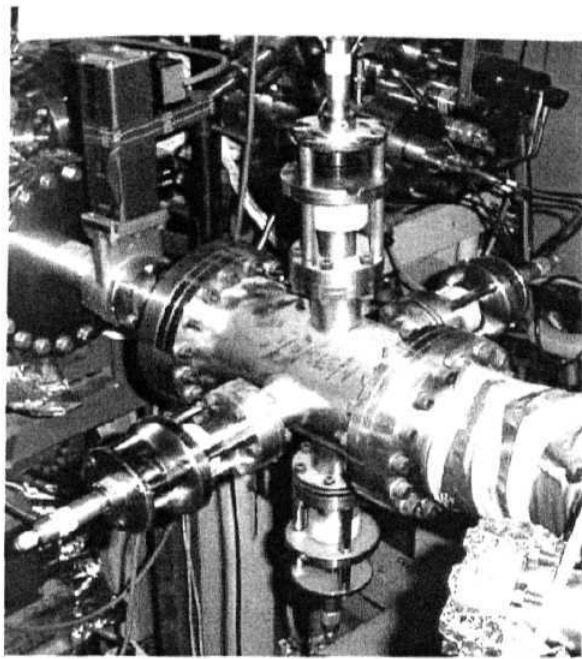


Fig. 3.23a:

Fig. 3.23b:

Fig. 3.23 Double slit made for GM chamber a) Image & b) Inner structure

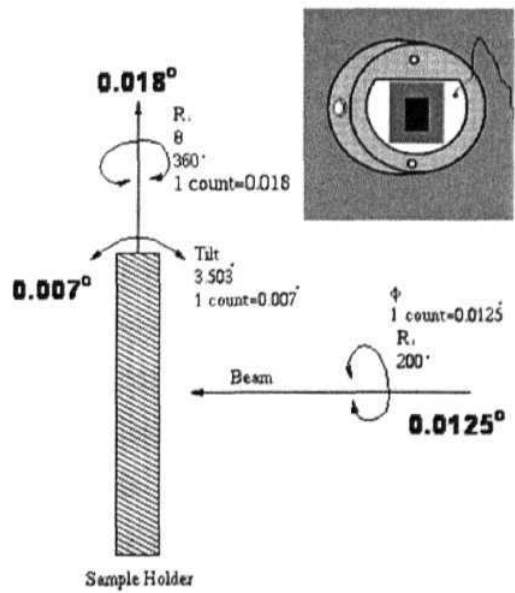


Fig. 3.24: GM Sample ladder and its degrees of freedom (inset: G10 Sample holder)

3.2.1.3 Automation and operation

Compatible software routines are written in C/C++ to integrate the existing data acquisition system (Freedom [14]) with the goniometer control. A CAMAC module has been designed and installed to instruct the stepper motor controls through data acquisition system. Any or all of the rotors can be initialized to their lower limits using the "Initialize" command. At a given time only one rotor can be operated while the other two can be initialized if required. Every time, the active rotor will first be initialized to its lower limit and then it will reach to the specified initial value. This method is used to avoid the possible backlash and also to keep the reference of rotor position during the power failure. Once initialized, the rotor will reach the final value in a given number of steps. Required spectra will be collected at each angle (step) for a given amount of time. At every interval the incident current will also be recorded using a CAMAC based Scalar module which is normally inputted by a digital current integrator. The program will also draw the online normalized angular scan corresponding to a given energy window. However the normalization is only optional. The program is user friendly and all inputs can be fed through popup windows shown in fig.(3.25). All the data can be saved event by event in list mode configuration. Offline routines have also been developed to obtain the angular scans from different energy windows depending on the requirements.

3.2.1.4 Experimental Procedure and Results:

40 MeV Si ions delivered from the 15MV Pelletron accelerator of NSC have been used as incident beam. A pair of double slits (described above) separated by roughly around 4m was employed to define the incident angle and also to get the fine and parallel beam. Two SSB Detectors were placed at 60° and 110° for alignment and data collection respectively as shown in Fig.(3.26). Forward angle was used for alignment process so as to reduce the irradiation time while back angle was used to improve the energy resolution. Channeling studies have been performed on the strained In_{0.1}Ga_{0.9}As layer grown on GaAs substrate at SSPL, Delhi using Molecular Beam Epitaxy (MBE). Three samples with different layer thickness (100 Å⁰, 250 Å⁰ & 400 Å⁰) have been investigated. However here we present only one channeling angular scan obtained from In_{0.1}Ga_{0.9}As

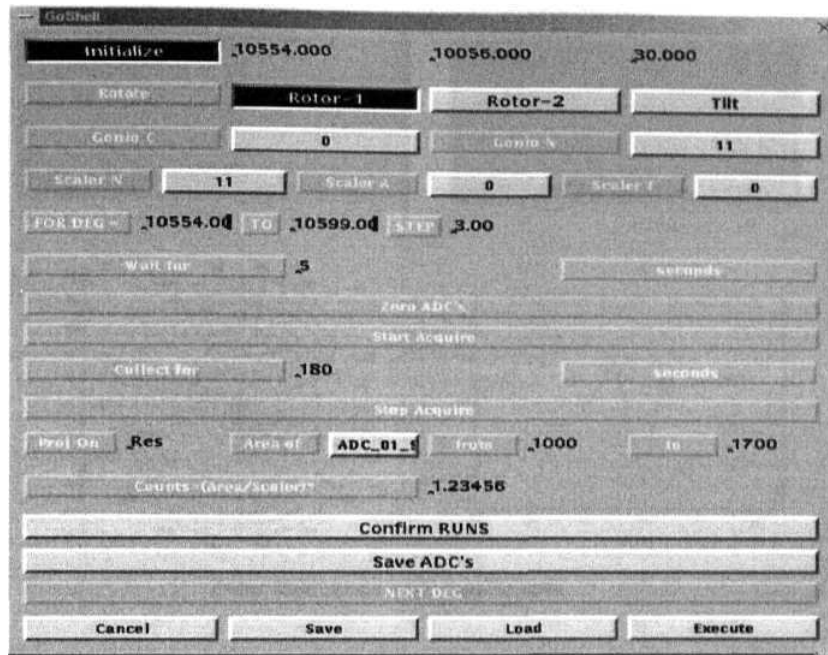


Fig. 3.25: Pop - Up window for accepting inputs to the automation program

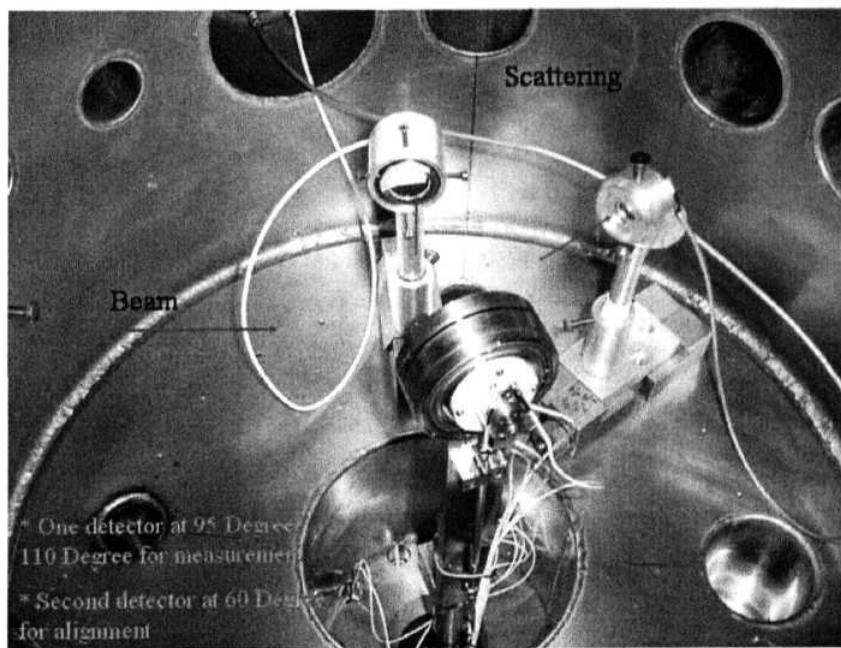
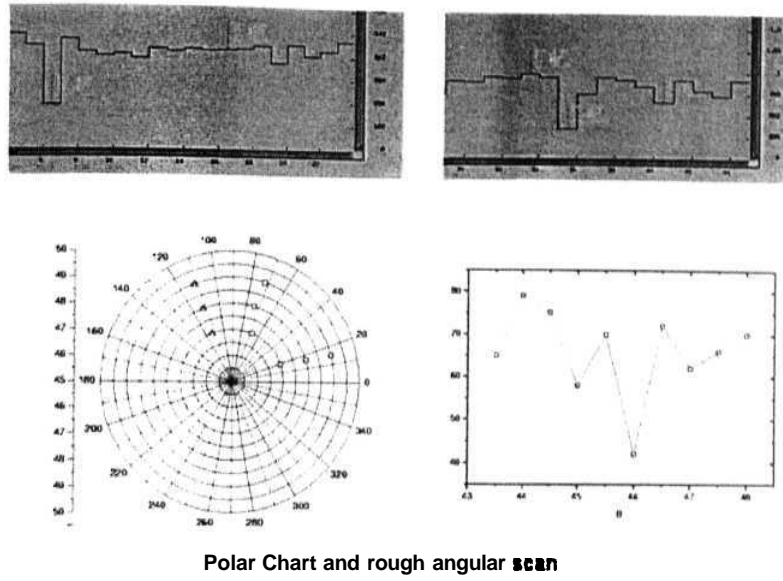


Fig. 3.26: Experimental setup for channeling measurements

* **scans** performed by automation **program**



Polar Chart and rough angular scan

Fig. 3.27: Φ Scans, Polar Chart & rough angular scan obtained using the automation program while searching for $\langle 110 \rangle$ axis.

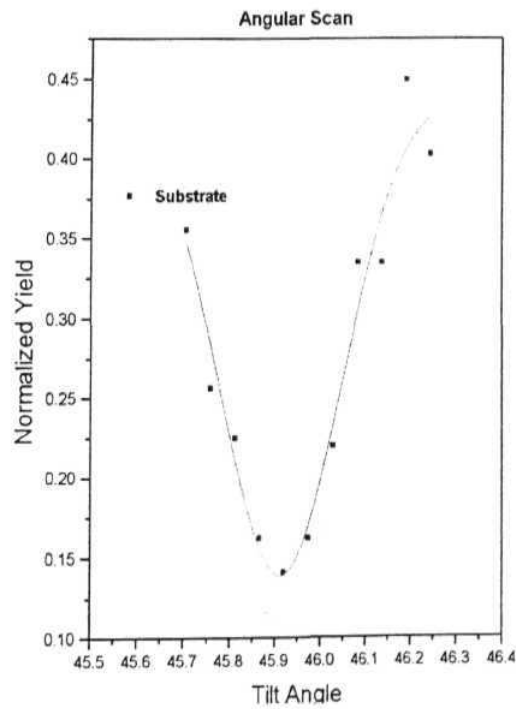


Fig. 3.28: A sample angular scan obtained from the substrate of $\text{In}_{0.1}\text{Ga}_{0.9}\text{As}$ (100\AA^0) / GaAs sample

We have followed the standard polar chart method [21] to locate the required axis. Fig(3.27) shows some Φ scans recorded while searching for planar dips as a part of alignment process. Fig.(3.27) also shows a polar chart used for mapping the axis and Fig(3.28) shows a sample angular scan obtained from the substrate of $\text{In}_{0.1}\text{Ga}_{0.9}\text{As}$ ($\text{Ga}_{0.9}\text{As}$)/GaAs sample. From this figure one can observe the good reduction of yield in channeling condition.

33 CONCLUSION

Good z-separation and depth resolution have been observed from the LAPSDT data [1]. The kinematic broadening caused by the large solid angle is taken care by implementing kinematic corrections in all the LAPSDT based ERDA experiments presented in this thesis. Large solid angle could be used to minimize the radiation damage during the measurement with the help of position sensitivity. 2D position sensitivity has also been obtained and the angular resolution is found to be better than the required value ($<0.1^\circ$) for measuring structural effects like blocking/ERDA patterns. Hence Channeling/Blocking - ERDA, Transverse heating/cooling of channeled ions, on-line radiation damage / modifications, sputtering and many such studies can be performed using this detector. Some of such experiments have already been performed by several users of NSC.

The "automated high energy channeling facility" has been tested and found to be working consistently. The facility has been checked three times in three different runs. Reasonably good reduction is obtained from all the scans that have been performed on epilayers. This facility has been used to measure the strain in the above mentioned samples. This facility can be used to perform any channeling/blocking experiments. It can give the information related to crystalline quality. Most importantly on-line damage studies can be performed to understand the SHI interaction with the crystal lattice. It is possible because the SHI beams are used for probing the crystalline quality and these beams can also be used to modify the crystal structure and other parameters. Such studies combined with blocking/ERDA will have more applicability in understanding the ion

solid interactions [22]. This technique then can be used for introducing the controlled damage in solids. Studies like ion beam induced amorphi-sation and re-crystallization can also be performed using this facility. Overall facility developed in this work is shown in fig. 3.29.

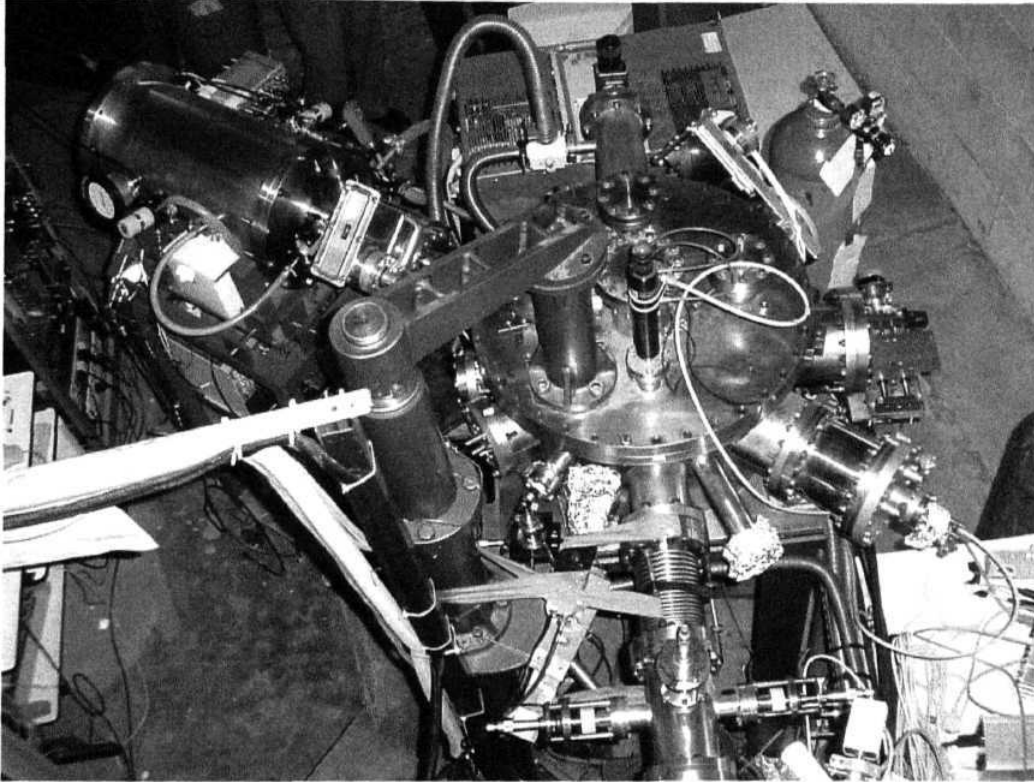


*Fig. 3.29: Image of the complete facility (LAPSDT & Channeling)
developed as a part this thesis*

3.4 REFERENCES

1. Development of a Large Area two dimensional Position Sensitive AE-E Detector Telescope, S. V.S. Nageswara Rao et. al. *NSC (New Delhi) annual report 63*, (2001-2002); Effect of field homogenization on position sensitivity of LAPSDT, S.A. Khan, S.V.S. Nageswara Rao et. al., *NSC (New Delhi) annual report 65*, (2001-2002); *Submitted an abstract to ICACS 20, Puri, India.*

3. Radiation Detection and Measurement, G.K. Knoll, *Wiley publishers*, (1999 3rd edition)
4. W. Assmann, *Nucl. Instrum. Meth.* B64, 267 (1992); W. Assmann, P. Hartung, H. Hurber, P. Staat, H. Steffens, and Ch. Steinhausen, *Nucl Instrum. and Meth.* **B85**, 726(1994).
5. H. Timmers, R.G. Elliman, T.R. Ophel, *Nucl. Instrum. Meth.* A447, 536 (2000).
6. S. Ghosh, D.K. Avasthi, T.Som, A. Tripathi, S.K. Srivastava, S.V.S. Nageswara Rao, F. Gruner and Walter Assmann, *Nucl. lustrum. Meth.* B190(1-4), 169 (2002); *NSC(New Delhi) annual report* 61, (1999-2000)
7. H. Timmers, T.D.M. Weijers, R.G. Elliman, *Nucl. lustrum. Meth.* B190, 393 (2002).
8. T.D.M. Weijers, H. Timmers, R.G. Elliman, *Nucl. lustrum. Meth.* **B190**, 397 (2002).
9. O. Bunemann, T.E. Cranshaw, J.A. Harvey, *Can. J. Res. All*, **191**, (1949).
10. T.E. Bortner, G.S. Hurst, W.G. Stone, *Rev. Sci. Instr.* 28, 103 (1957).
11. V. Palladino, *Nucl. lustrum. Meth.* B148, 35 (1978).
12. D.K. Avasthi and W. Assmann, *Current science* 80, 1532 (2001)
13. G. Rosner, B. Heck, J. Pochodzalla, G. Hawatsch, B. Kolb and A. Micazika, *Nucl. lustrum. Meth.* B188, 561 (1981).
14. FREEDOM, The LINUX based data acquisition system at NSC, B.P. Ajit Kumar, Et. al, *SANAI-97 held at BARC* on 5th Feb. (1997).
15. A.P. Pathak, S.V.S. Nageswara Rao, Azher M. Siddiqui, *Nucl. Inst. and Meth.* **B161-163**, 487 (2000).
16. Azher M. Siddiqui, S.V.S. Nageswara Rao, Anand P. Pathak, V. N. Kulkarni, R. Kesav Murthy, Eric Williams, Daryush Ila, Claudiu Muntele, K.S. Chandrasekaran and B. M. Arora, *J. Appl. Phys.* 90, 2824 (2001).
17. Azher M. Siddiqui, Anand P. Pathak, B. Sundarvel, Amal K. Das, K. Sekhar, B.N. Dev and B.M. Arora, *Nucl. lustrum. Meth.* B142, 389 (1998).
18. A.P. Pathak, S.V.S. Nageswara Rao, A.M. Siddiqui, G.B.V.S. Lakshmi, S.K. Srivastava, S. Ghosh, D. Bhattacharya, D.K. Avasthi, D.K. Goswami, P. V.

- Satyam, B.N. Dev and A. Turos, *Nucl. Insrt. Meth.* B193, 319 (2002).
19. B.N. Dev *Nucl. Insrt. Meth.* B156, 258 (2002) *and refs. there in.*
20. Development of Automated High Energy Channeling Facility at NSC, S.V.S. Nageswara rao, et. al., *NSC (New Delhi) annual report*, 66 (2001-2002).
21. W.K.Chu, J.W.Mayer, M.A.Nicolet, Backscattering spectrometry, *Acad. Press*, New York, (1978).
22. D.K. Avasthi, W. Assmann, H. Huber, H.D. Mieskes and H. Nolte, *Nucl. Instrum. Meth.* B142, 117(1998).

CHAPTER IV

ION BEAM MIXING AND STRAIN ENGINEERING

This chapter gives the details of irradiation and the characterization techniques performed to study the effects of ion irradiation on the crystalline and interface quality, composition / diffusion / mixing effects and the thickness of the individual layers. It is shown that the strain can be tuned using the SHI mixing without loss of the crystalline / interface quality. Thickness and fluence dependence studies have been performed on single layer samples. Effects of annealing (RTA) have also been discussed. The possibility of on-line monitoring and controlled modification of strain is shown in this work.

4.1 INTRODUCTION

As discussed in previous chapters, the integration of optoelectronic devices needs different bandgaps to be accommodated on a single wafer because photonics circuits demand different bandgaps for different devices. For example if we have to integrate a laser, wave-guide and any other optical device like a photo-detector then we need to choose different bandgap for wave-guide so as to reduce the absorption loss. Moreover, most of the time optical devices require alignment to within fractions of a micron and they should be stable under the operational conditions. Hence efficient circuits cannot be fabricated using discrete optical components. So spatial bandgap tuning of heterostructures and multilayer is important. Meeting such bandgap requirements is quite difficult during the growth. The alternative way then would be to alter the bandgap after growing the structures. Compositional disordering and mixing at the interface by Ion

Implantation and subsequent thermal annealing is normally employed [1-3]. An ion beam of a given fluence can cause intermixing of atomic layers at the interface, a phenomenon called Ion Beam Mixing.

Ion beam mixing has become simple and promising technique because the diffusion/migration of different elements is enhanced by the large concentration gradients exist at each interface. Although these structures are inherently metastable due to these concentration gradients, they are shown to be quite stable under normal operation even at elevated temperatures like 900° C [4]. Increase in temperature beyond a point, say critical temperature t_c (900° C for InGaAs based structures) causes the intermixing, but it cannot have any spatial selectivity. The value of this t_c can be reduced to a lower value say t_c^1 (around 600° C for InGaAs based structures) by creating some defects like vacancies and interstitials which enhance the diffusion process. Ion irradiation or implantation is found to be more suitable for introducing such defects. Suitable masks can be used to selectively implant the defects over specified area on a wafer and then the temperature of this wafer can be elevated to t_c^1 so as to get different bandgap on these selected spots while the bandgap in the other areas is unchanged. Lot of study has been performed to obtain this planar technology.

Xia et. al [4] gave a detailed review of the ion beam mixing of semiconductor superlattices along with several suitable characterization techniques including HRXRD. They gave an example [5,6] in which AlGaAs alloys were made at the selected areas on an AlAs/GaAs superlattice using Zn ion implantation and subsequent thermal annealing. It is interesting to note that the AlGaAs alloy stays as a single crystal and epitaxial to the surrounding superlattice regions. Since this discovery, impurity disordering in the temperature range of 600° C -900° C has been reported in many III-V compound semiconductor systems [7-12]. Charabonneu et. al [1] have shown that the blue shift occurs' in the QW bandgap of a QW laser due to ion irradiation and subsequent thermal annealing. InGaAs/GaAs and InGaAs/InP based laser structures have been studied using the photoluminescence (PL) as a diagnostic tool. The PL peak position was shown to be shifted due to the mixing effects. The broadening and distortion of PL spectrum of high

fluence sample (8.56 MeV As irradiation at 2.5×10^{14} ions/cm²) shows the structural deterioration of the QW laser. Hence different bandgaps can be obtained without loss of the sample quality by keeping the fluence below this value. The well thickness of the irradiated sample was also observed to be increased, using the cross-sectional TEM. In another experiment reported in 1999 [13], they have directly shown the shift in the emission wavelength of an ion mixed QW laser. The bandgap-tuned laser was characterized in terms of threshold current density and external quantum efficiency. They exhibit blue shift in the lasing spectra up to 63nm. This allows laser with a range of tuned wavelengths to be fabricated from a single wafer. Glodberg et. al [14] reported similar experiments in 1997. They have shown the emission spectra of four laser diodes produced from a single semiconductor wafer. The effects of multiple implants on the mixing of AlAs/GaAs have been studied by Venkatesan et. al. [15] using TEM and SIMS, to form AlGaAs alloy layers. The influence of ion mass and fluence on the intermixing of GaAs/AlGaAs quantum well structures using PL and SIMS has been studied in detail by H. Leier et. al. [16]. Diffusion length for Al was measured and compared with the existing theory. Many more experiments have been performed to study the ion beam mixing in semiconductor multilayers in this low energy region.

We study the effects of SHI irradiation on different properties of these materials. This SHI induced mixing, rather than the implantation and subsequent thermal annealing, is more suitable for the integration of optoelectronic devices because of the advantage that the interface mixing can be confined to a narrow region at the interface as against the lateral straggling effects in low energy ion implantation. Moreover SHI mixing studies attain importance from the fundamental need of understanding the energy transfer mechanism in this energy region. The high-energy beam loses its energy to the electronic subsystem of the target material. Then this energy will be transferred to the lattice atoms via the electron phonon coupling. There are two models namely "Coulomb explosion model [17]" and the "Thermal spike model [18]" to explain such energy transfer mechanisms. According to the Coulomb explosion model, a positive ion core along the ionizing path of the energetic beam repels the nearby atoms. This causes a radial motion of the atoms sitting around this core. This model is applicable for the

insulators like polymers. Thermal spike model assumes that the inelastic energy loss of the energetic beam produces a very high temperature, which exists for a very short time, thereby called as thermal spike. During the spike period the material will melt because these temperatures are very well above the melting temperatures. Diffusion occurs in this molten state but it cannot come back to the equilibrium because of the rapid quenching. Thermal spike is shown to be more responsible for the mixing occurring at the metal-metal and metal - semiconductor interfaces. SHI induced mixing (in various systems like metal-metal, metal-semiconductor and semiconductor-semiconductor) has been recently studied by several authors [19,20]. The basic thrust of such work is to understand the above mentioned energy transfer mechanism as well as to make new materials for novel device applications. Very few such studies have been reported in SLS.

Here we studied the effects of 130 - 200 MeV Ag ion irradiation on the $\text{In}_{0.53}\text{Ga}_{0.47}\text{As}/\text{InP}$ based lattice-matched and strained InGaAs/GaAs single layers / superlattice structure by HRXRD, and RBS/Channeling. Experimental details regarding the growth, irradiation and characterization are given in chapter2. The band structure of these materials depends on the thickness, atomic composition and strain of/in each layer. Hence as an initial step, we concentrate on the effects of ion beam mixing on these parameters. Hence the chapter's title is "Ion beam mixing and strain engineering" rather than "Band gap tuning ..." However strain engineering ultimately results in the bandgap modification. To the best of our knowledge, Ion beam mixing and strain engineering experiments of these materials in this high energy (100 MeV to 200 MeV Ag) region have not been reported so far.

4.2 THE P523 (A lattice Matched Superlattice System):

Ion beam mixing experiments have been performed to introduce strain in an initially lattice matched system (P523). RBS/C and HRXRD are used to study these mixing effects. Fig. 4.1 shows the $\langle 100 \rangle$ aligned and the corresponding random spectra of irradiated and unirradiated samples. A reduction up to 7% in the yield of $\langle 100 \rangle$ aligned to that of the random spectra is observed. These spectra show considerably good

crystalline quality of both the samples. Hence it is clear that the irradiation did not affect the basic lattice structure of the sample. $\langle 110 \rangle$ channeling angular scan probes the strain in such lattice mismatched structures [3, 19-24] as discussed earlier. 3.5 MeV He^{++} ions were used for such scans keeping the earlier reported steering effects in view [22-24]. The peak in the random spectra contains the contribution of the GaAs signal from the active superlattice. A very thin bin (about 20 channels) of the central portion of this peak is obtained by suitably subtracting the Indium background. Angular scan performed from such bins corresponds to the GaAs of InGaAs layer. This scan is compared with that of the scan obtained from the InP substrate region.

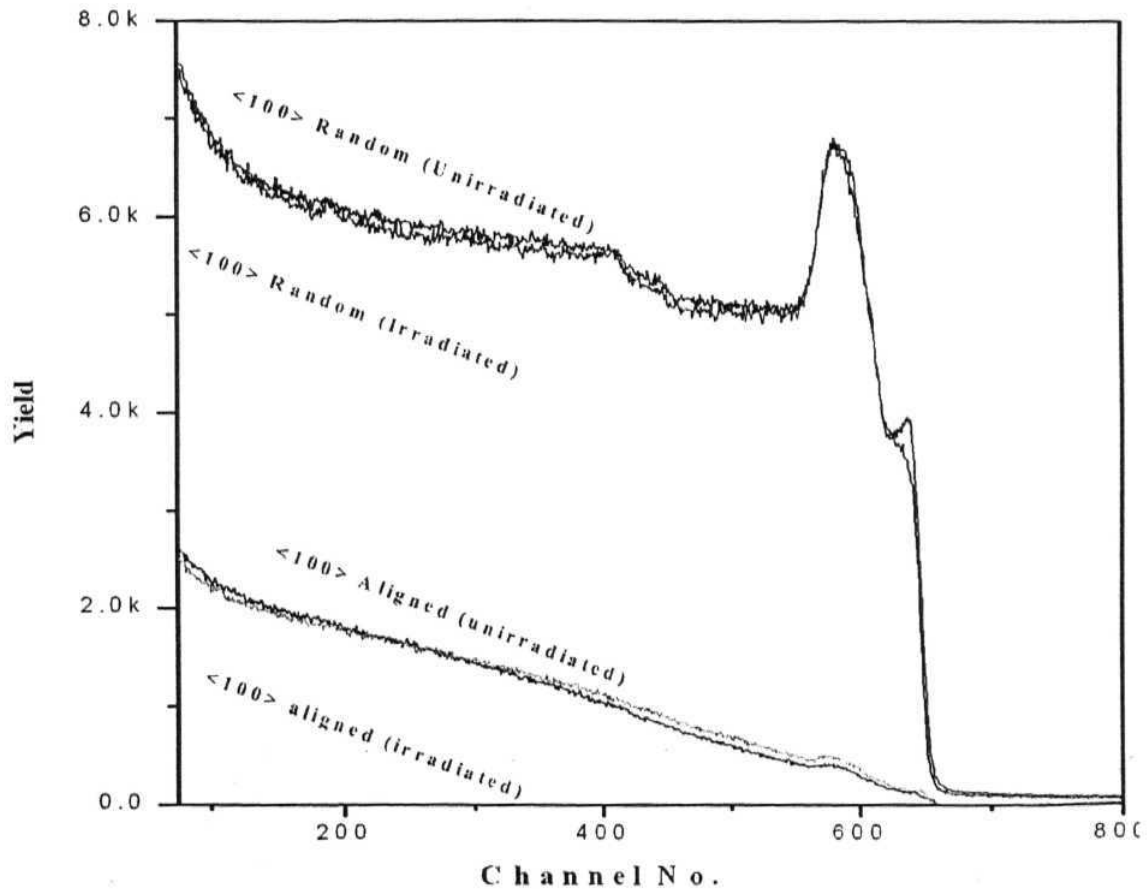


Fig. 4.1: $\langle 100 \rangle$ Aligned and random RBS spectra of P523U and P523 I,

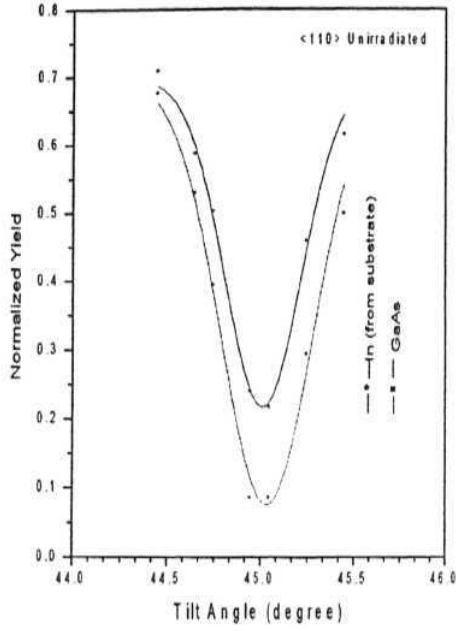


Fig. 4.2a

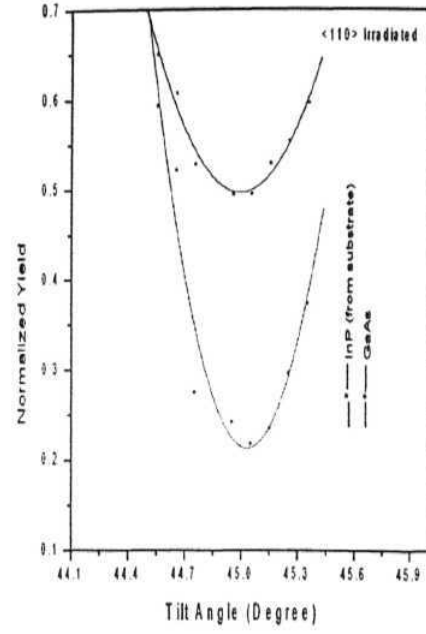


Fig. 4.2b

Fig. 4.2: $\langle 110 \rangle$ Channeling angular scans of (a) P523U and (b) P523I.

Fig. 4.2 a & b show $\langle 110 \rangle$ channeling angular scans of pristine and the irradiated samples respectively. The scan performed on the pristine sample does not show any strain within the experimental error. It is expected because the sample is lattice matched. The $\langle 110 \rangle$ angular scan of the irradiated sample is broadened when compared to that of the pristine sample. This reflects some structural differences at the surface caused by the heavy ion irradiation. Although the scan is considerably broad it has a good minimum indicating that the lattice is intact. Such effects are earlier observed when a thin amorphous layer is deposited on the single crystal silicon [25]. Such thin amorphous layer increases the divergence of the incident beam. However, good channeling spectra can be obtained from the underneath crystal. From fig. 4.2b it is observed that the minimum of InGaAs scan is shifted to about less than 0.1° with respect to that of the substrate, corresponding to a finite tensile strain which is less than 0.35%. The strain value is evaluated using the formula given by eq. 1.22. These measurements suggest the fact that the irradiation introduces a finite tensile strain in an otherwise lattice matched system but it did not allow us to estimate the exact strain values because of the experimental limitations to probe such low strain values.

Fig. 4.3 shows a zoom on the near surface region of $\langle 100 \rangle$ random spectra. The solid line corresponds to the unirradiated sample and the dashed line corresponds to the irradiated sample. The reduction of indium yield and the slope at the surface region of the irradiated spectrum indicates that the indium diffuses from the surface. The peak related to the GaAs also shifts towards the higher energy channels. These channels correspond to the surface Ga or As like atoms. The top InP layer of the pristine sample does not contain such impurities. So it can be inferred from this that there is a migration of Ga or As like atoms to the surface from the underneath layers.

Although the strain values are very low, there is a considerable change in the irradiated sample. Later these values were measured very accurately using HRXRD. Effects of annealing (RTA) have also been studied. Such study was extended to a high fluence (5×10^{13} ions/cm²) sample also. Including the pristine sample in every set, we classify all these samples (P523) into two sets namely low dose samples (P523U, URTA, I & IRTA) and high dose samples (P523U, 12 & 12RTA). Fig.4.4 shows the HRXRD spectra of low dose samples. These spectra are displaced (Shifted upwards) on the intensity axis for clarity. The inset shows the complete interference pattern of P523U. Similar spectra of high dose samples are shown in fig. 4.5. Very high number of satellite orders in the HRXRD spectra shown in these figures, indicate that the interfaces are very sharp and the boundaries are abrupt. Also indicated fact is that these interfaces remain considerably sharp even after irradiation. The width of the substrate peak varies with the material treatment. The narrowest peak (More Lorentzian like) is observed for the as grown sample and the broadest peak (More Gaussian like) is observed for the high fluence sample. This width is reduced by RTA procedure but did not reach the as grown value. This is caused mainly due to the implantation damage in the substrate region (about 13 nm deep). The reduction in the intensity of satellite peaks shows the interdiffusion of elements across the interfaces. Superlattice period and strain values are obtained using the simple HRXRD formulas (given in chapter 1) based on Bragg's law. Measured strain values and other crystal parameters are given in table 4.1. The dependence of strain on the ion fluence (after RTA) is shown in fig 4.6.

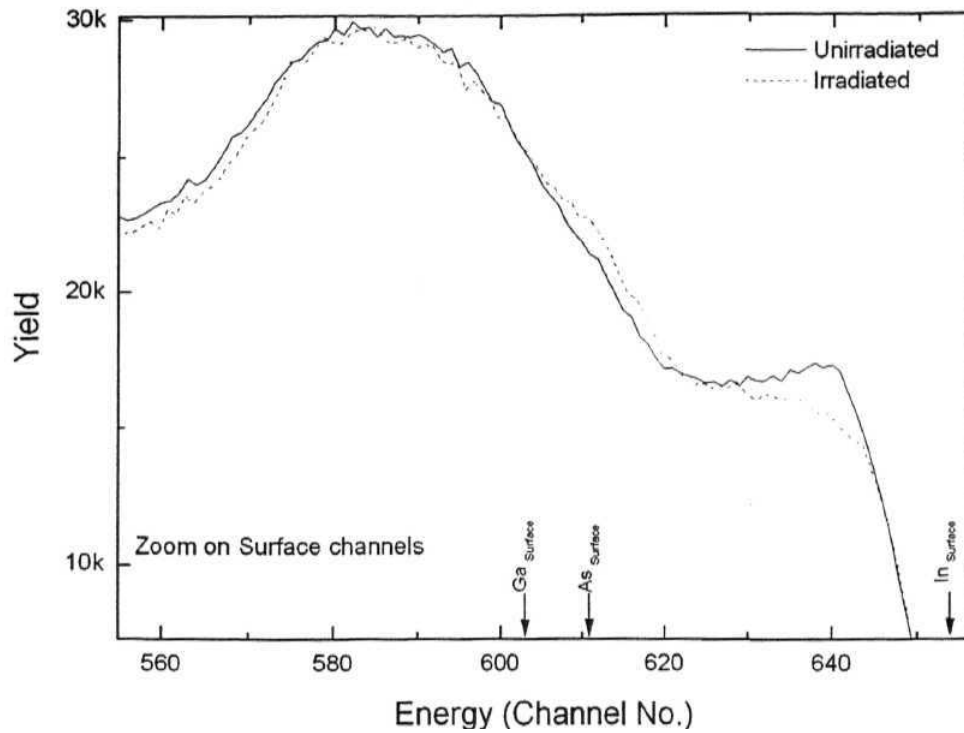
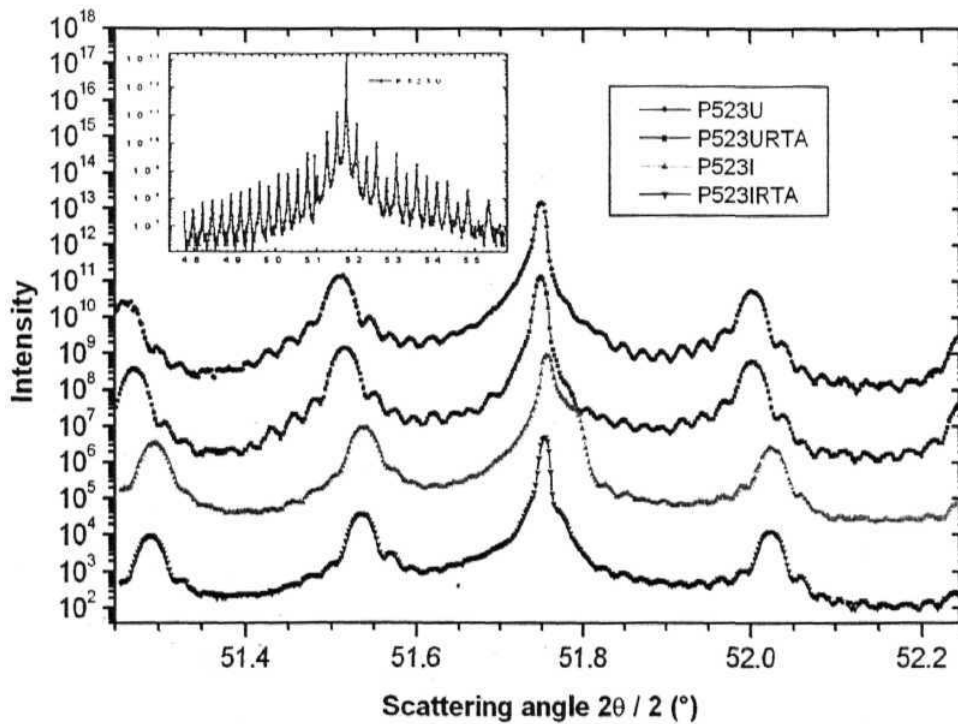
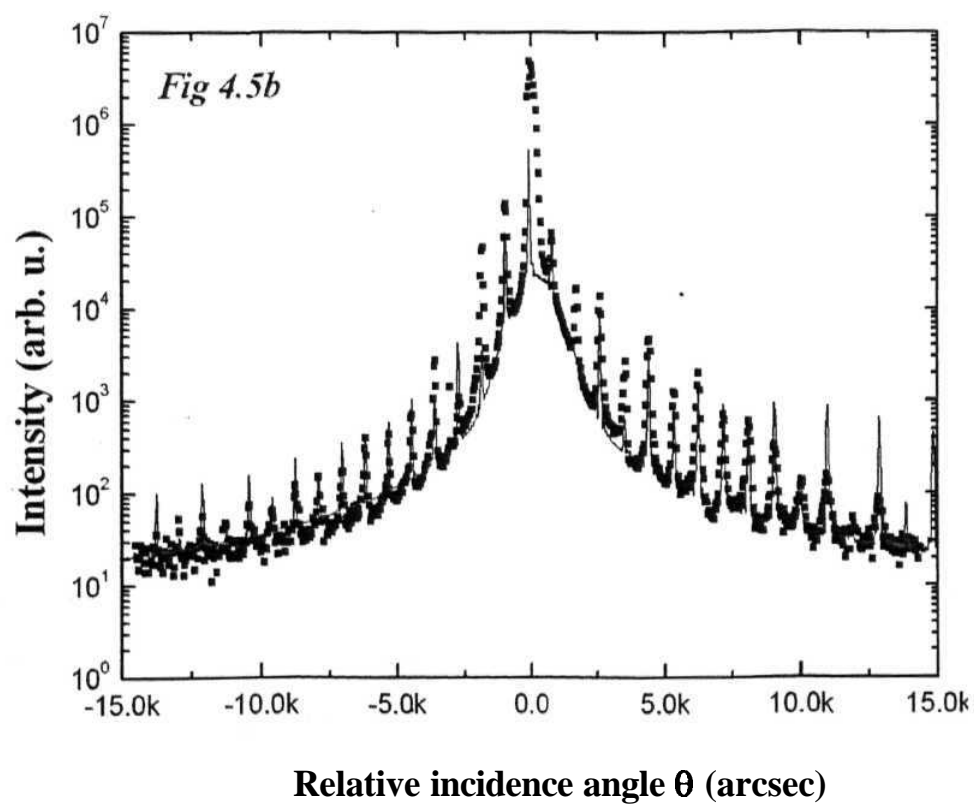
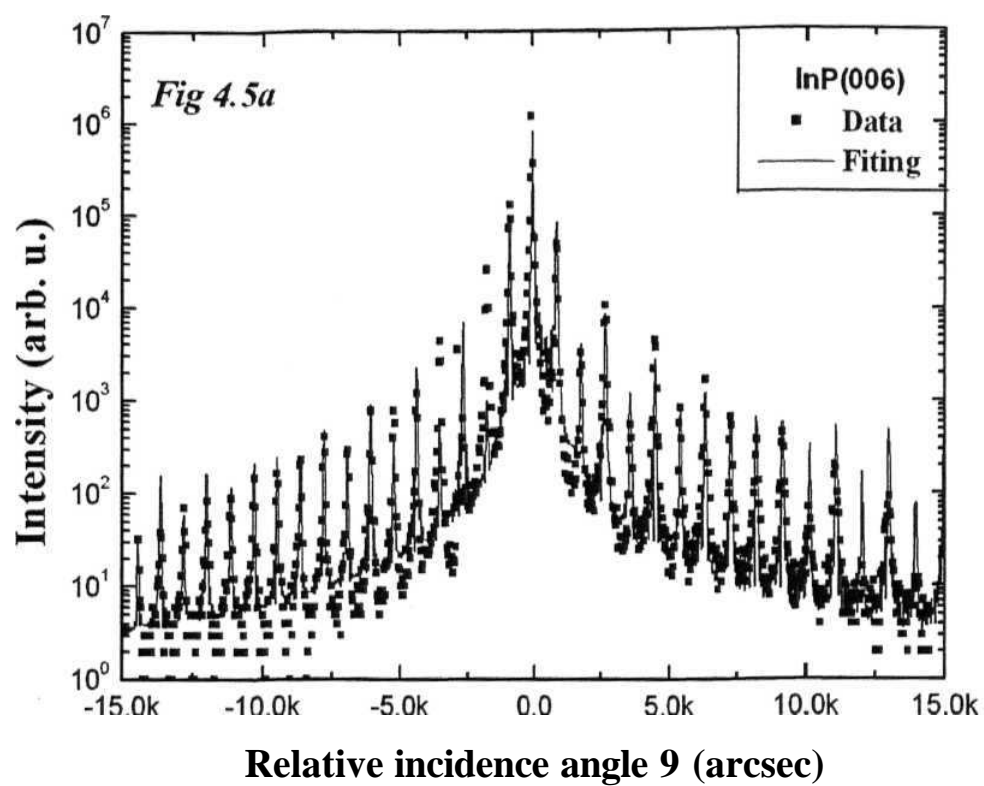


Fig. 4.3: A zoom on the near surface region of $\langle 100 \rangle$ random spectra (Fig. 4.1).



4.4: HRXRD spectra of low dose samples zoomed around the substrate peak, Maintaining the order given in label box; inset: complete interference pattern of P523 U.



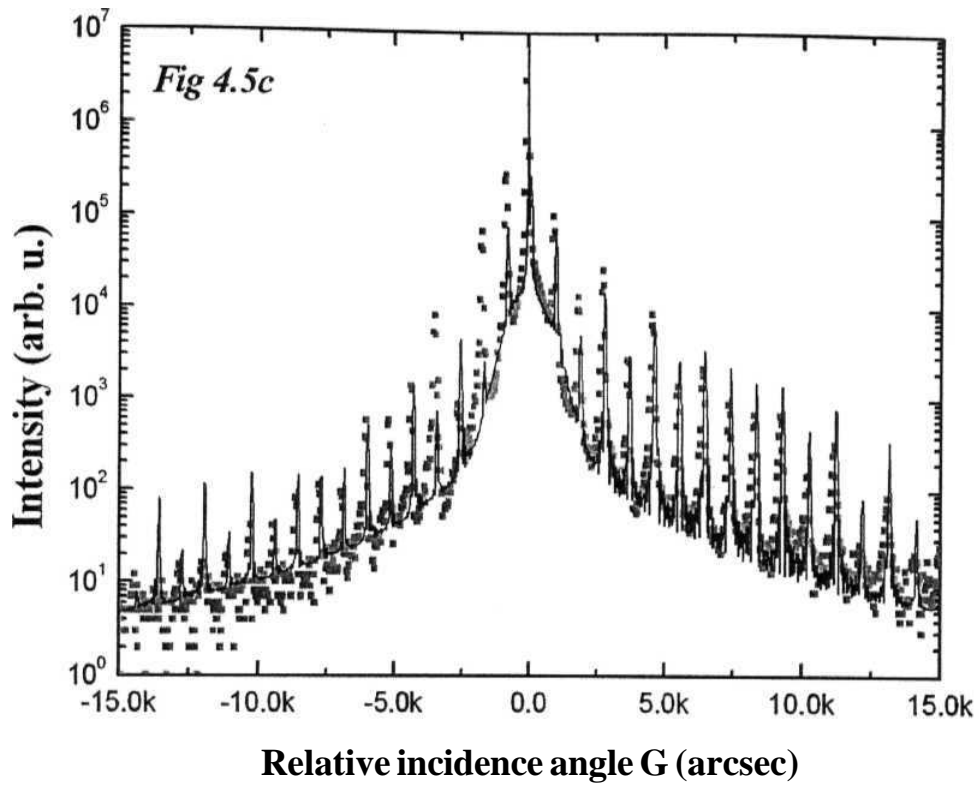


Fig. 4.5: HRXRD spectra and data fits: (a) P523U, (b) P523I2 & (c) P523I2RTA

Table 4.1 Measured strain and thickness values of P523 series

Sample	S (nm) (Nominal 30nm)	$(\Delta d/d)_{\perp}$
P523 U	28.90	-1.10×10^{-4}
P523 URTA	29.08	-1.44×10^{-4}
P523 I	29.01	-3.46×10^{-4}
P523 IRTA	28.93	-3.59×10^{-4}
523 I2	29.69	-
523 I2RTA	28.59	-6.92×10^{-4}

As a general trend [2] the period of the pristine sample is found to be less than that of irradiated samples. The mixing effects are more prominent for ion beam processed (high fluence) and annealed sample as expected. Simple irradiation changes the strain but the interface quality could be improved after annealing as it can be observed by the asymmetry in the substrate peak. However annealing alone doesn't change the strain value significantly. Hence a tensile strain is induced in an initially lattice matched system without loss of the sample quality.

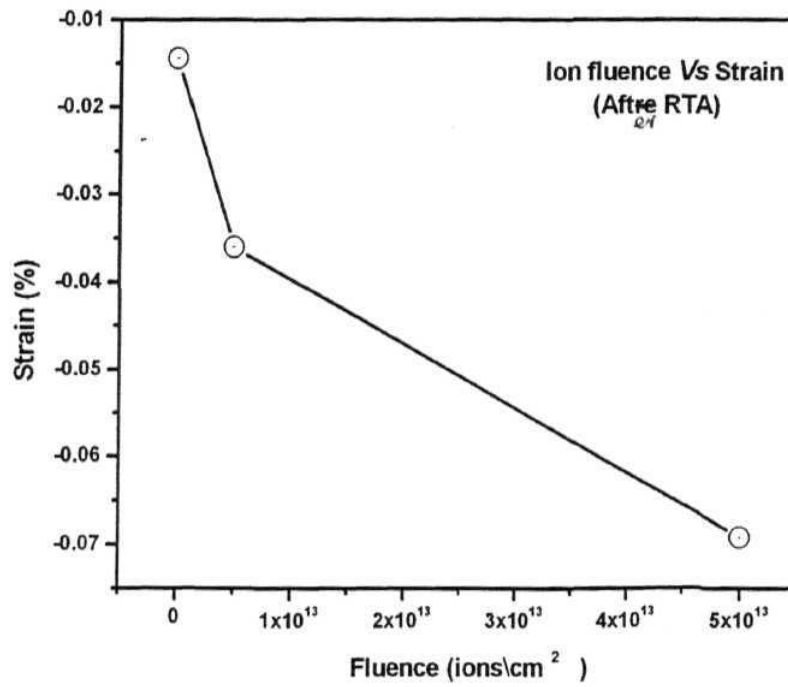
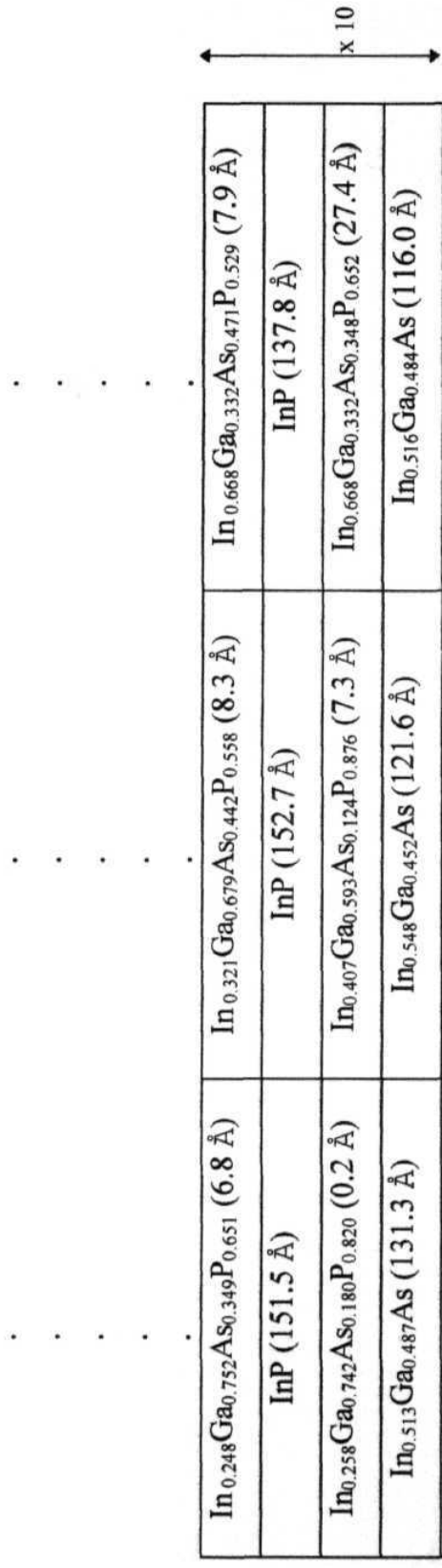


Fig. 4.6: Fluence dependence (P523)

TABLE 4.2: Structure details of the superlattice found from HRXRD (Composition)

Sample Name & Structure	Structure Details	P523U		P523I2		P523I2RTA	
		X	Y	x	y	x	y
In _x Ga _{1-x} As _y P _{1-y}	x 10 Layers	0.248	0.349	0.321	0.442	0.668	0.471
InP		-	-	-	-	-	-
In _x Ga _{1-x} As _y P _{1-y}		0.258	0.180	0.407	0.124	0.668	0.348
In _x Ga _{1-x} As		0.513	-	0.548	-	0.516	-
In _x Ga _{1-x} As _y P _{1-y}	Substrate	0.407	0.631	0.233	0.499	0.524	0.544
InP		-	-	-	-	-	-



For a detailed understanding we have analyzed the HRXRD data of high dose samples using a computer code RADS Mercury. The thicknesses and chemical content of all the layers are taken as free parameters of the fitting routine. Furthermore, a diffuse scattering profile (due to uncorrelated lattice defects) is added to the pure dynamicX-ray diffraction. Fig.4.5 shows the HRXRD spectra of these high dose samples along with proper fits. This analysis suggests that the diffusion process will form a thin $\text{In}_x\text{Ga}_{1-x}\text{AsP}_{1-y}$ on the top of every layer. This effect is observed even in the pristine sample; however the effect is more in irradiated and/or annealed samples. Table 4.2 shows structure of the sample which is obtained by fittings and table 4.3 shows the thickness of each layer. The thickness (superlattice period) values given in table 4.3 are little different from the values that are given in table 1. It is because the superlattice was considered as a homogeneous structure with perfect nominal structure while calculating these values from the interference pattern shown in fig.4.4. These tables suggest the fact that the diffusion is more effective in irradiated and annealed sample (P523I2RTA).

TABLE 4.3: Structure details of the superlattice found from HRXRD (Thickness)

Sample treatment	Multilayer period(λ) (\AA^0)	d_{InP} (\AA°)	d_{InGaAs} (\AA°)	d_{InGaAsP} above InP (\AA^0)	d_{InGaAsP} below InP (\AA^0)	Sum thickness of diffusion layers / X
P523U	289.8	151.5	131.3	6.8	0.2	0.024
P523I2	289.9	152.7	121.6	8.3	7.3	0.054
P523I2RTA	289.1	137.8	116.0	7.9	27.4	0.122

4.3 Application of LAPSDT (*Online observation of ion beam mixing using ERDA - LAPSDT*)

LAPSDT has been used to observe the online mixing in lattice matched InGaAs/InP superlattice (P520). The structure of P520 is same as that of P523 but grown in ~~different~~ batch. LAPSDT based ERDA experiment has been performed using 150 MeV ions at a recoil angle of 55° . Kinematic corrections have also been implemented. The projection of P band of the AE-E spectrum for different ion fluence is shown in

figure 4.7. A minimum fluence of 221×10^{12} ions/cm² was necessary to get sufficient statistics. Fig. 4.7a corresponds to this fluence and shows separate peaks corresponding to different layers. It should be noted that the sample contains *P* only in alternating layers which is reflected in fig. 4.7a. Fig. 4.7b, c & d correspond to higher fluences as shown in the respective figures. Higher fluences are chosen as multiples of the initial fluence so as to keep same statistics for all the spectra. Intermixing is clearly observed in this figure, the peaks in the *P* band are getting merged with increasing fluence. This type of online monitoring is necessary for achieving controlled modification. Moreover one can study all intermediate fluences rather than some selected fluences as done in off-line measurements. This a major advantage of ion beam characterization technique when compared to other off-line characterization techniques. In this work it is found that the mixing effect starts appearing from a fluence of 4.54×10^{12} ions/cm² in this system if irradiated by 150 MeV Ag ions. In addition to this work, LAPSDT has been used in several cases to determine the initial stoichiometry and layer thickness of some of the samples.

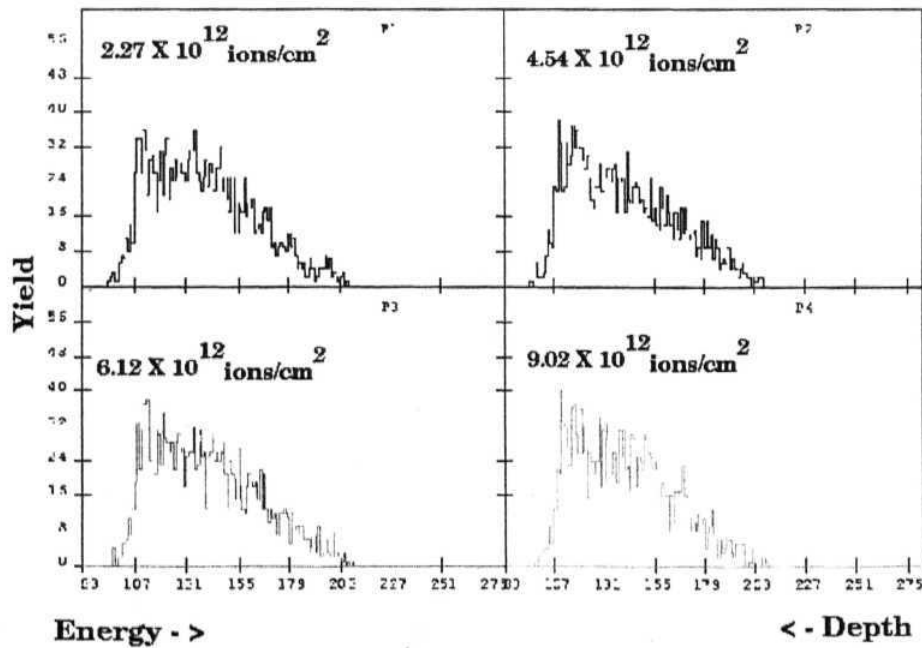


Fig. (4.7): Online observation of ion beam mixing using ERDA - LAPSDT (projection of *P* band) (a) top left; (b) top right; (c) bottom left & (d) bottom right; Corresponding fluence is given in each figure..

4.4 THE MQW5 and 4401 {Strained multi quantum wells):

Fig. 4.8a shows the HRXRD spectra of irradiated and unirradiated MQW5 which are displaced (Shifted upwards) on the intensity axis for clarity. It can be observed that the irradiation did not spoil these structures significantly. The measured superlattice periods, *In* content and the strain values are found to be lesser than that of the nominal values. Measured strain values of pristine and irradiated samples shown in table 44.

Table 44-

Sample	Double layer thickness (nm)	Main system		Secondary system	
		$(\Delta d/d)\%$	<i>In</i> content	$(\Delta d/d)\%$	<i>In</i> content
MQWU	20.15 \pm . 08	0.325%	0.07	0.164%	0.04
MQWI	21.18 \pm . 08	0.298%	0.06	0.120%	0.03

The reduction of *In* concentration represented by the reduction of the satellite intensities, in the irradiated sample reflects the gradual diffusion of *In* from InGaAs layers. Correspondingly there is a reduction of strain from 0.325% to 0.298%. Although the measured periods of both the samples are found to be less than the nominal value, there is a 10Å° difference between MWQ5U and MWQ5I. The superlattice period of the irradiated sample is found to be 10Å° larger than that of pristine sample. An increase in the well thickness or in the superlattice period is observed in all samples including the P523. Such increase in well thickness is observed in the low energy mixing experiments also [1]. The other InGaAs/GaAs based systems, which will be discussed in next section, also show similar behavior. The reduction in the compressive strains can also be seen in table 4.4 in which strain values of all samples are provided. Here we defined a quantity $\Delta \epsilon\%$ as a percentage ratio of the change ($\Delta \epsilon$) in strain due to the irradiation to that of the pristine sample. This helps in comparing the mixing effects in different samples.

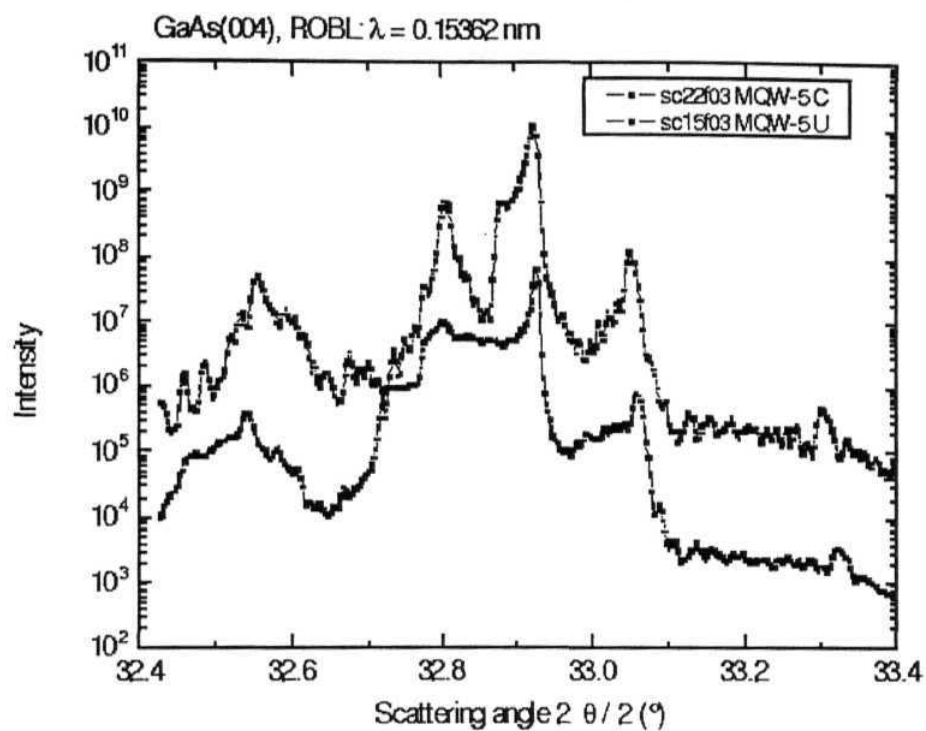


Fig. 4.8a:

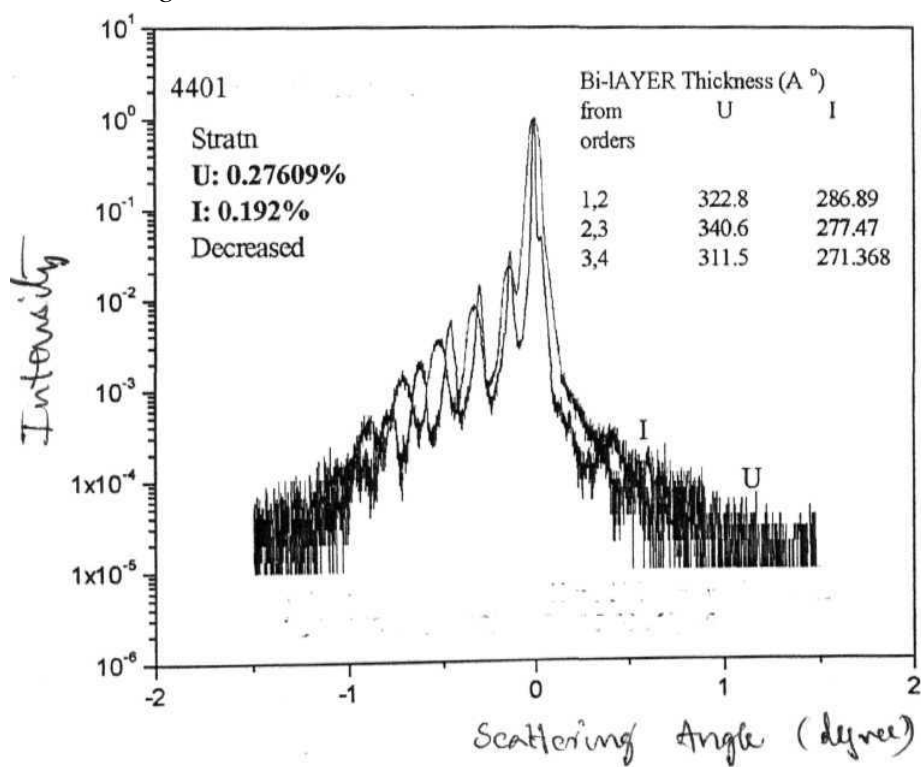


Fig. 4.8b:

Fig. 4.8: HRXRD Spectra of (a) MQW5U & I and (b) 440 IU & I

Fig 4.8b shows the HRXRD spectrum measured on 4401U and 44011. The strain value (0.192%) measured in 44011 is less than that (0.27609%) of the pristine sample 4401U indicating the reduction of compressive strain. Actually the superlattice period calculated from the satellite peaks should not depend on the order of those particular satellite peaks as long as they are consecutive peaks. But here in this sample the thickness values measured from different orders of the HRXRD spectra turned out to be different as shown in figure 4.8b. For example the superlattice period of 4401U is found to be 322.8\AA , 340.6\AA & 311.5\AA when calculated from 1st & 2nd, 2nd & 3rd and 3rd & 4th orders. This might be caused due to the possible in homogeneity of the superlattice structure. Here the super lattice period is found to decrease after irradiation as against to all other samples. This inconstancy is caused due to in homogeneity / ambiguous measurement and hence this case may be treated separately. So these values are not considered while drawing the overall conclusions of this chapter.

4.5 SINGLE STRAINED LAYER SYSTEMS

(Thickness and ion fluence dependence)

The dependence of layer thickness and the ion fluence on the mixing effects of single strained layer structures have been studied using HRXRD. Figs. 4.9 show the HRXRD spectra of such single layer structures. The layer peak of 41011 is shifted towards substrate peak when compared to that of the 4101U. Clear shift can be observed in fig. 4.9a which indicates the reduction of compressive strain. Fig. 4.9b Shows similar spectra for 2601 series. From this figure it is clear that the shift increases with increase in fluence. HRXRD data of all the samples have been fitted using the MADMAX simulation software. Fig. 4.9c shows one such fitting for 2601 series of samples, as an example. Measured strain values (obtained from MADMAX - HRXRD fittings) are given in table 4.4. Reduction of compressive strain due to ion irradiation is observed consistent with all other samples.

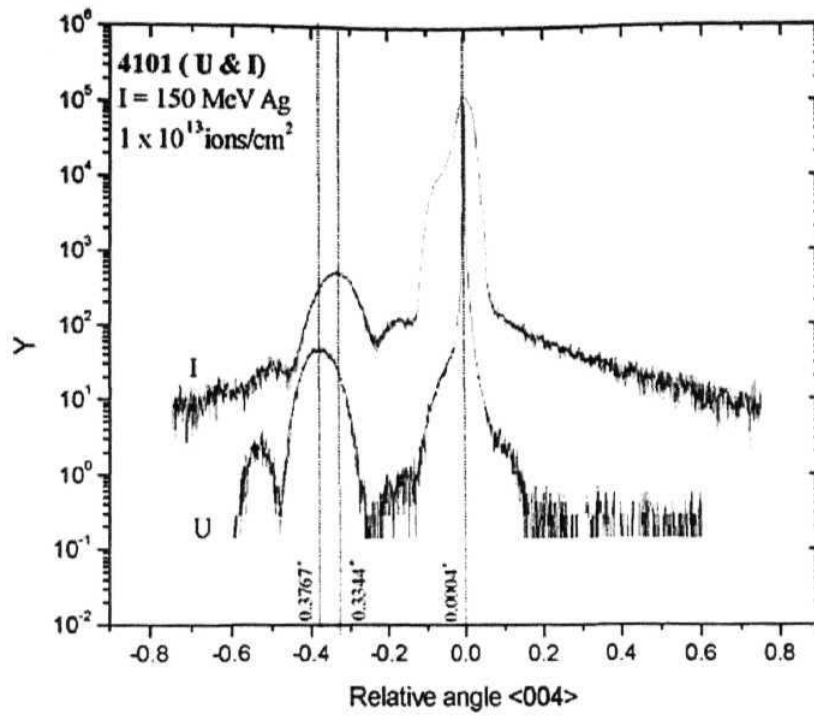


Fig. 4.9a: HRXRD spectra on 4101U & 4101I (i.e 4101113)

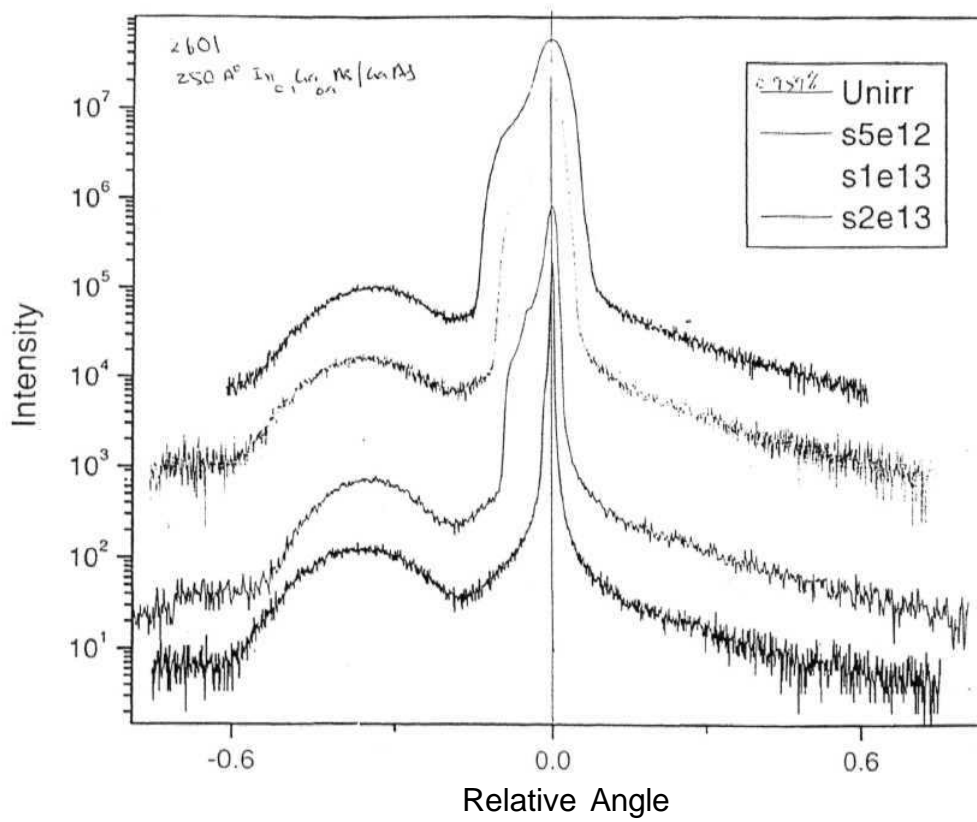


Fig. 4.9b: Fluence dependence: HRXRD on 2601 series

150MeV Ag on In_{0.1}Ga_{0.9}As (250Å) /GaAs

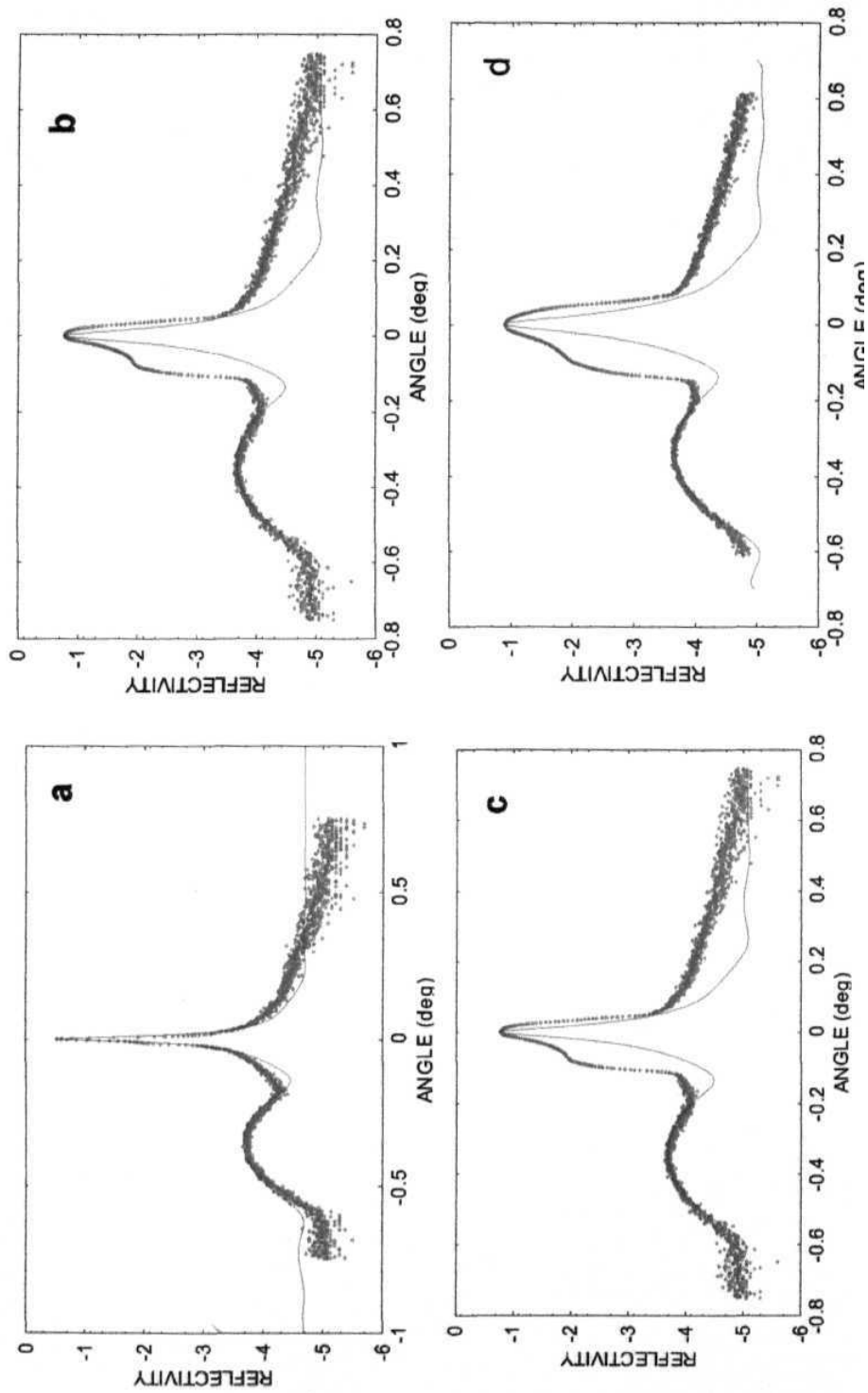


Fig. 4.9c: MADMAX –HRXD fittings
a) 2601U, b) 2601512, c) 2601113 & d) 2601213

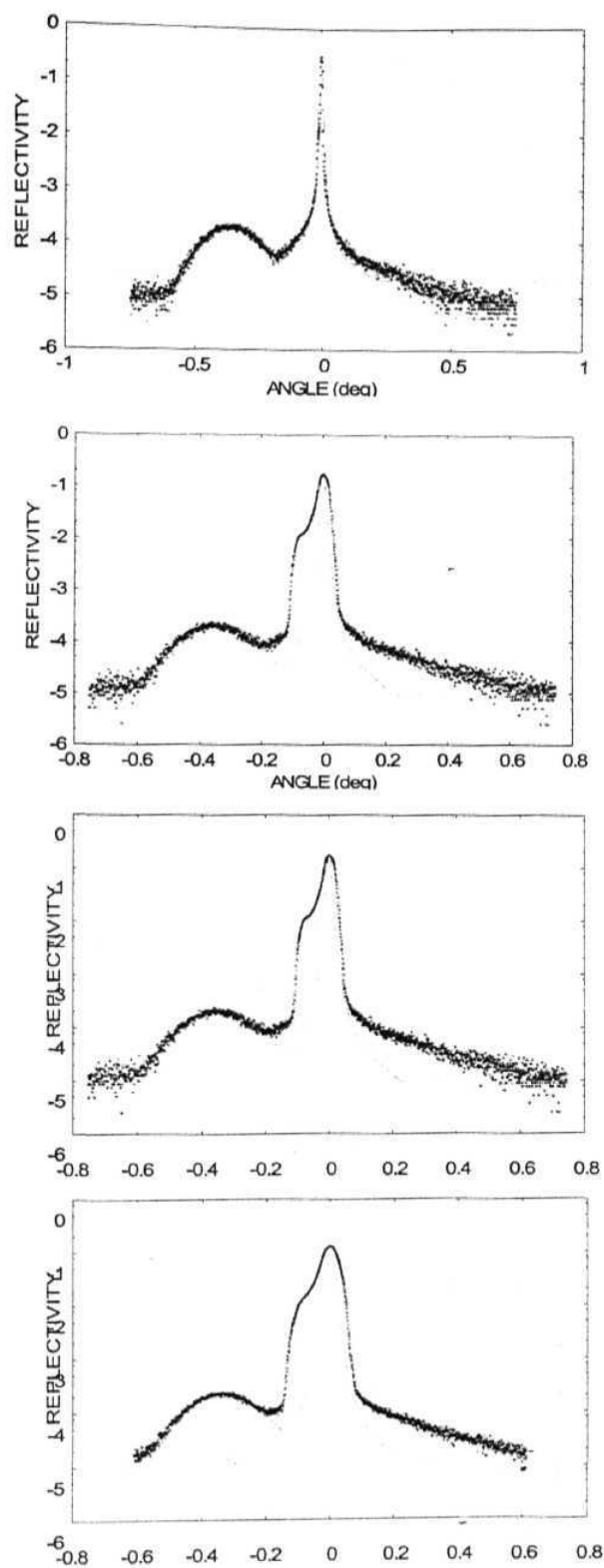


Fig. 4.9c: MADMAX -HRXRD fittings (2601U, 2601512, 2601113 & 2601213 from top:
Thick solid scatter graph is data while the thin solid line is the MADMAX fitting)

Ion fluence dependence studies have been performed on a single strained (2601: 250 Å⁰ In_{0.1}Ga_{0.9}As) layer grown on GaAs substrate. HRXRD experiments have been performed to study the effects that are caused by ion beam mixing. Measured values of thickness (210 Å⁰) and composition ("In": 7.5 %) are less than that of nominal values. These details and strain values are provided in table 4.5 along with all other samples. Fig.(4.10) shows the influence of ion fluence (Q) on the strain and composition. The compressive strain decreases linearly with increase in Ion fluence and exactly fits to a straight line ($\epsilon_t = 0.01017 - 2.7 \times 10^{-17}Q$). Similarly the indium content will also reduce linearly with increase in fluence. Here the maximum fluence was 2×10^{13} ions/cm² in contrast to P523I2 where the maximum fluence was 5×10^{13} ions/cm². Hence from fig (4.6) and fig (4.10) one can observe a linear dependence of strain with increase in fluence. It is inferred that the slope will change after a critical fluence (fig. 4.6). Similar nature is observed for all considered samples. The dependence of thickness and all other parameters can be observed from table 4.5 where we present the data of all samples including several single layer samples. We have considered single layer samples (4201, 26091 & 4101) for the thickness dependence on the mixing effects. Effects of irradiation increase with increase in layer thickness. This is because the initial strain energy in thick layers is more when compared to thin samples. This strain energy will decrease by promoting the diffusion of *In* during irradiation.

From the following table it is also observed that the irradiation effects are more prominent in multi-layers when compared to single layer samples.

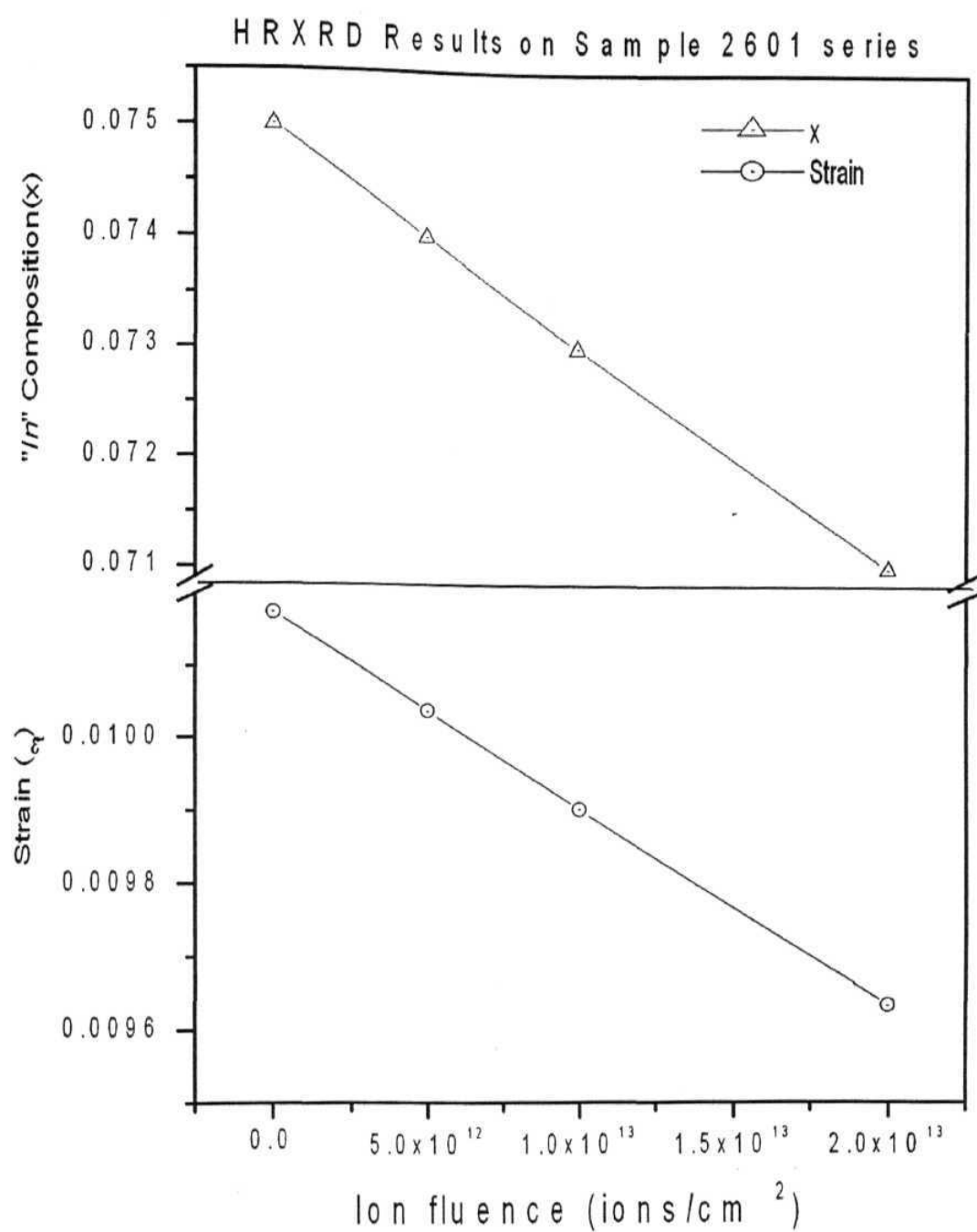


Fig.4.10: Influence of ion fluence (Q) on the strain and composition (2601)

Table 4.5: Ion beam mixing - HRXRD: Complete set of results presented in this chapters

Sample	Thickness / Superlattice period (\AA)	Indium content (x)%	$e\pm\%$	Ae	$\Delta \epsilon\%$
4201 (100\AA)	100	7.2	0.9769	0.1351	13.82
42011 (1×10^{13})		6.2	0.8418		
2701 (150\AA)*	150	8	1.0848	0.0674	6.2131
270111 (5×10^{12})	150	7.5	1.0174		
2601 (250\AA)	210	7.5	1.0174	0.0135	1.3269
2601512		7.4	1.0039		
2601113	-	7.2	0.9904	0.027	2.6538
2601213	-	7.1	0.9634	0.0538	5.2879
4101 (400\AA)	450	7.5	1.0174	0.108	10.615
41011 (1×10^{13})		6.7	0.9094		
MQW5	20.15	7	0.325	0.027	8.308
MWQ5I	21.18	8	0.298		
4401	See text (section 4.4)		0.2706	0.0787	29.07
4401I	see text (section 4.4)		0.192		
P523U	28.9		-0.011	0.0236	214.54
P523RTA	29.08	-	-0.0144		
P523I	29.01	-	-0.0346	0.0249	226.36
P523IRTA	28.93	-	-0.0359	0.582	529.09
P523I2	29.69				
P523I2RTA	28.59		-0.0692		

"-" Not calculated /not needed /given earlier, Spectrum not clear and not included in any interpretation/discussion

4.6 CONCLUSIONS

The general trend in all the samples indicates the gradual diffusion of *In* from surface and the migration of *Ga* or *As* like atoms to the surface regions due to the SHI irradiation and/or annealing processes. The compressive strain is found to decrease in the initially compressive strained samples and tensile strain is induced in an initially lattice matched system. General trend indicates the increase in the superlattice period after the irradiation. The effect of irradiation increases with increase in the fluence and initial layer thickness. Ion beam mixing effects are more prominent multi-layer samples when compared to single layer structures. Strain energy will promote the mixing effects and hence the initial effective strain energy plays a key roll in the ion beam mixing effects. Implantation damage in the substrate deep below ($\sim 13\ \mu$) the epilayers is observed some of the samples and it could be annealed out up to an extent using the RTA. It is shown that the SHI irradiation can be used to tune the strain without much loss of the quality of the samples.

4.7 REFERENCES

1. S. Charabonneu, P.J. Poole, P.G. Pive, M. Buchanan, R.D. Goldberg and I.V. Mitchell, *Nucl. Inst. and Meth.* B106, 457 (1995).
2. J.W. Wan, D.A. Thompson and J.G. Simmons, *Nucl. Instr. Meth.* B106, 461 (1995).
3. V. Hofsa B, J. Kuhn, C. Kaden, V. Harle, H. Bolay, F. Scholz, H. Schweizer, H. Hillmer, R. Losch and W. Schlapp, *Nucl. Instr. Meth.* B106,471 (1995).
4. W. Xia, S.N. Hsu, C.C. Han, S.A. Papert, B.Zhu, C. Cozzolino, P.K.L. Yu and S.S. Lau, *Nucl. Instrum. Meth.* B59/60, 491 (1991).
5. W.D. Laidig, N. Holonyak Jr., M.D. Camras, K. Hess, J.J. Coleman, P.D. Dapkus and J. Bardeen, *Appl Phys. Lett.* 38, 776 (1981).
6. N. Holonyak Jr., W.D. Laidig, M.D. Camras, J.J. Coleman and P.D. Dapkus, *Appl. Phys. Lett.* 39, 776 (1981).
7. D. Deppe and N. Holonyak Jr., *J. Appl. Phys.* R93, 64 (1988).

8. K.H. Lee, H.H. Park and D.A. Stevenson, *J. Appl. Phys.* 65, 1048 (1989).
9. J.M. Dallesasse, W.E. Piano, D.W. Nam, K.C. Hsieh, J.E. Baker and N. Hplonyak Jr., *J Appl. Phys.* **66**, 482 (1989).
10. W.D. Laidig, J.W. Lee, P.K. Chiang, L.W. Simpson and S.M. Bedair, *J. Appl. Phys.* 54, 6382(1983).
11. B. Tell, J. Shah, P.M. Thomas, K.F. Brown-Goebeler, A. DiGiovanni, B.I. Miller and U. Koren, *Appl. Phys. Lett.* 54, 1570 (1989).
12. S. O'Brien, D.P. Bour and R.J. Shealy, *Appl. Phys. Lett.* 53, 1859 (1988)
13. S. Charabonneu, P.J. Poole, Y. Feng, G.C. Aers, M. Dion, M.Davies R.D. Goldberg and I.V. Mitchell, *Appl. Phys. Plett.* 67, 2954 (1995).
14. R.D. Goldberg, I.V. Mitchell, P. Poole, D. Labrie, H. Lafontaine, G.C. Aers, R. Williams, M. Dion, S. Charbonneau, K. Ramanujancha and G.C. Weatherly, *Nucl. Instrum. Meth.* **B127/128**, 418 (1997).
15. T. Venkatesan, S.A. Schwarz, D.M. Hwang, R. Bhat, H.W. Yoon and Y. Arakawa, *Nucl. Instrum. Meth.* **B19/20**, 777 (1987).
16. H. Leier, A. Forchel, G. Horcher, J. Hommel, S. Bayer, H. Rothfritz, G Weimann and W. Schlapp., *J. Appl Phys.* 67, 1805 (1990).
17. R.L. Fleisher, P.B. Prile and R.M. Walker, Nuclear tracks in solids, *Univ. of California Press*, California (1975).
18. Z.G. Wang, Ch. Duforur, E. Paumier and M. Toulemonde, *J. Phys.* C6, 6733 (1994)
19. W. Assmann, M. Dobler, D.K. Avasthi, S.Kruiser, H.D. Mieskes, H. Nolte, *Nucl. Instrum. Meth.* **B146**, 271 (1998).
20. C. Dufor, Ph. Bauer, G. Marchal, J. Grilhe, C. Jgoven, J. Pacaud, J.C. Jousset, *Euro Phys. Lett.* **21**, 671 (1993).
21. A.P. Pathak, S.V.S. Nageswara Rao, A.M. Siddiqui, G.B.V.S. Lakshmi, S.K. Srivastava, S. Ghosh, D. Bhattacharya, D.K. Avasthi, D.K. Goswami, P. V. Satyam, B.N. Dev and A. Turos, *Nucl. Insrt. Meth.* **B193**, 319 (2002).
22. A. M. Siddiqui, S.V.S. Nageswara Rao, A. P. Pathak, V. N. Kulkarni, R. Kesav Murthy, E. Williams, Daryush Ila, Claudiu Muntele, K.S. Chandrasekaran and B.

- M. Arora, *J. Appl. Phys.* 90,2824 (2001).
23. A.P. Pathak, S.V.S. Nageswara Rao, A. M. Siddiqui, *Nucl. Inst, and Meth.* **B161-163**,487 (2000).
24. Shin Hashimoto, Y.Q. Feng and W.M. Gibson, *Nucl. Inst, and Meth.* **B13**, 45 (1986).
25. W.K. Chu, J.W. Mayer and M.A. Nicolet, Backingscattering Spectrometry, *Academic Press*, New York (1978).

CHAPTER V

HIGH ENERGY CHANNELING

40 MeV Si channeling studies have been performed on the strained $\text{In}_{0.1}\text{Ga}_{0.9}\text{As}$ layer grown on GaAs substrate using Molecular Beam Epitaxy (MBE). Three samples with different layer thickness have been investigated in this study. These experiments have been performed using the currently developed automated high energy channeling facility. These details are given in this chapter

5.1 INTRODUCTION

Rutherford backscattering spectroscopy and channeling (RBS/C) is a well established technique [1-4] to determine the nature and the concentration of crystal imperfections. Recently it has widely been used to measure the lattice strains present in technologically important structures like strained layer superlattices (SLS) [5-8]. The strain being a key parameter is very important to study. RBS/C has been employed to measure such strains by several researchers because it is a direct and depth resolved method. These details with specific methods to determine lattice strains are discussed in initial chapters.

Basically strain measurements are based on the determination of the direction of the off-normal axis of strained layer, which is shifted with respect to that of substrate. This small shift ($\Delta\Psi$) between epilayers and the substrate gives a measure of strain ($\Delta\Psi/\sin\Psi\cos\Psi$). Hence the accuracy of the strain measurement by RBS/channeling depends on the sharpness of the channeling angular scan. As discussed earlier the sharpness of these angular scans increases with increase in incident particle energy. Therefore the strain resolution and the

sensitivity of the method are improved in high energy channeling [6-8]. If the energy is too low then the results are misleading steering effect due to the broad critical angles [6,9]. At incident energies that result in critical angles comparable or larger than the tilt due to the lattice strain, angular scan measurement is not reliable due to the beam steering effect, in that some of the channeled ions become random in one layer, although aligned in an other large

In fact there are two major difficulties in high energy channeling experiments. They are the alignment process which becomes difficult due to the small critical angles and the radiation damage. Both these problems can be taken care by using the currently developed automated channeling facility. One has to reduce the effective ion fluence during the measurement to minimize the possible damage. The scattering cross-section can be improved by choosing heavy incident ions and a forward angle detection. At the same time the forward angle detection deteriorates the energy resolution so we used this method only for alignment. Required spectra are collected using a detector placed at back scattering angles. In the following sections we discuss the experimental conditions, results and conclusions drawn from these experiments respectively.

5.2 EXPERIMENTAL

40 MeV Si ions delivered from the 15MV Pelletron accelerator of NSC, New Delhi have been used as incident beam. A pair of double slits separated by roughly around 4m was employed to define the incident angle and also to get the fine and parallel beam. Two SSB Detectors were placed at 60° and 110° for alignment and data collection respectively. Channeling studies have been performed on the strained In_{0.1}Ga_{0.9}As layer grown on GaAs substrate. Three samples with different layer thickness (100 Å⁰, 250 Å⁰ & 400 Å⁰) have been investigated in this study.

5.3 RESULTS AND DISCUSSION

The "automated high energy channeling facility" has been tested and found to be working consistently. Fig. 5.1 shows the angular scans obtained from different samples. Reasonably good reduction is obtained from the scans that are performed on epilayers. They are either fitted by Gaussian or second order polynomial functions [6]. Each figure consists of two angular scans corresponding to epilayer and substrate. These curves are obtained from corresponding depth windows of same set of RBS spectra collected at different angles in the vicinity of the off-normal axis ($\langle 110 \rangle$). The minimum of the angular scan obtained from the substrate does not match with that of the epilayer. That is the centers of the two angular scans that are obtained from the same sample and from the same set of RBS spectra do not match each other. It is because the ax channel in the layer is tilted when compared to that of the substrate due to the strain. The minima of all the curves that are obtained from epi-layers are shifted towards lower angles when compared to respective substrate scans. This indicates the fact that the samples are compressively strained.

The strain value ($\epsilon_t = 0.4\%$) obtained from Fig. 5.1a i.e for the 250 \AA^0 sample turns out to be less when compared to that of the expected value ($\sim 1\%$ [6]). This may be caused due to irradiation effect during the alignment process. The ion irradiation causes ion beam mixing and will reduce the strain in the layer as discussed in the previous chapter [8]. Hence for the other samples we took angular scans on the fresh spot just by shifting the beam position by 1 or 2mm vertically (or horizontally) after axis is found. Very small but fine search is sufficient to remap the axis if it is misaligned due to the above mentioned linear motion. Fig. 5.1b shows the angular scans obtained on a fresh spot (unirradiated portion) of 400 \AA^0 sample. The strain value obtained from the measured angular misalignment is still less (0.56%). However in this figure one can see that the angular shift is well resolved when compared to earlier low energy channeling measurements. It clearly shows the advantage of the high energy channeling measurements. These strain values are less when compared to nominal values. This can be understood up to an extent from HRXRD results presented in the previous chapter which suggest the less In content (6% to 7% to that of the nominal 10%) in all these samples.

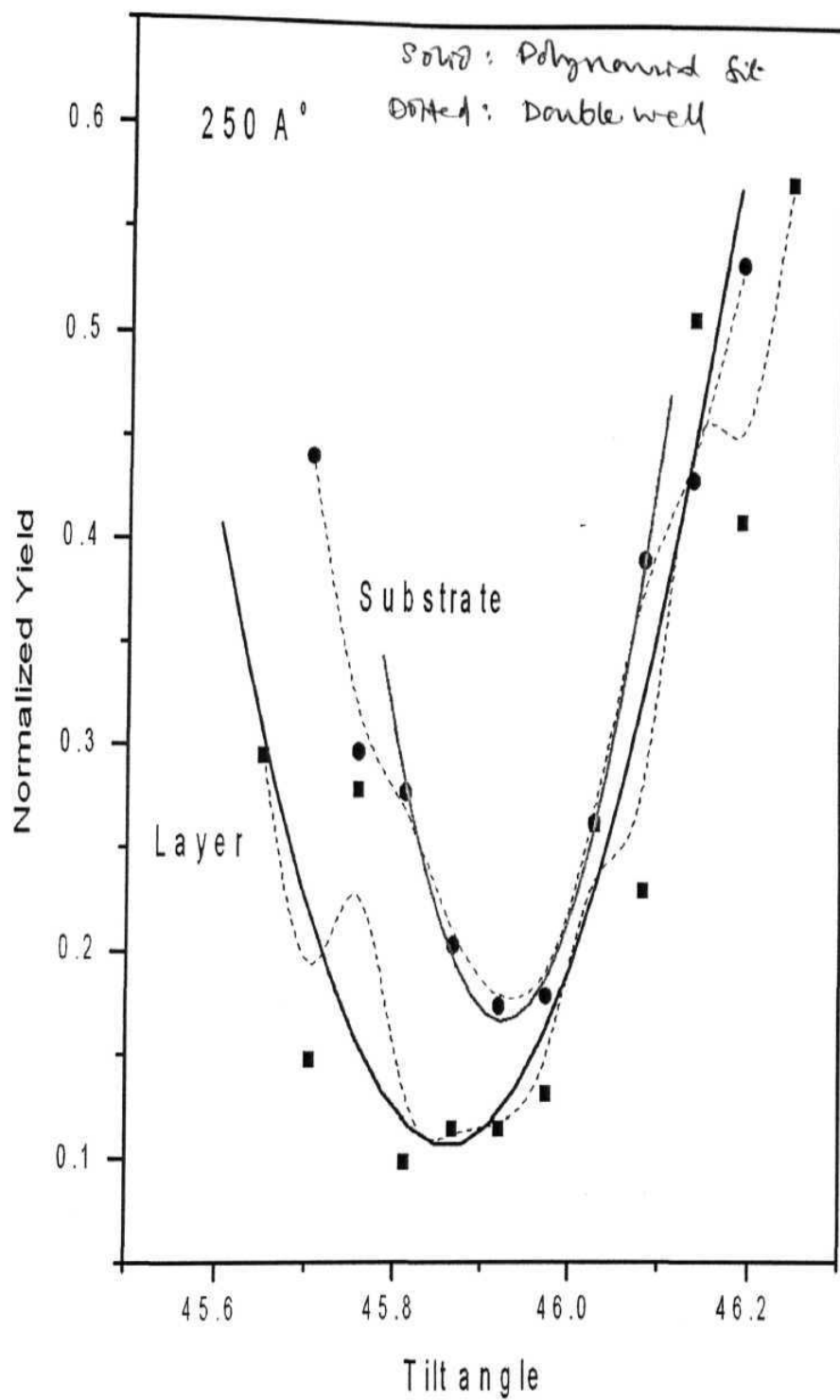


Fig. 5.1a: Channeling angular scan around $\langle 110 \rangle$ axis for 250Å sample

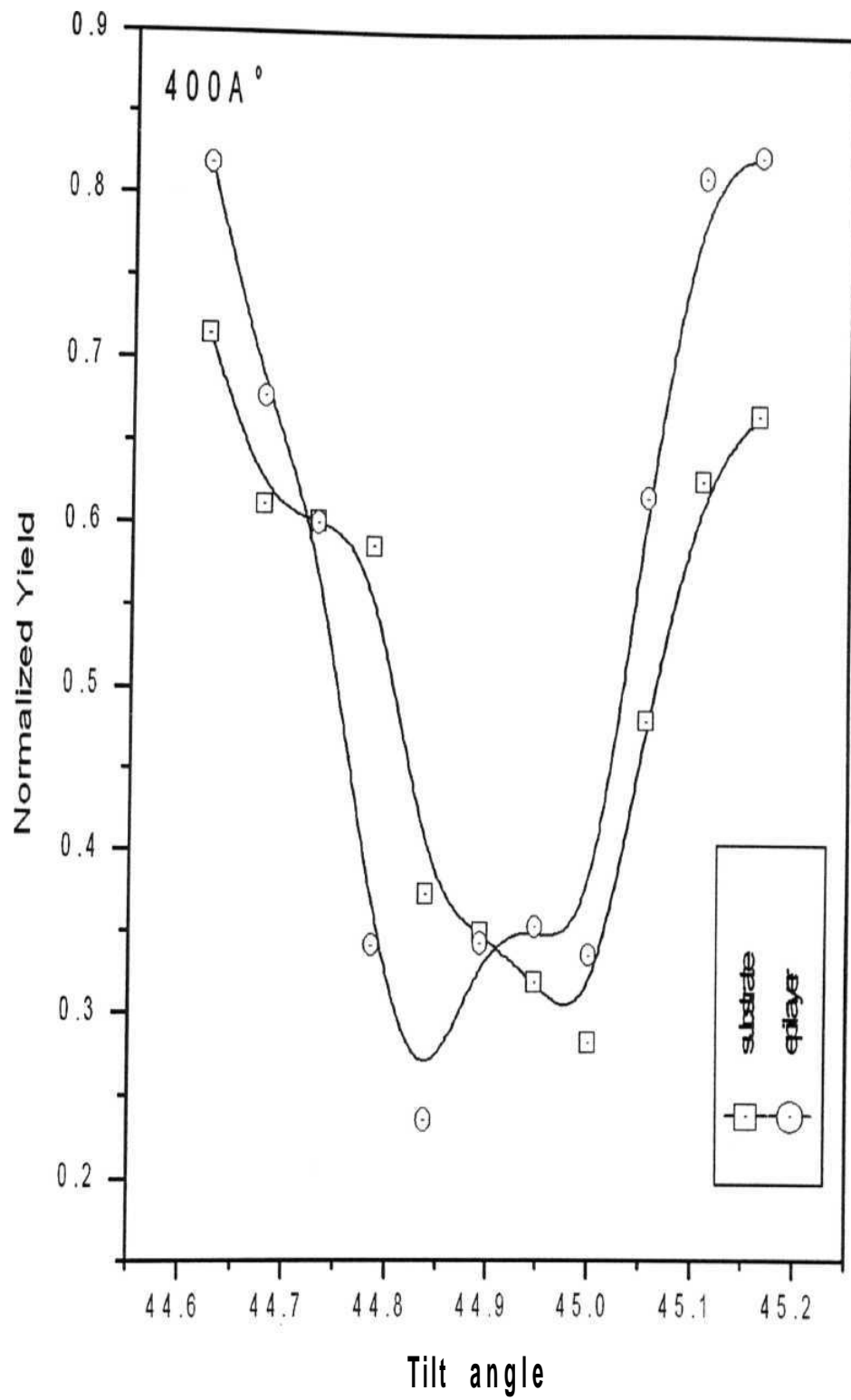


Fig. 5.1b: Channeling angular scan around $\langle 110 \rangle$ axis for 400Å sample

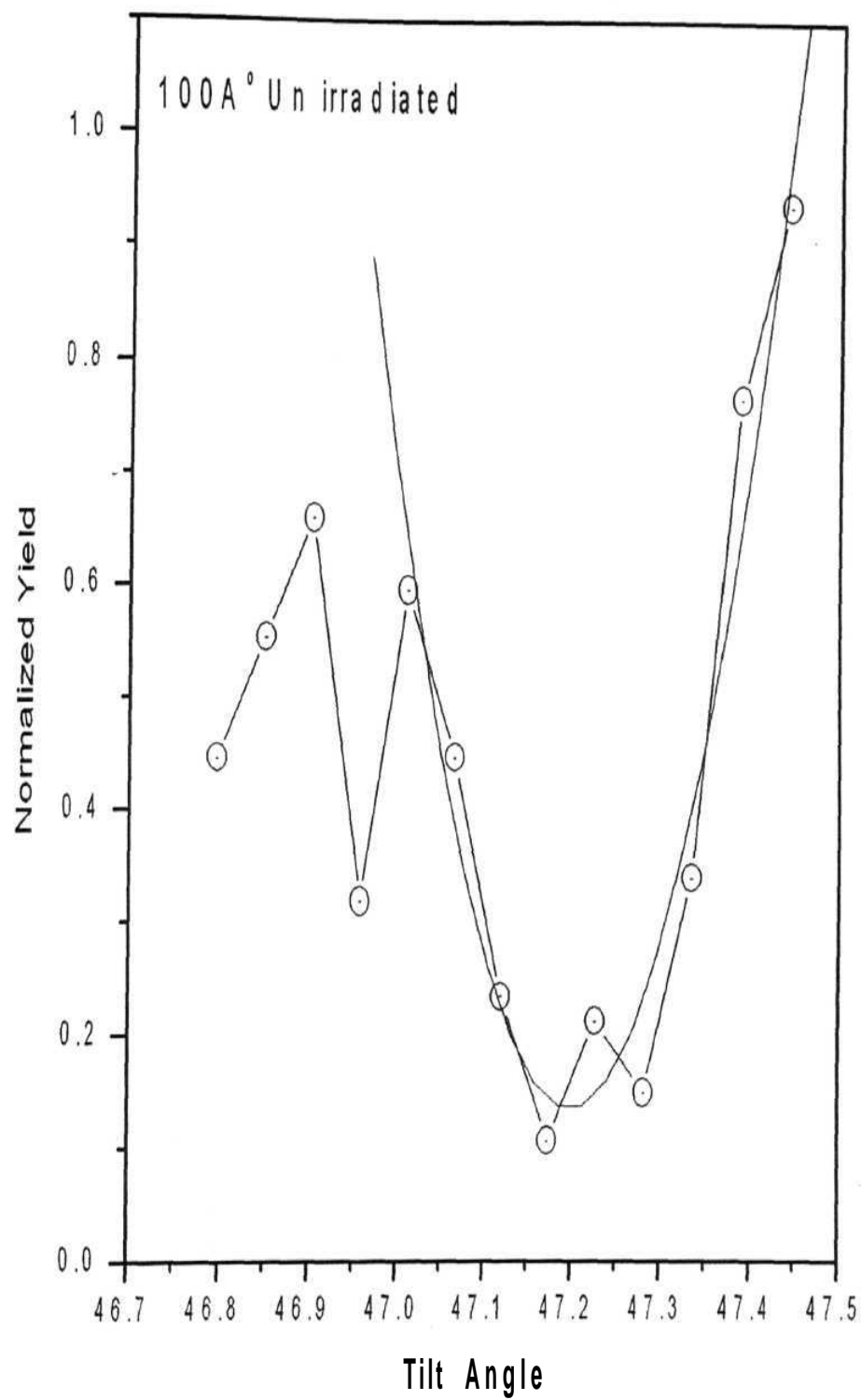


Fig. 5.1c channeling angular scan measured around $\langle 110 \rangle$ axis for 100 Å sample (from epi layer) on fresh spot

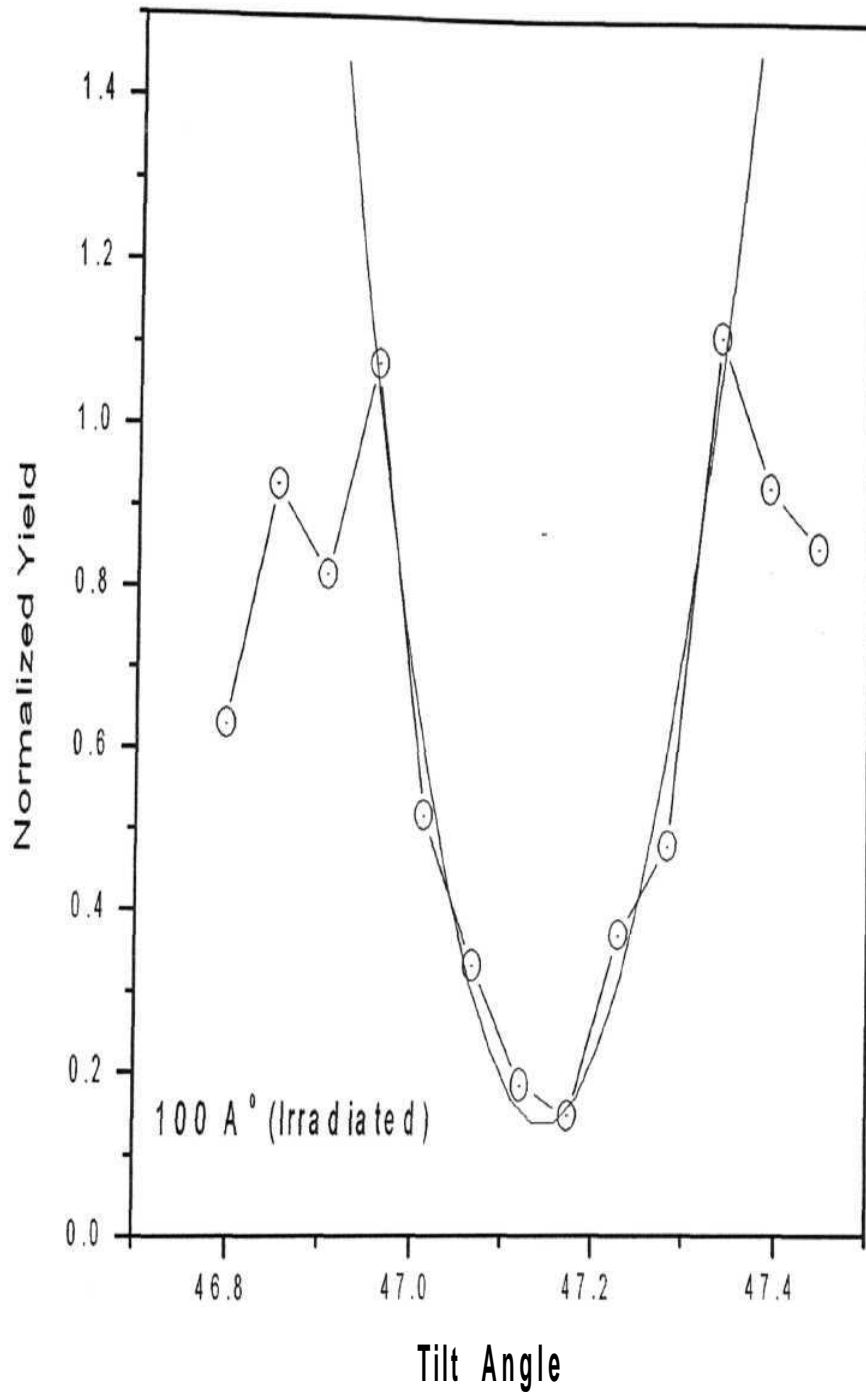


Fig. 5.1d

Fig. 5.1 d: Channeling angular scan around $\langle 110 \rangle$ axis for 100Å° sample (from epilayer) on irradiated spot.

Fig. 5.1c shows the angular scan obtained from the fresh spot of 100A° sample. Considerable asymmetry is observed in this angular scan. The yield goes down on the lower angle side when compared to that of the higher angle side. However the angular scan (fig. 5.1d) measured in the same energy window of the same sample but on the irradiated spot does not show any such asymmetry. This indicates that this asymmetry is directly related to the strain present in the layer. The effect is reduced due to the decrease in strain in the vicinity of the irradiated portion. Such asymmetric scans have been observed earlier by L.C. Feldman et. al.[10] in highly strained $\text{Si}_x\text{Ge}_{1-x}/\text{Ge}$ multi layers. Here the layers are very thin (mono layers) when compared to the channeling wavelength of the probing beam. These asymmetric angular scans are analyzed using Monte-Carlo simulations. The atomic rows of the tilted (strained) layers look like interstitial impurities. This asymmetry is a good tool to measure the low strain values if Monte Carlo simulations are used to analyze the channeling data. This will improve the resolution of the measurement.

As discussed earlier, the measured strain values are less than the expected values. This may happen because of three possible reasons. One of them is the possibility of strain relaxation during the sample growth. Although HRXRD measurements give expected strain values, we cannot rule out this possibility at this stage. HRXRD measurement along asymmetric directions, energy dependent dechanneling studies or some microscopic measurements might resolve this problem. One can estimate the in-plane and out of plane lattice constants using asymmetric x-ray reflections [6] to verify this possibility of strain relaxation. Similarly energy dependent dechanneling measurements can be performed to estimate the dislocation density at the interface.

The other reason for "low strain values" might be due to the possible errors in the depth profiling of RBS spectra. Especially the measured strain values in the case of thin samples (100 A° and 250A°) are too low. The effective thickness has been calculated considering the sample tilt (45° for this case of <110> direction) for depth profiling as usual. The angular scans obtained from substrate and epilayers are too close (fig. 5.1a for 250 A° sample, not shown for 100A° sample) and hence the measured strain values are too low when compared to HRXRD measurements. Even if the incident beam is aligned to the axial direction of the epilayers the yield may not go down if there is a small contribution from the substrate GaAs to this angular scan. However one may expect a small reduction due to the decreased scatterings in the epilayers. However one may get the actual

dip along the axial direction of substrate only. Such a feature of second minimum can be seen in fig. 5.1a and fig. 5.1c. If we consider these second minima for strain calculations then we got comparable results. These strain values measured for 100A° and 250A⁰ sample are 0.696% and 1.12% respectively, which are comparable with HRXRD results (0.852% and 1.017% respectively). These calculations are performed just to see whether this second dip corresponds to the epilayers or not but at this stage we cannot comment further on this part. Although this minimum appears in two samples measured during two different experiments, the data points in the vicinity of this dip are very low. In addition to this the asymmetry in the <110> axis of these samples may also cause such subsidiary minima in the angular scans. Such an extra dip is not observed in 400A° sample as it is considerably thick.

Finally, it seems that the channeling measurements give low strain values when compared to other methods (like HRXRD & Raman Spectroscopy [6]). Either it may be an inherent problem in the channeling measurements or it may happen due to the possible material modification during the measurement. We have greatly reduced the irradiation time (during the measurement) by employing a separate detector for alignment purpose at the forward angle and the currently developed automated high energy channeling facility. This can further be reduced by using the newly developed LAPSDT for channeling measurements. The application of this detector in ERDA channeling will improve the measurement quality with its Z-separation capability. It may not be possible to completely avoid the modification of strain during the high energy channeling measurements but there is certain advantage in this technique if we want to study the dynamic changes in strain during the irradiation. This is possible with the on-line monitoring of material properties using blocking-ERDA. This type of dynamic study is not possible with other off-line measurements. Although many other techniques exist to measure the accurate strain values, ion beam methods are best suited to study the online modification and hence to achieve the controlled modification of material properties.

5.4 CONCLUSIONS

The advantage of high energy channeling to measure lattice strains is shown in this work. Results obtained on the irradiated spots are consistent with the corresponding results of previous

chapter. They indicate that the ion irradiation will reduce the compressive strain. Asymmetric angular scans have been observed in 100\AA sample. Measured strain values are very low when compared to the expected values. The conclusion on this part is still open for discussions as pointed out in last paragraphs. Some more experiments are needed to settle this issue.

A blocking experiment has also been performed for the first time in SLS. This is preliminary result and needs to be refined before presenting it. So we did not include these results in this thesis but this is a simple and direct method to measure strains. It will also indicate the possibility of online monitoring and controlled modification of strain (strain engineering) in SLS.

5.5 REFERENCES

1. Chu W.K, Mayer J.W, Nicolet M.A, Backscattering spectrometry, *Acad. Press*, New York (1978)
2. Feldman L. C, Mayer J. W. and Picraux S. T., *Materials Analysis by Ion Channeling*, *Acad. Press*, New York (1982).
3. Gemmell D. S, *Rev. Mod. Phys.* 46, 129 (1974).
4. Pathak A. P., *Radiation Effects and defects* 30, 193 (1976).
5. Semiconductors and semimetals vol. 33, ed. Persall et al, *Acad. Press*, New York (1991).
6. Siddiqui A.M, Nageswara Rao S.V.S, Pathak A.P, Kulkarni V. N., Kesav Murthy R, Eric Williams, Daryush Ila, Claudiu Muntele, Chandrasekaran K.S and Arora B. M., *J. Appl. Phys.* 90, 2824(2001).
7. Pathak A.P, Nageswara Rao S.V.S, Siddiqui A.M, *Nucl. Inst. and Meth.* B161-163, 487 (2000).
8. Pathak A.P, Nageswara Rao S.V.S, Siddiqui A.M, Lakshmi G.B.V.S, Srivastava S.K, Ghosh S, Bhattacharya D, Avasthi D.K, Goswami D.K., Satyam P.V, Dev B.N and Turos A, *Nucl. Insrt. Meth.* B193, 319 (2002).
9. Shin Hashimoto, Feng Y.Q. and Gibson W.M, *Nucl. Inst, and Meth.* B13, 45 (1986).
10. Feldman L.C, Bevk J, Davidson B.A, Gossmann H. J , and Mannaerts J.P., *Phys. Rev. Lett.* 59(6), 664 (1987).

CHAPTER VI

EFFECTS OF STRAINS AND DEFECTS IN MULTILAYERS ON THE CHANNELING RADIATION

This chapter introduces the "Channeling Radiation (CR)" from the light relativistic particles like electrons and positrons, which is very much sensitive to the shift/tilt existing at the interfaces of SLS. It also introduces the quantum mechanical formulation of the channeling theory and gives the procedures to estimate the effects of defects on channeling and channeling radiation in quantum mechanical framework. Results obtained in these methods on the effects of stacking faults and strains in SLS will be presented in detail. The theory developed on SLS will be useful for strain measurements using the channeling radiation and has become an important part of the thesis.

6.1 INTRODUCTION

Scattering studies play vital role in the development of radiation physics and allied areas of material science. These studies laid a strong base for the present day's science and technology. Channeling, a special case of such scattering process, has been a powerful tool in the defect diagnosis. In this connection, the light particles like electrons and positrons are being used because of their sensitivity in probing irregularities and crystal imperfections present in solids [1,2]. Although we don't have the experimental facilities to perform such studies, we tried to put some light in terms of theory. We developed a simple quantum mechanical framework to study the defects and strains

present in SLS. Here we start with the definition of channeling for the sake of completeness while previous chapters discuss the concept of channeling in detail.

When energetic charged particles are injected along high symmetry crystallographic directions of a single crystal, then because of the ordered structure of the crystal atoms, such particles will undergo a correlated series of small angle gentle collisions, leading to a phenomenon known as channeling. The oscillatory motion of such channeled charged particles results in a special kind of electromagnetic radiation called as "channeling radiation (CR)" which is qualitatively different from other types of radiations [3-14]. Radiation energies are detectable only when light relativistic particles like electrons/positrons are being channeled, because of the great enhancement of energies due to relativistic effects combined with the Doppler shift. In the rest frame of projectile, the relativistic motion results in Lorentz contraction along the axis or plane and hence the strength of the continuum potential is enhanced by a factor γ (where $\gamma = (1 - v^2/c^2)^{-1/2}$). In the lab frame the emitted radiation frequency is Doppler shifted in the forward direction by a factor 2γ . So the overall enhancement in the frequency is of the order of $2\gamma^2$ and hence the energy is shifted to KeV or MeV range from eV or KeV range.

Channeling of such light relativistic particles should be treated in the quantum mechanical framework. Here the longitudinal motion is considered to be nearly free particle type whereas the transverse motion is bounded by the atomic planes (axes). This confined motion results in the discrete bound states in the transverse continuum potential. Channeling radiation results due to the transitions among various transverse energy levels. Such radiation was in fact observed experimentally first for positrons [15] and later for electrons [16,17]. This subject has been reviewed quantum mechanically [3,18], where the characteristics of this radiation has been studied using an interatomic potential operative between the atomic strings/planes. The direct observation of this radiation has opened possibilities of new application as a tool for defect characterization. Hence quantum mechanical estimates of the radiation parameters like for example, frequencies, line widths, effects of monochromaticity etc., are of great importance in the light of

defect diagnosis. Apart from this, the X-rays generated during channeling, open new perspectives in plasma physics research, laser technology and medicine.

Many simulation programs based on Monte Carlo methods are devoted to describe the channeling phenomenon and related effects. These programs mainly study the shape and different parameters of the channeling angular scan (Angular dependence of scattering yield). Such scans are important to study the crystal structure, defects and thermal vibrations of lattice atoms. Complicated techniques based on statistical methods are needed to describe classical channeling phenomenon where as simple quantum mechanical methods can be implemented to study the light particle channeling. Keeping these points in mind, we have developed quantum mechanical formulations both for positron and electron channeling radiation in virgin crystals. Channeling angular scans are obtained by calculating the initial occupation probabilities of various states at the entry surface. In addition the influence of tilt angle / shift near the interfaces of the multi-layers on the channeling radiation has been calculated and discussed.

6.2 CR FROM POSITRONS AND ELECTRONS

The channeling radiation emitted by the light particles (viz. e^+ , e^-) and its characteristics like radiation intensity, monochromaticity, line widths etc., are studied by incorporating spontaneous transitions among the transverse energy levels and these quantum mechanical estimates are in good agreement with experimental data [3-10]. Most of the theoretical investigations in this direction have been based on nearly perfect crystal situations. However, no crystal is perfect in real life hence it is important to understand the role of these defects on channeling radiation. In addition to these intrinsic defects the lattice strain in SLS will also influence the trajectory of channeled particles and hence the corresponding channeling radiation. So it is important to incorporate the effects of various defects on CR. In fact there are some very interesting results based on the electron/positron channeling radiation experiments carried out by Park and coworkers [10] using perfect and imperfect diamond crystals where, nitrogen platelets are buried intrinsically deep inside these crystals. These platelets are equivalent to extended defects:

SFs with respect to one set of planes (i.e. along (1 1 1) and (1 10)) and dislocations with respect to another set of planes (along (10 0) direction). These experimental results suggest that the presence of these platelets cause substantial reduction in the spectral line widths (the centroid being intact) for positrons on one hand and shift in the frequency for electrons on the other. These results suggest that such radiation studies can be used as a tool for defect characterization through the intensity and line width measurements.

6.3 THE MODEL

For electron channeling, the electrons in the ground state of the transverse energy spectrum are dechanneled faster than those in excited states. This is because the electrons corresponding to lower transverse energy states oscillate around the atomic planes with a smaller amplitude so that overall they spend larger fraction of their time in the vicinity of atomic planes or axes and hence get dechanneled at a faster rate than those corresponding to higher transverse energy, i.e., excited states. This mechanism tends to dechannel the ground state in the transverse energy spectrum of electrons much faster. The electron because of its attractive nature towards target nuclei, takes spiral path (known as *rosette-motion* [19]) under the influence of axial channeling and the transverse potential is two dimensional. However in the planar case it oscillates about the atomic plane in the transverse space and the corresponding planar transverse potential seen by these electrons is one dimensional hydrogen atom type and can be expressed as

$$V(x) = -\frac{A}{|x|} \quad 6.1$$

where A contains the information about host crystal parameters and projectile charge.

For positrons, because of opposite charge, situation is reversed to that for electrons [20]. The transverse potential for positrons is well approximated by simple harmonic oscillator, given by

$$V(x) \approx V_0 + \frac{1}{2}kx^2 \quad 6.2$$

where V_o and k depend on host crystal parameters and projectile charge.

The ground state wave function of the positron is strongly localized about the channel axis ($x = 0$) so that the particle is confined along this axis. These particles refer to well-channeled configuration as they have fewer tendencies to hit the atomic plane directly. On the other hand, the excited states will have more tendencies to cause dechanneling, since these particles come closer to host atoms (plane or axes). The corresponding Schrodinger equation governing the transverse motion is given by

$$\left[\frac{-\hbar^2}{2\gamma m} \nabla^2 + V(x) \right] \Psi = E_{\perp} \Psi \quad (6.3)$$

where $V(x)$ is the corresponding continuum planar potential for electron/positron and E represents standard transverse energy eigen states. The corresponding wave function for planar channeled positron is that of the standard harmonic oscillator with the coupling constant α given by.

$$\psi_n^+ = \left(\frac{\alpha}{\sqrt{\pi} 2^n n!} \right)^{\frac{1}{2}} \exp(-\alpha^2 x^2) H_n(\alpha x) \quad (6.4)$$

The detailed calculation of eigen functions of planar channeled electron involves hypergeometric functions and this is explained in Ref. [21]. These wave functions are obtained for both even and odd parity states by matching them at $x=0$. In the present quantum formulation we will make use of these wave functions which are given by

$$\psi_n^- = \sqrt{\frac{2}{a_0^3 n^5 (n!)^2}} \exp(-|x|/na_0) \{x\} L_n^1(2|x|/na_0) \quad (6.5)$$

Here L represent associated Laguerre polynomials of first kind and the function $\{x\}$ is defined as x if $|n\rangle$ is even and $|x|$ if $|n\rangle$ is odd and with the usual meanings for all other symbols [11,12].

Effects of defects and strains have been studied with corresponding wavefunctions obtained by applying the necessary correction terms to the continuum potential.

6.4 THE MOTIVATION

(Transition probabilities at the stacking boundary)

The basic motivation behind this work has been the quantum mechanical formulation given by Goteti et. al.[11-14], to study the effects of extended defects on channeling/dechanneling. Here we present an example *{slacking faults}* combined with our contribution to those model calculations. Later in the next sections we present the effects of defects/strains on the channeling radiation.

A stacking fault is an example of obstruction without any distortion in the channel where the potential valleys present on the one side of the fault are shifted w.r.t the potential hills on the other side. For any particle passing through the stacking fault, the longitudinal component of energy is not much affected but the transverse energy undergoes a change. So quantum mechanically it's a transition of the particle from one harmonic (Hydrogen atom like) potential to other similar potential shifted by an amount a_s , the stacking shift. Hence by incorporating the shift in the right side wave function one can calculate the matrix element at the stacking boundary. This matrix element governs the transitions among the various available states. Here an expression for transition probability T_n on the basis of sudden approximation for transition for a given initial state $|n\rangle$ to any final state $|m\rangle$ is obtained.

$$T_n = \sum_{m=0}^{m_{\max}} |\langle m | n \rangle|^2 \quad 6.6$$

Here the matrix element $\langle m | n \rangle$ is given by

$$\langle m | n \rangle = \frac{\exp(-\alpha^2 a_s^2 / 4)}{\sqrt{\pi 2^{m+n} m! n!}} \int_{-\infty}^{\infty} \exp\left\{-\left(t + \frac{b}{2}\right)^2\right\} H_n(t) H_m(t+b) dt = \frac{\exp(-\alpha^2 a_s^2 / 4)}{\sqrt{\pi 2^{m+n} m! n!}} I_{mn} \quad 6.7$$

Where $b = aa_{s+}$

In fact the above integral runs from $-d_p/2$ (half the channel width) to $d_p/2$ but the limits are considered to be infinity assuming that the wavefunction dose not have any tails outside the channel. This assumption applies to all integrals considered in this chapter. Ofcourse $-d_p/2$, $d_p/2$ are considered during the numerical evaluation of integrals. These matrix elements were first calculated by Goteti et. al. [11] for limited number of maximum states using mathematical induction and they have discussed the behavior of these transitions in detail. Here we have solved the integral analytically and gave a simple and compact formula as follows.

Consider the generating function of Hermite polynomials

$$\sum_{n=0}^{\infty} H_n(x) \frac{t^n}{n!} = \exp[-t^2 + 2xt] \quad 6.8$$

$$\Rightarrow \sum_{n=0}^{\infty} H_n(x+a) \frac{t^n}{n!} = \exp[-t^2 + 2(x+a)t] \quad 6.9$$

$$= \left[\sum_{n=0}^{\infty} H_n(x) \frac{t^n}{n!} \right] \exp(2at) \quad 6.10$$

By comparing the coefficient of t^n on both sides of the eq. 6.10

$$H_n(x+a) = \sum_{r=0}^n {}^n C_r (2a)^r H_{n-r}(x) \quad 6.1$$

Using the equation (eq. 6.11) we can write

$$H_m(t+b) = H_m\left[\left(t + \frac{b}{2}\right) + \frac{b}{2}\right] = \sum_{r=0}^m {}^m C_r (b)^r H_{m-r}\left(t + \frac{b}{2}\right) \quad 6.12$$

and

$$H_n(t) = H_n\left[\left(t + \frac{b}{2}\right) - \frac{b}{2}\right] = \sum_{s=0}^n {}^nC_s (-b)^s H_{n-s}\left(t + \frac{b}{2}\right) \quad 6.13$$

Substituting the equations 6.12 and 6.13 into 6.7

$$I_{mn} = \sum_{s=0}^n \sum_{r=0}^m {}^mC_r {}^nC_s (-1)^s (b)^{s+r} \int_{-\infty}^{\infty} \exp\left\{-\left(t + \frac{b}{2}\right)^2\right\} H_{n-s}\left(t + \frac{b}{2}\right) H_{m-r}\left(t + \frac{b}{2}\right) dt \quad 6.14$$

Now the integral can be solved using the orthogonal property of Hermite polynomials

$$I_{mn} = \sum_{s=0}^n \sum_{r=0}^m {}^mC_r {}^nC_s (-1)^s (b)^{s+r} 2^{n-s} (n-s)! \sqrt{\pi} \delta_{n-s, m-r} \quad 6.15$$

Hence I_{mn} has a value only if $n-s = m-r$ and hence

$$r = m-n+s \quad 6.16$$

By substituting eq. 6.16 into 6.15 and simplifying we get the general expression for $\langle m|n \rangle$ given in ref. [11]

$$\langle m | n \rangle = \frac{\exp(-b^2/4)}{\sqrt{2^{n+m}} m! n!} \left[\sum_{r=\max(0, m-n)}^m (-1)^{n-m+r} 2^{m-r} {}^mC_r \frac{n!}{(n-m+r)!} \right] \quad 6.17$$

The most generalized and compact expression for the above expression is written in terms of associated Laguerre polynomials [22].

$$\langle m | n \rangle = \left(\frac{m!}{2^{n-m} n!} \right)^{1/2} \exp(-b^2/4) (-b)^{n-m} L_m^{n-m}(b^2/2) \quad 6.18$$

The corresponding matrix element for planar channeled electron is evaluated from the integral

$$\langle m | n \rangle = C_{nm} \int_{-d_p/2}^{d_p/2} \exp\left(-\frac{1}{A_0 mn} [n|x+b| + m|x|]\right) \{x+b, x\} L_m^1\left(\frac{2|x+b|}{mA_0}\right) L_n^1\left(\frac{2|x|}{nA_0}\right) dx \quad \dots \quad 6.19$$

$$\text{where } C_{mn} = \left(\frac{2}{A_0^3 (mn)^{5/2}} \right)$$

This integral has been solved numerically by splitting it into various intervals [23] and the results are shown in fig.(6.1). The total dechanneling probability for the ground state of electron is very sensitive to stacking shift as seen from the fig.(6.1), in contrast to the positron case where the excited states show such behavior while the ground state calculation show almost Gaussian in shape [11]. This reflects the fact that the dechanneling of electrons and positrons is qualitatively different because of their opposite charges and this is revealed clearly in the present quantum dechanneling calculations. These predictions in fact explain the conclusions drawn by *Park et. al.* [10] where, radiation spectrum yields affected by the platelets clearly indicate that the positrons with smaller amplitudes (ground state particles) can survive even after encountering the shift, while those in electron case show higher tendency to get dechanneled. These are highlighted in the present quantum description. The ground state for channeled electron is localized along the plane while the excited states extend over to the either side of the atomic plane. Therefore the particles in excited states of the transverse energy spectrum propagate with higher amplitudes as compared to those in ground state. This can also be realized from the corresponding angular scans presented in the next section.

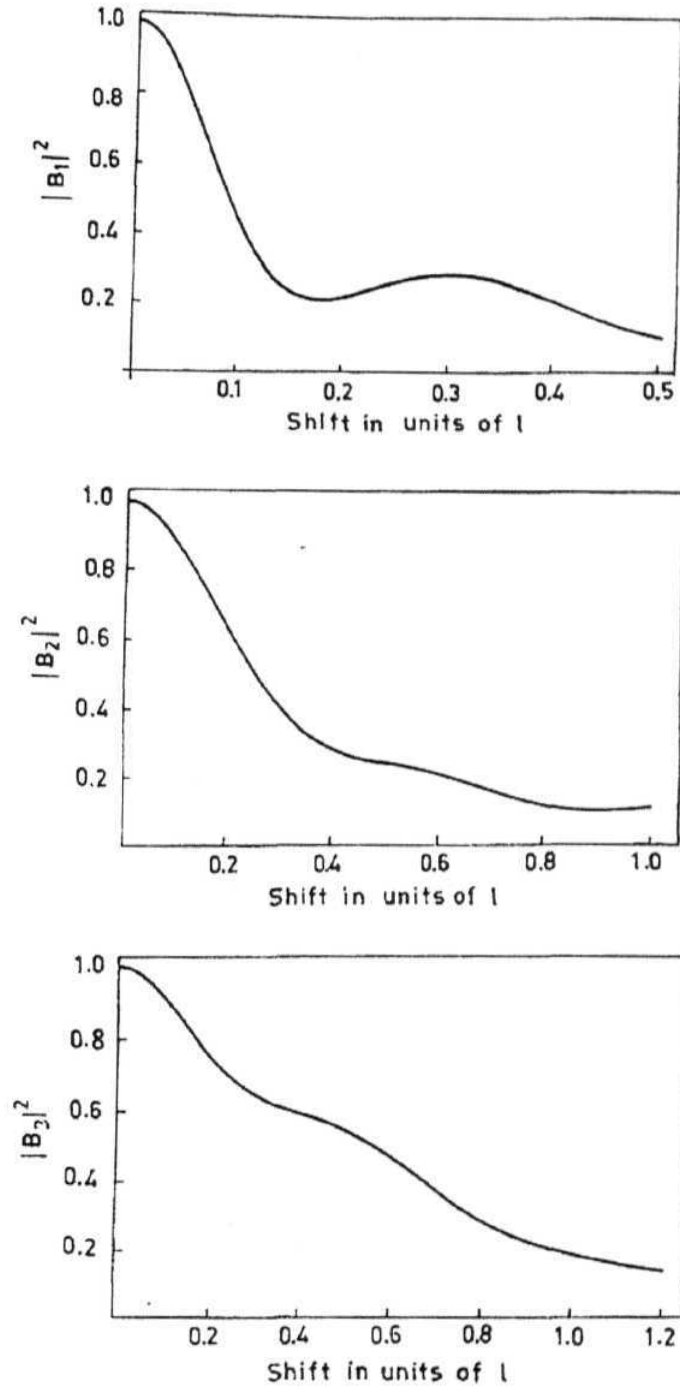


Fig. 6.1: Occupation probabilities of all possible states due to the redistribution after crossing the stacking boundary (for planar channeled electrons)

6.5 INITIAL OCCUPATION PROBABILITY

When high energetic electron/positron beam is injected into the crystal, depending upon the angle of incidence and beam divergence, the particle flux gets populated among various quantized energy levels. These two factors will effect the subsequent population of excited states. When the angle of incidence is large (within the critical angle), the transverse eigen state population is more as compared to small incident angle and less divergent situations. The initial value of quasi-momentum is defined by matching Bloch wavefunction to the incident plane wave at the crystal surface. By matching the wavefunction at the crystal entry face, we obtain an expression for the initial population of the energy levels (Π_n) as

$$\Pi_n = \left| \int_{-d_p/2}^{d_p/2} \exp(iq_x x) \psi_n(x) dx \right|^2 \quad 6.20$$

where, q_x is the quasi-momentum in transverse space. This integral has to be solved numerically [23] for the case of electrons due to the complexity involved. For positron case an analytical expression is obtained as shown below

$$\Pi_n^+ = \left(\frac{\alpha}{\sqrt{\pi 2^n n!}} \right) \left| \int_{-\infty}^{\infty} \exp\left(iqx - \frac{\alpha^2 x^2}{2} \right) H_n(\alpha x) dx \right| \quad 6.21$$

$$= A \left| \int_{-\infty}^{\infty} \exp\left(\frac{-t^2}{2} \right) H_n(t + i\eta) dt \right|^2 \quad 6.22$$

where $\eta = q/\alpha$, $t = (\alpha x - i\eta)$ and $A = \frac{\exp(-\eta^2)}{\alpha \sqrt{\pi 2^n n!}}$

Using the eq. 6.11 (with $r = n-r$) the above integral can be written as

$$\Pi_n^+ = A \left| \sum_{r=0}^n {}^nC_r (2i\eta)^{n-r} \int_{-\infty}^{\infty} \exp\left(\frac{-t^2}{2}\right) H_n(t) dt \right|^2 \quad 6.23$$

$$= A \left| \sum_{r=0}^n {}^nC_r (2i\eta)^{n-r} \int_{-\infty}^{\infty} \exp\left(-\left(\frac{t}{\sqrt{2}}\right)^2\right) H_r\left(\frac{t}{\sqrt{2}}\right) H_n\left(\frac{t}{\sqrt{2}}\right) dt \right|^2 \quad 6.24$$

The above equation can be expanded using the general properties of **Hermite** polynomials as follows

$$\Pi_n^+ = A \left| \sum_{r=0}^n \frac{n! (2i\eta)^{n-r}}{r! (n-r)!} 2^{-\frac{r}{2}} \sum_{m=0}^r \frac{r!}{m! (r-m)!} \int_{-\infty}^{\infty} \exp\left(-\left(\frac{t}{\sqrt{2}}\right)^2\right) H_m\left(\frac{t}{\sqrt{2}}\right) H_n\left(\frac{t}{\sqrt{2}}\right) dt \right|^2 \quad 6.25$$

Once again the above equation has been solved using the orthogonal properties of Hermite polynomials.

$$\Pi_n^+ = A(\sqrt{2})^2 \left| \sum_{r=0}^n \frac{n! (2i\eta)^{n-r}}{r! (n-r)!} 2^{-\frac{r}{2}} \sum_{m=0}^r \frac{r!}{m! (r-m)!} (\sqrt{\pi} 2^m m! \delta_{m, r-m}) \right|^2 \quad 6.26$$

Hence Π_n^+ has a definite value only if $m = r-m = r/2$. So r must be an even integer and can be written as $2s$ ($r=2s$) for an integer s . Substituting these values into eq. 6.26 we get

$$\Pi_n^+ = 2\pi A \left| \sum_{s=0}^{\lfloor n/2 \rfloor} (-1)^s \frac{n!}{s! (n-2s)!} (2s)^{n-2s} \right|^2 = 2\pi \left(\frac{\exp(-\eta^2)}{\alpha \sqrt{\pi} 2^n n!} \right) |H_n(\eta)|^2 \quad 6.27$$

Hence

$$\Pi_n^+ = \frac{\sqrt{\pi}}{\alpha n! 2^{n-1}} \exp\left\{-\frac{q_x^2}{\alpha^2}\right\} \left| H_n\left(\frac{q_x}{\alpha}\right) \right|^2 \quad 6.28$$

The above expression gives the relation between the incident angle and the occupation probability of any particular state (n). The maximum number of bound states (n_{\max}) can be obtained by equating the total transverse energy to the depth of the planar potential [24]. n_{\max} increases with mass and the energy of the incident particle and hence the motion becomes classical. Low n_{\max} situation should be considered in quantum mechanical framework. Here we consider both the situations with different values of n_{\max} . Fig. (6.2a) shows the incident angle dependence on the various states for the case of $n_{\max} = 3$. It is clear from the figure that the lower states have more occupation probability while excited states are less populated. As expected, the ground state shows a Gaussian distribution around the center of the channel. Higher states are populated if the incident angle is increased. Total channeling probability shows the wiggles that are generally observed in the experiments with planar-channeled positrons [24-26]. In fact from figure 6.2a one can visualize the shape of angular scan for the cases where $n_{\max} = 1$ and 2 because they are simply the superposition of all lower states. Hence from this figure one can determine the shape of angular scans for these two cases. Shape of such scans is in good agreement with existing theoretical and experimental results. Fig. (6.2b) shows the channeling angular scan obtained from these calculations for pure classical situation with $n_{\max} = 12$. Such high number of states is considered so as to see more wiggles and also to confine our calculations to the pure classical regime.

Pedersen et. al., [25] performed planar channeling experiments in both classical and quantum regimes using 1.2 MeV positrons along different planes of single crystal Si. They measured the angular scans in back scattering mode and compared their results with 9-beam theory for three values of n_{\max} ($n_{\max} \sim 1, 2$, & 5 along {115}, {110} & {100} planes respectively). For the pure quantum case, the shape of the angular scan obtained experimentally [25] for $n_{\max} = 1$ also matches with our calculations (Fig. (6.2a)). Andersen et. al., [26] considered the case of $n_{\max} = 8$ also. Qualitatively all these results

[25-26] are in good agreement with our present calculations. The shape of the angular scan comes in a quite natural way from simple quantum concepts. However quantitative results can be obtained by estimating the exact values of a and n_{\max} which depend on the probing beam and the target material.

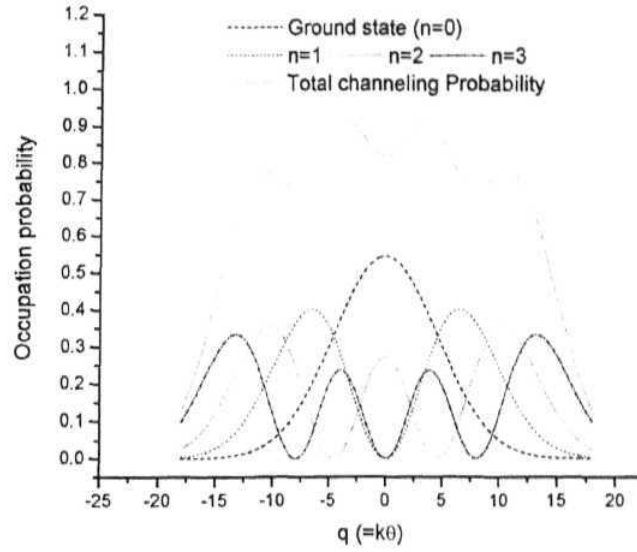


Fig. 6.2 (a) $n_{\max} = 3$

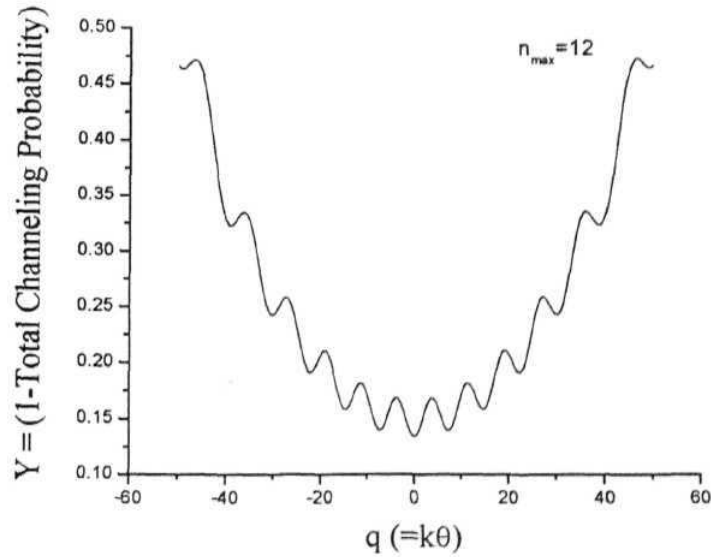


Fig. :6.2(b): form $n_{\max} = 12$.

Fig. (6.2): Incident angle dependence on the various states

Similar angular scans are computed numerically [23] for the case of electron with $n_{\max} = 3$ as shown in fig.(6.3). This figure clearly indicates the fact that the excited states have more occupation probability while lower states are less populated. More rigorous and refined experiments are to be carried out for both electrons and positrons because of their importance in relativistic case. Especially for the electron case sufficient experimental data is not available to study the effects of defects/strains. The complexity involved in the electron wavefunction reflects on the further calculations. It is difficult to attain analytical solutions and hence numerical methods were used. Hereafter we consider only positrons and will present analytical results.

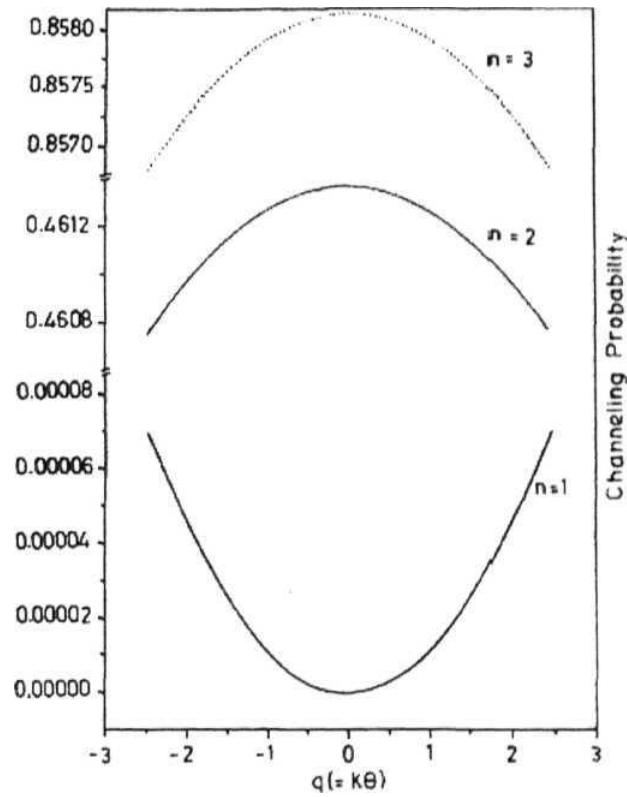


Fig. 6.3: Occupation probabilities of all possible channeled states versus incident angle at the surface (for electron case).

6.6 EFFECTS OF SLS ON CR

When the particle flux approaches the tilted portion of the SLS, some of the particles get dechanneled because of direct obstructions across the interface and this beam attenuation depends on initial phase at the entry surface. As a result, the subsequent dechanneling is attributed partly to (i) the abrupt shift in the atomic planes (denoted by a_{sls}) and (ii) their relative orientation angle ' θ '. This angle influences the population redistribution in xy - *plane*. If the layers are less strained, $\theta \sim \theta_c$ (i.e., critical angle) and the shift $a_{sls} \sim a_{TF}$, majority of the particles are expected to survive during their passage through the strained portion between the multi-layers. The intensity of a transition line obtained for an incident plane wave with a definite transverse momentum ($p_{in, \perp}$) proportional to the initial population. However, if there are irregularities/imperfections in the crystallographic channels, then the population re-distribution near the defect sites should also be suitably incorporated. The expression for population re-distribution (Π^+_{sls}) is obtained by matching the wave functions across the boundary, near the strained portion.

$$\Pi_{sls} = |B_m|^2 = \sum_{n=0}^{n_{\max}} \left| \int e^{iK\theta} \phi_n(x) \phi_m(x + a_{sls}) dx \right|^2 \quad 6.29$$

$$= e^{-(b^2 + \beta^2)/2} \sum_{n=0}^{n_{\max}} \left| \frac{1}{\sqrt{\Pi 2^{m+n} n! m!}} \int \exp \left\{ - \left(t + \frac{b - i\beta}{2} \right)^2 \right\} H_n(t) H_m(t + b) dt \right|^2 \quad 6.30$$

Where $t = \alpha x$ and $|\beta| = K0/a$ with K being the longitudinal component of the momentum. By denoting $b^2 + \beta^2 = \lambda^2$, the above integral has been solved analytically and result is expressed in terms of associated Laguerre polynomials given by

$$\Pi_{SLS}^+ = e^{-r^2/2} \left(\sum_{n=0}^{n_{\max}} \frac{(\min\{m, n\})!}{(\max\{m, n\})!} \left(\frac{r^2}{2} \right)^{|n-m|} \left[L_{\min(m,n)}^{|n-m|} \left(\frac{r^2}{2} \right) \right]^2 \right) \quad 6.31$$

The integral has been solved in the same procedure that had been adapted to solve the integral involved in eq. 6.7 with

$$H_n(t) = \sum_{r=0}^n {}^nC_r (-1)^r (b - i\beta)^r H_{n-r} \left(t + \frac{b - i\beta}{2} \right) \text{ and}$$

$$H_m(t+b) = \sum_{s=0}^m {}^mC_s (-1)^s (b + i\beta)^s H_{m-s} \left(t + \frac{b - i\beta}{2} \right)$$

The effects of stacking shift or the tilt at the tilted interface of an SLS can be studied from the eq. 6.31. Fig. (6.4) shows the interdependence of stacking shift and tilt on the occupation probability of ground state from all initial states after passing the interface. Maximum probability is observed when both shift and tilt is zero as expected, because ground state is most populated in the case of positron channeling. However excited states have lower occupation probability after passing the defected region. Fig. (6.5a) shows similar graphs for an excited state $m = 3$. Here it is observed that the tendency of occupying higher states is more in the presence of defects. A cross-sectional view of $m=3$ case is shown in fig. (6.5b) for clarity, which suggests the oscillatory behavior of the occupation probability of this state. Such transitions between the states contribute to the intrinsic channeling radiation caused by spontaneous transitions. Hence it is necessary to take these effects into account while calculating the radiation intensity and other radiation characteristics.

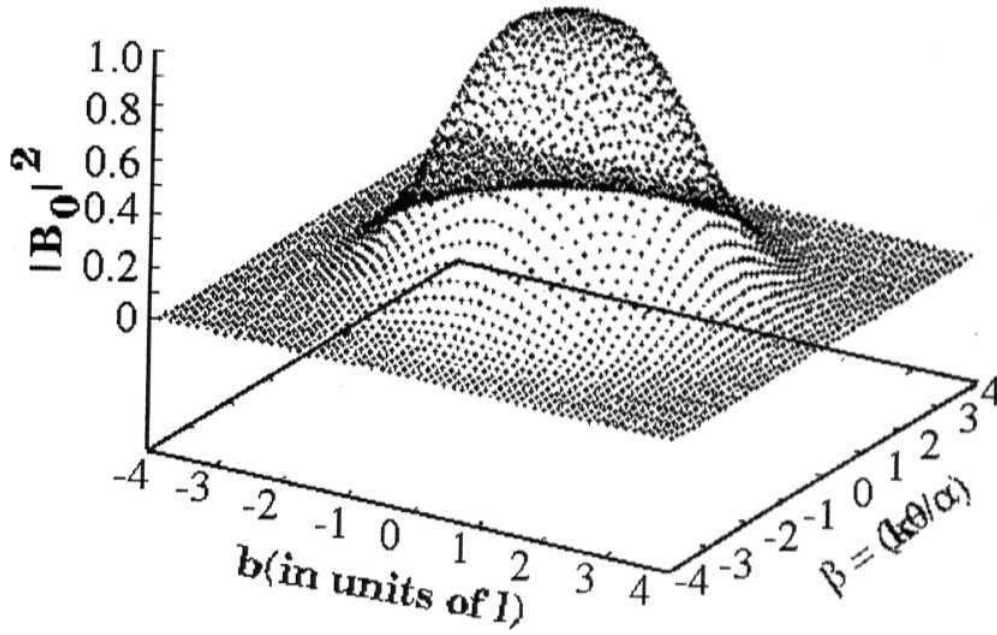


Fig 6.4: Interdependence of stacking shift and tilt on the occupation probability of ground state from all initial states after passing the interface.

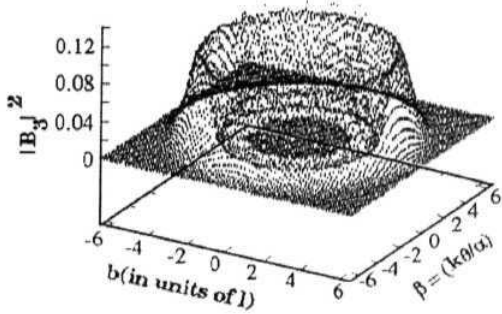


Fig. 6.5 a

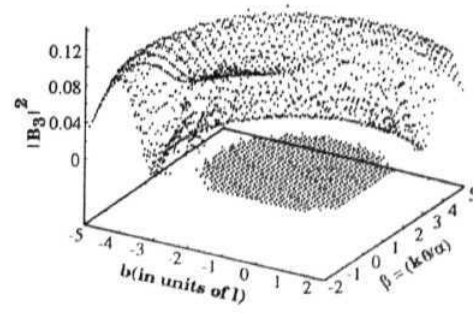


Fig. 6.5b

Fig 6.5: (a) Interdependence of stacking shift and tilt on the occupation probability of an excited state ($m=3$) from all initial states after passing the interface, (b): Cross-sectional view of (a)

6.7 EXPRESSIONS FOR RADIATION INTENSITIES

The intensities of various spectral peaks associated in the transmission of the particle in dipole approximation are governed by various factors like the matrix element $|\langle m|n\rangle|^2 (= |\mathbf{P}_{nm}|^2)$, the initial population of channeled states Π_n and the dechanneling of the particle flux near the faulted region. If 's' is the penetration depth of the particle beam into the crystal, the dechanneling effects can be phenomenologically introduced by a depletion factor D_n which is given by

$$D_n(t) = (s_n/t)(1 - \exp(-s/s_n)) \quad 6.32$$

where s_n denotes depletion length of the state $|n\rangle$ in a crystal of thickness V [20]. The effective population governing the emission of channeling radiation over the crystal thickness ' t ' is given by

$$\Pi_{\text{eff}}(t) = \Pi_n D_n(t) |\mathbf{B}_m|^2 \quad 6.33$$

Total intensity of given transition peak in the channeling radiation spectrum is governed by what is called strength factor given by $F_{mn} = |\mathbf{p}_{mn}|^2 \Pi_{\text{eff}} D_n$. The absolute radiation intensity is given by

$$N = 2(1 + \beta^{-1}) \alpha \omega \left(\frac{L}{c} \right) (mc)^{-2} |\langle u_f | p_x | u_i \rangle|^2 \frac{\delta\Omega}{4\pi} \Pi_{\text{eff}} \quad 6.34$$

where detector solid angle $\delta\Omega \ll \pi$ and Π_{eff} is effective fractional population of state after stacking fault boundary and ω is photon energy emitted in forward direction. β , L and c have their usual meanings [3].

6.8 CONCLUSIONS

Complete procedure has been discussed here to study the effects of defects/strains on the channeling and related effects using the quantum mechanical models **developed by** Gotati. et. al [11-14]. The case of stacking fault has been taken as an example to study the dechanneling of planar channeled electrons [23] and positrons [22,27]. These earlier results are improved and more general as well as compact expressions are given for the transition probabilities at the stacking boundary. Important physical concepts have been discussed in detail. The theory has been extended to study the effects of SLS on channeling radiation.

The total dechanneling for the ground state of electron is very sensitive to stacking shift/tilt (fig. 6.1) in contrast to the positron case where the excited states show such behavior while the ground state population distribution is Gaussian in shape, as expected. This reveals the fact that the dechanneling of electrons and positrons is qualitatively different because of their opposite charges. These predictions in fact explain the conclusions drawn by Park and coworkers [10] where, radiation spectrum yields affected by the platelets clearly indicate that the positrons with smaller amplitudes (ground state particles) can survive even after encountering the shift, while those in electron case show higher tendency to get dechanneled. Here the resolution of electron/positron radiation spectra in (1 0 0) direction is very difficult and only a bump is noticed from the yields, suggesting severe dechanneling of these particles due to distortions originated by the platelets. This attenuation effect is severe and especially in the case of positrons because these wave functions are localized along the middle axis of the planar channel and hence the readjustment to the distortion might be very difficult. In addition, the beam attenuation in dislocation case of positrons/electrons also indicates the importance of relativistic effects on planar curvature. The electron data in similar situation indicates better yield (compared to the one noticed for positron case) as some of the initially well channeled electrons propagate through these distortions and get channeled as they are steered along the atomic sites. Contrary to the positron channeling,

such readjustment is quite possible for electrons. In addition, the distortion dechanneling in this case is expected to be less compared to the dechanneling due to obstruction.

Expressions for the initial population of different states at the surface of an SLS and for the population re-distribution due to the strain / shift preset at the interfaces are obtained quantum mechanically [22,23&27]. The expression for initial population yields the channeling angular scans that are generally performed. On the other hand the expression for population re-distribution helps in determining the tilt or shift existing in the system. Results obtained from this formulation are qualitatively in good agreement with the earlier calculations and also with the experiments [25,26]. Shape of the channeling angular scans is obtained in a quite natural way using simple quantum concepts, instead of using complicated statistical methods. It is shown that the ground state is more populated (less populated) for positrons (electrons) when compared with the excited states. The effects of stacking shift and the tilt present in the multi-layered semiconductor structures are described using the graphical representation for the case of positrons. It is observed that the higher states are more populated in the presence of defects.

An expression is obtained to estimate the effect of stacking shift / tilt on the radiation intensities. This has two fold applications. It can be used to estimate the required shift/tilt to obtain the maximum intensity and on the other hand it can be used to measure the strain present in SLS. This formulation can also be used to estimate the other radiation parameter like line width etc. Theory can be extended to the case of electron channeling radiation also. More rigorous and refined experiments are to be carried out for both electrons and positrons because of their importance in relativistic case. Subsequently, detailed theoretical calculations in accordance with experimental observations are to be carried out. At this point it can only be concluded that extensive research work is needed in this direction both in theoretical and experimental areas.

6.9 REFERENCES

1. Peter J. Schultz, Guiti R. Massoumi and W.N. Lennard, *Nucl. Instrum. Meth.* 90, 567(1994).
2. M.J. Pusaka and R.M. Nieminen, *Rev. Mod. Phys.* 66, 842 (1994).
3. M. A. Kumakhov, and R. Wedell, (ds.) *Radiation of relativistic light particles during interaction with single crystals*; (spektrum Akadcmischer verlag, 1991)
4. R. L. Swent, R. H. Patnell, H. Park, J. O. Kephart R. K. Klein, S. Datz, R. H. Fearick and B. L. Berman *Phys. Rev.* B29, 52 (1984).
5. V. V. Beloshitsky and A. A. Bobrov, *Nucl. Instrum. Meth.* B 72, 395 (1992).
6. M. Gouanere *et. al.*, *Phys. Rev.* B38, 4352 (1988).
7. J. Augustin, A. Schafer and W. Greiner, *Phys. Rev.* A51, 1367 (1995).
8. B. L. Berman *Rad. Eff. and Defects in Solid*, 122-123, 277 (1991), *and other papers in this issue*.
9. S. Datz, R. W. Fearick, H. Park, R. H. Patnell, R. L. Swent, J. O. Kephart and B. L. Berman, *Nucl. Instrum. Meth.* B2, 74 (1984).
10. H. Park, R.H. Patnell, R.L. Swent, J.D. Kephart, B.L. Berman, S. Datz and R.W. Fearick, *J. Appl. Phys.* 55, 358 (1984).
11. L. N. S. Prakash Goteti and Anand P. Pathak, *J. Phys.* C9, 1709 (1997).
12. L. N. S. Prakash Goteti and Anand P. Pathak, *Phys. Rev.* 58, 5243 (1998).
13. L. N. S. Prakash Goteti and Anand P. Pathak, *Phys. Rev.* B59, 8516 (1999).
14. L. N. S. Prakash Goteti, "Quantum models for effects of extended defects on ion-channelinng", *Ph.D thesis, University of Hyderabad (1999)*.
15. M. J. Alguard, R. L. Swent, R. H. Pantell, B. L. Bermen, S. D. Bloom and S.Datz, *Phys. Rev. Lett.* 42, 1148 (1979).
16. R. H. Pantell and M. J. Alguard *J. Appl. Phys.* 50, 798 (1979):
17. R. Wedell, *Phys. Stat. Sol.* B99, 12 (1980).
18. M. A. Kumakhov and R. Wedell *Phys. Stat. Sol.* B84, 581 (1977)
19. J. U. Andersen, E. Bonderup, E. Laegsgaard and A. H. Sorensen, *Phys. Scripta*, 28,308(1983).

20. W. Heitler, "The quantum theory of radiation", 3rd. ed., *Clarendon Press*, Oxford. (1954).
21. Loundon *Am. J. Phys.* 27, 649 (1959).
22. S.V.S. Nageswara Rao, L.N.S. Prakash Goteti and Anand P. Pathak, *Ind. J. Phys.* 76B(4), 443, 2002.
23. A.P. Pathak, L.N.S. Prakash Goteti and S.V.S. Nageswara Rao, *Nucl. Instrum. Meth. B193*, 188(2002).
24. D.S. Gemmell, *Rev. Mod. Phys.* 46, 129 (1974).
25. M. J. Pedersen, J.U. Andersen and W. M. *Rad. Eff* 12, 47 (1972).
26. J.U. Andersen, W. M. Augustynan and E. Uggerhøj, *Phys. Rev. B* 3, 705, (1971)
27. S.V.S. Nageswara Rao, L.N.S. Prakash Goteti and Anand P. Pathak, *Nucl. Instrum. Meth. B* 319, 118 (2002).

CHAPTER VII

CONCLUSION

This chapter summarizes all conclusions drawn from different experiments and calculations performed as a part of this thesis and also address the possibilities of further work in this direction. The detailed chapter wise conclusions are given at the end of each chapter.

7.1 INSTRUMENTATION

A Large Area two-dimensional Positions Sensitive AE-E Detector Telescope (LAPSDT) and an automated high energy channeling facility have been designed (fig. 3.29) and developed as a part of this thesis work [1,2]. The performance of these facilities has been tested and these facilities have been utilized for performing the thesis experiments. Presently these two facilities are open to all universities and institutes in India at NSC, New Delhi.

Good z-separation and depth resolution have been observed from the LAPSDT data [1]. The kinematic broadening caused by the large solid angle is taken care by implementing kinematic corrections in LAPSDT based ERDA data. These kinematic corrections could be implemented indigenously for the first time in India. Hence large solid angle could safely be used to minimize the radiation damage during the measurement. This detector has been used to observe the online mixing in lattice matched InGaAs/InP superlattice. We found that the mixing effect starts appearing from a fluence of 4.54×10^{12} ions/cm² in this system if irradiated by 150 MeV Ag ions. 2D position

sensitivity has also been obtained and the angular resolution is found to be better than the required value ($<0.1^\circ$) for measuring structural effects like blocking/ERDA patterns. Hence many new experiments can be performed using this detector.

The "automated high energy channeling facility" has been tested and found to be working consistently [2]. The facility has been checked three times in three different runs. Reasonably good reduction in aligned yield has been obtained from all the scans that have been performed on epilayers. This indicates the good performance of the facility and the crystalline quality as well. InGaAs/GaAs samples have been characterized using this facility. Measured strain values (Ex: 0.56% for 400\AA Sample) are little lower than that of the nominal ($\sim 1\%$) values. HRXRD also confirms that the indium content and hence the strain (0.7%) in these samples less than those of the nominal values. Asymmetric angular scans have been observed in 100\AA $\text{In}_{0.1}\text{Ga}_{0.9}\text{As}/\text{GaAs}$ sample. This asymmetry is a good parameter to measure the low strain values if Monte Carlo simulations are used to analyze the channeling data.

7.2 ION BEAM MIXING AND STRAIN ENGINEERING

It is, shown that the strain in SLS can be tuned using SHI mixing without loss of the quality of the samples [3]. The common trend in all the samples indicates the gradual diffusion of *In* from surface and the migration of *Ga* or *As* like atoms to the surface regions due to the SHI irradiation and/or annealing processes. The compressive strain is found to decrease in the initially compressive strained samples and tensile strain is induced in an initially lattice matched system. General trend indicates the increase in the superlattice period after the irradiation. These facts are revealed by both RBS/Channeling and HRXRD measurements. Thickness, chemical composition and strain values of each layer of all the irradiated and pristine samples are determined and presented in tabular forms (in Chapter 4). The crystalline and interface quality of both the irradiated and the unirradiated samples are found to be considerably good from these measurements. Hence the heavy ion irradiation did not spoil the basic structure of the lattice. Broadening in the

substrate peak in HRXRD spectra is due to the implantation damage in the substrate region ($\sim 13\mu$ below the **epi-layer**), which could be annealed out up to some extent by RTA. Fluence dependence and layer thickness dependence on the mixing effects in single InGaAs layers grown on GaAs substrate have been studied using HRXRD. Mixing effect increases linearly with increase in fluence. Similarly such effects are found to increase with increase in layer thickness. This is because the initial strain energy in thick layers is more when compared to thin samples. This strain energy will decrease by promoting the diffusion of *In* during irradiation. Detailed discussion is given in chapter 4.

7.3 HIGH ENERGY CHANNELING

The importance of high energy channeling in lattice strain measurements has been discussed and pointed out [4]. High energy channeling experiments have been proposed and performed to measure the strains. Irradiation time has been greatly reduced by using the currently developed automated channeling facility. In addition to this we have also used a forward detector for alignment purpose where resolution is not a primary requirement. This will improve the count rate due to high scattering cross-section at forward angles. These methods have been implemented so as to minimize the possible damage during the channeling measurements. In fact this is the first experiment to study the channeling in the high energy region in **scattering** mode, *i.e 40 MeV Si on GaAs at 90/100 degree*. Some discussion is given in section 7.1. Here It is shown that this high energy channeling is a sensitive technique to measure the lattice strains. A blocking pattern has also been recorded for the first time in SLS using the forward scattering of 40 MeV Si, which suggests a new and easy method to measure the strains. However this blocking data has not been included in this thesis due to poor statistics. Online **monitoring** and controlled modification of strain (strain engineering) is possible with blocking-ERDA in these structures.

.4 CHANNELING RADIATION IN SLS

Quantum mechanical models have been developed to describe the effects of strains and defects on channeling of light relativistic particles like electrons and positrons [5]. Channeling of these relativistic particles is very sensitive to crystal imperfections. It is found that the total dechanneling for the ground state of electron is very sensitive to stacking shift/tilt in contrast to the positron case where the excited states show such behavior while the ground state calculation show almost Gaussian in shape. It is shown that the ground state is more populated (less populated) for positrons (electrons) when compared with the excited states. This reveals the fact that the dechanneling of electrons and positrons is qualitatively different because of their opposite charges. These calculations and predictions in fact explain the results of Park and coworkers [6].

When these relativistic particles are channeled along major planes or axes, they emit a special kind of radiation called channeling radiation. Here we have studied the effects of strains/defects on this channeling radiation. Expressions for the initial population of different states at the surface of an SLS and for the population redistribution due to the strain / shift preset at the interfaces have been derived quantum mechanically. The expression for initial population yields the channeling angular scans that are generally performed. On the other hand the expression for population redistribution helps in determining the tilt or shift existing in the system. Results obtained from this formulation are qualitatively in good agreement with the earlier calculations and also with the experiments [7]. Shape of the channeling angular scans is obtained in a quite natural way using simple quantum concepts, instead of using complicated statistical methods. It is observed that the higher states are more populated in the presence of defects.

An expression is obtained to estimate the effect of stacking shift / tilt on the radiation intensities. This has two fold applications. It can be used to estimate the required shift/tilt to obtain the maximum intensity and on the other hand it can be used to measure the strain present in SLS. This formulation can also be used to estimate the other

radiation parameter like line width etc. Theory can be extended to the case of electron channeling radiation also. In fact the available experimental data is not sufficient to compare our theoretical models. Lot of experimental and theoretical work is due in this important area of research.

7.5 FUTURE PROSPECTS

The capability of the channeling technique can be enhanced by integrating both the facilities (LAPSDT & automated high energy channeling) that are developed as part of this thesis work (fig. 2.29). Blocking/ERDA can be performed using this facility. Blocking experiment is simple and can be performed with very low fluence when compared to channeling measurements. It allows the online modification of strain and hence controlled modification of strain is possible with. A grate verity of new phenomenon can be studied using this facility. For example, several new experiments like channeling/blocking - ERDA, Transverse heating & cooling of channeled ions, Stopping Powers of channeled ions, re-crystallization, online sputtering, mixing & radiation damage studies can be performed with the currently developed facility. These experiments maybe performed as a continuation of this work.

The possibility of spatial band gap tuning for the integration of optoelectronic devices has been discussed and proved in this thesis. This band gap tuning technique can be pursued using PL. STM/TEM and other characterization techniques may also be used to promote this kind of work. To establish these techniques one has to rigorously work on the fluence dependence studies. Diffusion properties of constituent elements can also be studied. Controlled modification studies are to be pursued to establish this useful technology.

Channeling radiation theory can be extended to calculate radiation frequencies, line widths for both positrons and electrons. Axial channeling studies can also be performed. Efforts are to be put in the development of channeling radiation based characterization techniques. More rigorous and refined experiments are to be carried out

for both electrons and positrons because of their importance in relativistic case. Subsequently, detailed theoretical calculations in accordance with experimental observations are to be carried out. At this point it can only be concluded that extensive research work is needed in this direction both in theoretical and experimental areas.

As a last word, this thesis sets up a stage to perform several rigorous experiments and studies to establish the controlled spatial band gap tuning which is a primary requirement for the integration of optoelectronics circuits. The theoretical models, experimental conclusions and experimental facilities that have been developed in this work are helpful to pursue such studies. This work actually lays a base for the constructive work in the area of "*Ion beam research*" in general and the "*Ion Beam Characterization and Engineering of Strains in Semiconductor Multilayers*" in particular.

7.6 REFERENCES

1. Development of a Large Area two dimensional Position Sensitive AE-E Detector Telescope, S.V.S. Nageswara Rao et. al. *NSC (New Delhi) annual report, 63, (2001-2002)*; Effect of field homogenization on position sensitivity of LAPSDT, S.A. Khan, S.V.S. Nageswara Rao et. al., *NSC (New Delhi) annual report, 65, (2001-2002)*; *Accepted for poster presentation at ICACS 20, Puri, India.*
2. Development of Automated High Energy Channeling Facility at NSC S.V.S. Nageswara rao, et. al., *NSC (New Delhi) annual report, 66, (2001-2002)*; Automation of Channeling experiment for lattice strain measurements using high energy ion beams, S.V.S. Nageswara Rao et. al. (Poster: Presented at CAARI 2002, University of North Texas, Denton, USA).
3. A.P. Pathak, S.V.S. Nageswara Rao et. al. *Nucl. Insrt. Meth.* B193, 319 (2002); Ion beam irradiated effects on the strain in GaAs/InGaAs layers, S.V.S. Nageswara Rao, A.P. Pathak et. al. (Presented in an International conference PS1

2002 , March 4-8 Puri, India.. Proceedings in **World Scientific** are in process);
 Swift heavy ion mixing in In_{0.12}Ga_{0.88}As/GaAs strained layer superlattice,
 S.V.S. Nageswara Rao, et. al.; Solid State Physics (India) 44; Ion beam studies of
 strains/defects in semiconductor multi layers, A.P. Pathak, S.V.S. Nageswara Rao
 et. al, Presented at CAARI 2002, University of North Texas, Denton, USA.

4. A.P. Pathak, A.M. Siddiqui and S.V.S. Nageswara Rao, *Nucl. Instr. Meth. B*, 161-163, 487, 2000; AIP Series, 576, 476, 2001; A.M. Siddiqui, S.V.S. Nageswara Rao et. al, *J. Appl. Phys.* 90, 2824, 2001; Energetic ion beams for measurement and modification of strain in strained superlattices, Proc. DAE-BRNS workshop on thin films and multilayers, 68-71, oct. 1999.
5. A.P. Pathak, L.N.S. Prakash Goteti and S.V.S. Nageswara Rao, *Nucl. Instr. Meth. B*, 193, 188, 2002; *Ind. J. Phys.*, 76B(4), 443, 2002; Quantum description for the effects of strained layered superlattices on channeling radiation, S.V.S. Nageswara Rao et. al. *submitted to Nucl. Instr. Meth. B* (revised according to referee comments), Solid State Physics (India) 43 (2000); 44 (2001).
6. H. Park, R.H. Patnell, R.L. Swent, J.D. Kephart, B.L. Berman, S. Datz and R.W. Fearick, *J. Appl. Phys.* 55, 358 (1984).
7. M. J. Pedersen, J.U. Andersen and W. M. *Rad. Eff.*, 12, 47, 1972.; J.U. Andersen, W. M. Augustynan and E. Uggerhøj, *Phys. Rev. B* 3, 705 (1997).

S.V.S. NAGESWARA RAO

(NAGESH)

Senior Research Fellow

School of Physics

University of Hyderabad

Hyderabad-500 046, India

nageshphysics@yahoo.com

appsprs@uohyd.ernet.in

Objective: To pursue research in basic and applied Physics.

Present status

Ph.D. (Physics) [9th Sept. 1997 - to date]: Presently working on the PhD thesis. Thesis synopsis has been submitted to the university.

Thesis title: Ion Beam Characterization And Engineering of Strain in Semiconductor Multi-Layers

Thesis supervisor: Prof. Anand P. Pathak, School of Physics,
University of Hyderabad. Hyderabad 500 046, India.

Number of publications

<i>Refereed publications:</i>	9
<i>Conference proceedings:</i>	7
<i>NSC Annual reports:</i>	10
<i>To be communicated:</i>	6

Educational Qualifications

M.Sc(Tech.) Physics with specialization in Electronics and Space Physics
JNTU College of Engineering, Anantapur, Jawaharlal Nehru Technological
University, Hyderabad, AP, India First class with Distinction, 77.8% (1994-1997).

B.Sc (Mathematics, Physics & Electronics) A.M.A.L. College, Anakapalle,
Andhra University, Waltair, AP, India, First Class, 64% (1991-1994).

Special Presentations

Invited Talk (for Prof. Pathak)

"Ion Beam studies of Strains/Defects in Semiconductor Multi layers" CAARI 2002,
University of North Texas, Denton, USA.

Poster Presentation

"Automation of Channeling Experiment for Lattice Strain Measurements using High Energy
Ion beams", CAARI 2002, University of North texas, Denton, USA.

Young Scientist Presentation

"Channeling radiation from relativistic electrons and positrons" NCAMP XIII Jan 2001
IACS, Kolkata, India.

Special achievements:

Second rank: M.Sc.(Tech.) electronics and space physics course for the batch 1994-97

Memberships

Graduate Member, Institute of Physics, London (Grad. Inst. P, London)

Technical Skills

<i>Mechanical</i>	; Working experience on all common workshop machines. Design, drawing and development of mechanical parts needed for performing experiments.
<i>Experiment</i>	: Ion Beam Analysis & Modification (RBS, ERDA, Channeling, Blocking, Transverse Heating/cooling of channeled ions, stopping power measurements, Ion implantation, Ion beam Mixing, High resolution XRD). Working experience in an accelerator (15MV pelletron tandem accelerator) based laboratory. Handling ultra high vacuum systems, radiation detectors (surface barrier, ion implanted position sensitive detectors & ionization chambers), data acquisition and control.
<i>Research:</i>	Literature survey, Planning and performing different kinds of experiments, Theoretical modeling, Design & Development of experimental facilities, Proposing new problems and writing research projects. Data Collection, Analysis, interpretation, Presentations & Publishing results.
<i>Computation:</i>	
<i>Languages</i>	: <i>Pascal and C</i>
<i>Assembly Language</i>	<i>8085 & 875J</i>
<i>Operating System</i>	<i>DOS, WINDOWS, UNIX and LINUX</i>
<i>(As Platform)</i>	
<i>Simulation Programs</i>	<i>TRIM, RUMP and FREEDOM (ERDA)</i>

Personal Details

Date Of Birth	08-06-1974
Marital Status	Unmarried
Languages Known	English, Hindi and Telugu
Residential Address	C/O Sri. Y.V. Chendra Sekhar Rao 2-2-1130/24/1, New Nallakunta Hyderabad - 500 044, Ph: +91-40 - 7667946/7673893 e-mail: nsaniali@yahoo.com

Experience:

I have Five years of experience in Research and Development in the area of experimental and theoretical aspects of Ion-solid interactions (Accelerator based research in materials science). I have developed two experimental facilities namely " A Large Area two dimensional Position Sensitive AE-E Detector Telescope" and "An automated high energy channeling facility" at Nuclear Science Centre, New Delhi with the collaboration of Dr. D.K. Avasthi, as a part of my thesis work. I have performed my thesis experiments using these facilities. These facilities are presently open for the user community of NSC. My research interest includes the Ion beam characterization and engineering of material properties using swift heavy ions, especially the spatial bandgap tuning of semiconductor multilayers using ion beam mixing methods for the integration of optoelectronic circuits. I have participated in the experimental and developmental activities of ion beam based materials science research at NSC. I have performed (or participated in) several experiments like sample growth, HRXRD (at TIFR-Mumbai and SSPL-Delhi), Raman spectroscopy (at IGCAR-Kalpakkam), and *He* RBS-Channeling at (IOP-Bhubaneswar and IIT-Kanpur). I have also participated in the development of a large area gas detector (with Dr. S. Ghosh) and in several irradiation and ERDA-Experiments at NSC. I have also studied the theoretical aspects of channeling radiation in SLS.

I also have 5 months experience in hardware and software design using micro controllers in the Programmable Control Systems (PCS) laboratory of Bharat Heavy Electricals Limited BHEL (R&D), Hyderabad. (6th Sem. Of M.Sc)

Please see : List of NSC annual reports (Participation in variety of experimental and developmental activities at NSC and the experience in collaborative research and team work) and List of Publications (Experience related to the thesis problem)

References (Addresses of two scientists who are familiar to my work)

1. Prof. Anand P. Pathak, School of Physics, University of Hyderabad, Hyderabad 500046, India. *{Thesis supervisor}* e-mail apps@uohyd.ernet.in. Ph. 040 3010181 Fax +91 40 3010181/3010227/3010120
2. Dr. D.K. Avasthi, Nuclear Science Centre, Post box No. 10502, Aruna Asaf Ali Marg, New Delhi 110 067, India e-mail dka@nsc.ernet.in Ph. 011 6893955 Fax +91 11 6893666

LIST OF PUBLICATIONS

Refereed Journals: (Published / accepted for publication)

1. Defects and Strain studies in semiconductor multilayers, A.P. Pathak, S.V.S. Nageswara Rao, A.M. Siddiqui, *Nucl Instr. Meth. B*, 161-163, 487, 2000.
2. Strain Measurements of semiconductor multilayers by Ion channeling, High resolution XRD and Raman Spectroscopy, Azher M. Siddiqui, S.V.S. Nageswara Rao and Anand P. Pathak, AIP Series, 576, 476, 2001.
3. Ion Chnanneling, high resolution x-ray diffraction and Raman spectroscopy in strained quantum wells, Azher M. Siddiqui, S.V.S. Nageswara Rao, Anand P. Pathak, V. N. Kulkarni, R. Kesav Murthy, Eric Williams, Daryush Ila, Claudiu Muntele, K.S. Chandrasekaran and B. M. Arora, */ Appl. Phys.* 90, 2824, 2001.
4. Ion beam studies in strained layer superlattices, A.P. Pathak, S.V.S. Nageswara Rao, A.M. Siddiqui, G.B.V.S. Lakshmi, S.K. Srivastava, S. Ghosh, D. battacharya, D.K. Avasthi, D.K. Goswami, P. V. Satyam, B.N. Dev and A. Turos, *Nucl Insrt. Meth. B*, 193, 319, 2002.
5. Electronic sputtering of Fullerene films by swift heavy ions, S. Ghosh, D.K. Avasthi, T. Som, A. Tripathi, S.K. Srivastava, S.V.S. Nageswara Rao, F. Gruner and W. Assmann, *Nucl Instr. Meth. B*, 190 (1-4), 169, 2002.
6. Channeling radiation from relativistic electrons - study of stacking faults and dislocations, A.P. Pathak, L.N.S. Prakash Goteti and S.V.S. Nageswara Rao, *Nucl. Instr. Meth. B*, 193, 188, 2002.
7. Channeling radiation from relativistic electrons and positrons, S.V.S. Nageswara Rao, L.N.S. Prakash Goteti and A.P. Pathak, *Ind. J. Phys.*, 76B(4), 443, 2002.
8. DE/dx measurements for heavy ions with $Z=6-29$ in poly corbonate, A. Sharma, P.K. Diwan, S. Kumar, S.K. Sharma, V.K. Mittal, S.V.S. Nageswara Rao, B. Sannaki, S. Ghosh, and D.K. Avasthi. *Nucl Instr. Meth. B*, 194(1), 7, 2002.
9. Quantum description for the effects of strained layered superlattices on channeling radiation, *submitted to Nucl Instr. Meth. B* (In Press)

Communicated:

1. Ion beam irradiated effects on the strain in GaAs/InGaAs layers, S.V.S. Nageswara Rao, et. al. (Presented in an International conference PSI 2002 , March 4-8 Puri, India.. Proceedings in *World Scientific* are in process)

Published in Conference Proceedings:

1. Energetic ion beams for measurement and modification of strain in strained superlattices, D.K. Avasthi, S.V.S. Nageswara Rao and A.P. Pathak, Proc.. DAE-BRNS workshop on thin films and multilayers, 68-71, oct. 1999.
2. Quantum description of the electron dechanneling by stacking faults, L.N.S. Prakash Goteti, S.V.S. Nageswara Rao and A.P. Pathak, Solid State Physics (India) 43, 322, 2000.
3. Electronic sputtering of Fullerene films by swift heavy ion impact, S. Ghosh, D.K. Avasthi, T. Som, A. Tripathi, S.K. Srivastava, S.V.S. Nageswara Rao, F. Gruner and W. Assmann, Solid state physics (India) 43, 280, 2000
4. Quantum description of the effects of defects on channeling radiation, Anand P. pathak, L.N.S. Prakash Goteti and S.V.S. Nageswara Rao, proc. APF conf. April 13-15, 2000 (in press),[*National symp. On atomic physics at the frontiers*].
5. Swift heavy ion mixing in $\text{In}_{0.12}\text{Ga}_{0.88}\text{As}/\text{GaAs}$ strained layer superlattice, S.V.S. Nageswara Rao, G.B.V.S. Lakshmi, A.M. Siddiqui, S.Ghosh, S.K. Srivastava, D.K. Avasthi, R.K. Jain, F. Eichhorn and A.P. Pathak, Solid State Physics (India) 44 (In Press, presented in DAE-SSP 2002)
6. Quantum description for the effects of strained layer super lattices on channeling radiation, S.V.S. Nageswara Rao, L.N.S. Prakash Goteti, G.B.V.S. Lakshmi, Azher M. Siddiqui and Anand P. Pathak, Solid State Physics (India) 44 (In Press, Presented in DAE-SSP2002)
7. Theory of charged particle probes to modern advanced materials, A.P. Pathak, S.V.S. Nageswara Rao, A.M. Siddiqui, L.N.S. Prakash Goteti and G.B.V.S. Lakshmi (Proce. International conference on Accelerator physics organized by NSC, New Delhi, in process)